Studies in Systems, Decision and Control 253

Harsh S. Dhiman
Dipankar Deb

Decision and Control in Hybrid Wind Farms

Springer

Studies in Systems, Decision and Control

Volume 253

The series "Studies in Systems, Decision and Control" (SSDC) covers both new developments and advances, as well as the state of the art, in the various areas of broadly perceived systems, decision making and control–quickly, up to date and with a high quality. The intent is to cover the theory, applications, and perspectives on the state of the art and future developments relevant to systems, decision making, control, complex processes and related areas, as embedded in the fields of engineering, computer science, physics, economics, social and life sciences, as well as the paradigms and methodologies behind them. The series contains monographs, textbooks, lecture notes and edited volumes in systems, decision making and control spanning the areas of Cyber-Physical Systems, Autonomous Systems, Sensor Networks, Control Systems, Energy Systems, Automotive Systems, Biological Systems, Vehicular Networking and Connected Vehicles, Aerospace Systems, Automation, Manufacturing, Smart Grids, Nonlinear Systems, Power Systems, Robotics, Social Systems, Economic Systems and other. Of particular value to both the contributors and the readership are the short publication timeframe and the world-wide distribution and exposure which enable both a wide and rapid dissemination of research output.

** Indexing: The books of this series are submitted to ISI, SCOPUS, DBLP, Ulrichs, MathSciNet, Current Mathematical Publications, Mathematical Reviews, Zentralblatt Math: MetaPress and Springerlink.

More information about this series at http://www.springer.com/series/13304

Harsh S. Dhiman · Dipankar Deb

Decision and Control in Hybrid Wind Farms

Springer

Harsh S. Dhiman
Department of Electrical Engineering
Institute of Infrastructure Technology
Research and Management (IITRAM)
Ahmedabad, Gujarat, India

Dipankar Deb
Department of Electrical Engineering
Institute of Infrastructure Technology
Research and Management (IITRAM)
Ahmedabad, Gujarat, India

ISSN 2198-4182 ISSN 2198-4190 (electronic)
Studies in Systems, Decision and Control
ISBN 978-981-15-0274-3 ISBN 978-981-15-0275-0 (eBook)
https://doi.org/10.1007/978-981-15-0275-0

I dedicate this book to almighty for giving me enough patience and strength throughout my journey. I thank my parents Renu & Sanjay, brother Hardik and the love of my life Shiwangi for motivating me to the ends of the world.
—Harsh S. Dhiman

I dedicate this book on Decision and Control to the Supreme Controller for providing whatever decision making ability I have in me. I thank my wife Indulekha and my son Rishabh for providing me unending love and support.
—Dipankar Deb

Preface

Depleting coal resources have raised alarming signals for installation of renewable energy systems (RES). The popularity of renewable sources is in cohesion with power ecosystem with benefits like cleaner production and lower tariff rates, making it reliable and secure candidate for electricity demands globally. Research and development in wind and solar technologies has seen a tremendous rise in the past two decades which, has attracted investors to put their money into these projects. European countries like Denmark, Germany, Sweden, and England have installed large offshore wind farms to cater their country's load demands. China, on the other hand, has been actively involved in manufacturing services, and India is on the developing side of wind energy portfolio.

The book focuses on the two most important aspects of the wind farm operation, that is, decision and control. The first part of the book deals with decision-making processes in wind farms. Modern-day decision-making is a volatile process that is sensitive to the internal and external factors which can directly influence decision-makers' decision. The introductory chapter on decision-making covers prime methods to evaluate a set of alternatives for given criteria. A part of the chapter is also dedicated to sensitivity analysis and how it influences decision-making. We also introduce the concept of hybrid wind farms and enlist the different strategies a operator can face to achieve optimal farm operation. Hybrid wind farm operation is governed by a set of alternatives that the wind farm operator must choose to ascertain optimal dispatch of wind power to the utility grid. The decision-making is accompanied by accurate forecasts of wind speed that must be known beforehand. Errors in wind forecasting are to be compensated fairly by pumping power from reserve capacity to the grid in terms of battery energy storage system (BESS). Alternatives, based on penalty cost, are assessed based on certain criteria, and MCDM methods are used to evaluate the best choice. Further, considering the randomness in the dynamic phenomenon in wind farms, a fuzzy MCDM approach is applied to the decision-making process to evaluate the best alternative for the hybrid wind farm operation. Case studies from the wind farms of the USA are presented with numerical solutions to the problem.

The second part deals with the control aspect, in particular with yaw angle control, that aids in power maximization in wind farms. A novel transfer function-based methodology is presented that controls the wake center of the upstream turbine(s). LIDAR-based numerical simulations are carried out for wind farm layouts. An adaptive control strategy is implemented to achieve the desired yaw angle for upstream turbines. The proposed methodology is tested for two wind farm layouts. Wake management is also implemented for hybrid wind farms, where BESS life enhancement is studied. The effect of yaw angle on the operational cost of BESS is assessed, and the case studies for wind farm datasets from the USA and Denmark are carried out. Overall, this book provides a comprehensive decision and control aspect for hybrid wind farms which may be useful from an industrial point of view.

Ahmedabad, India
August 2019

Harsh S. Dhiman
Dipankar Deb

Acknowledgements

The achievement of this goal would not have been possible without the assistance of the Institute of Infrastructure Technology Research and Management (IITRAM) that provided necessary infrastructural support for writing this book. The authors are also grateful to Multidisciplinary Publishing Institute (MDPI) for allowing us to use related content for the book. We would like to thank the scientific and research organizations and agencies like Wind Energy Center and University of Massachusetts for online access to wind speed datasets. We would like to express our sincere gratitude to Dr. Meera Vasani, Associate Dean, and Ms. Wati Longkumer for English proofreading.

Ahmedabad, India
August 2019

Harsh S. Dhiman
Dipankar Deb

Contents

About the Authors

Harsh S. Dhiman was born in Chandigarh, in 1992 and is currently pursing Ph.D. in Department of Electrical Engineering from Institute of Infrastructure Technology Research and Management (IITRAM), Ahmedabad, India under the supervision of Prof. Dipankar Deb. He obtained his Master's degree in Electrical Power Engineering from Faculty of Technology & Engineering, The Maharaja Sayajirao University of Baroda, Vadodara, India and B. Tech in Electrical Engineering from Institute of Technology, Nirma University, Ahmedabad, India. His current research interests include Hybrid operation of wind farms, Hybrid wind forecasting techniques and Wake management in wind farms.

Dipankar Deb completed his Ph.D. from University of Virginia, Charlottesville under the supervision of Prof. Gang Tao, IEEE Fellow and Professor in the department of ECE in 2007. In 2017, he was elected to be a IEEE Senior Member. He has served as a Lead Engineer at GE Global Research Bengaluru (2012-15) and as an Assistant Professor in EE, IIT Guwahati 2010-12. Presently, he is a Professor in Electrical Engineering at Institute of Infrastructure Technology Research and Management (IITRAM), Ahmedabad. He is a Student Startup and Innovation Project Coordinator at IITRAM. He mentor students to build Intellectual property Rights (Patents). His research interests include Control theory, Stability analysis and Renewable energy systems.

Acronyms

AEP	Annual energy production
AHP	Analytic hierarchy process
BESS	Battery energy storage system
CFD	Computational fluid dynamics
COPRAS	Complex proportional assessment
CPS	Cumulative priority score
EKF	Extended Kalman filter
ELECTRE	Elimination and choice translating reality
ERM	Energy reservoir model
FLORIS	FLOw Redirection and Induction in Steady State
HAWT	Horizontal axis wind turbine
IPC	Individual pitch control
KF	Kalman filter
KKT	Karush–Kuhn–Tucker
LIDAR	Light detection and ranging
LSSVR	Least square support vector regression
MAPE	Mean absolute percentage error
MCDM	Multi-criteria decision-making
MPAC	Model predictive active control
NIS	Negative ideal solution
OCV	Open-circuit voltage
PC	Penalty cost
PI	Proportional–integral control
PIS	Positive ideal solution
PROMETHEE	Preference ranking organization method for enrichment evaluation
PS	Priority score
RMSE	Root mean squared error
SAW	Simple additive weighting
SoC	State of charge

SOWFA	Simulation for On/Offshore Wind Farm Applications
SVR	Support vector regression
TOPSIS	Technique for Order of Preference by Similarity to Ideal Solution
UKF	Unscented Kalman filter
WFLOP	Wind farm layout optimization
WRA	Wind resource assessment

List of Figures

List of Tables

Chapter 1
Fundamentals of Wind Turbine and Wind Farm Control Systems

Wind is a randomly varying resource that needs to be appropriately tapped using wind turbines typically anchored to the ground and subjected to different torques and loads with changing atmospheric conditions. There are significant challenges in modeling such behaviors, and such issues become further complex in the case of offshore wind turbines, hilly terrains, and during ramp events which are extensively dealt with in this book. In this chapter, we present fundamental aspects of wind turbine blade-pitching control, wake control, and also wind reserve power maximization strategy. Micro-siting is an issue in wind farms that affects the total power generated from the farm, and is interrelated to turbine control and wake effect.

1.1 Introduction

Modern wind turbines operate in the region characterized by a cubic relation between extracted wind power and magnitude of wind speed. Performance of a wind turbine, in terms of power capturing capability is not solely dependent on wind speed but also on the orientation of the rotor blades and rotor hub. Control of this multidimensional dependence is one of the key areas in wind energy research. Mathematically, wind power extracted by a turbine with rotor area A from moving air with a velocity v is given as

$$P(t) = \frac{1}{2}\rho A v^3(t) C_p(\lambda, \beta), \tag{1.1}$$

where $C_p(\lambda, \beta)$ is the power coefficient dependent on the tip-speed ratio λ and blade-pitch angle β. The term C_p essentially reflects the turbine capability in terms of the aerodynamic efficiency which has a maximum theoretical value of 0.59. A wind turbine starts to extract power at a particular speed known as cut-in speed v_{in} which ranges typically from 2.5 to 5 m/s. Further, the region from cut-in speed to rated speed (speed at which the wind turbine is designed to optimally operate) is the region where the turbine is primed to operate. For wind speeds greater than rated speed, the turbine

H. S. Dhiman and D. Deb, *Decision and Control in Hybrid Wind Farms*,
Studies in Systems, Decision and Control 253,
https://doi.org/10.1007/978-981-15-0275-0_1

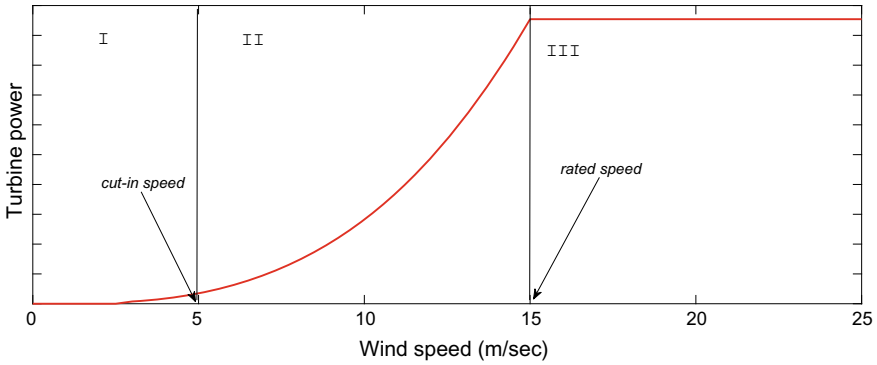

Fig. 1.1 Wind turbine power curve

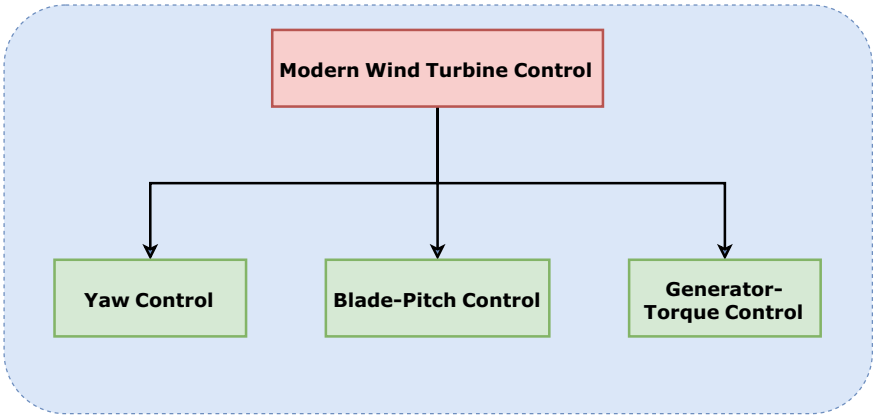

Fig. 1.2 Types of modern wind turbine control

stalls power production owing to the generator capability limits in terms of armature rating. If the turbine is operated above rated speed, collateral damage to the turbine components like rotor shaft, gearbox, and yaw bearings is possible thus jeopardizing the wind farm operation. Figure 1.1 depicts the wind turbine power curve with three regions where the turbine operation is defined. Region I, where no power extraction is observed as the wind speed is less than cut-in speed. Region II, where the wind power follows cubic relationship with incoming wind speed.

Figure 1.2 illustrates the types of wind turbine controls that are being used in modern wind power plants.

The yaw control is used for aligning the yaw toward the wind direction for extracting maximum power from the wind. Over the years, yaw control of wind turbine(s) as well as wind farm has gained a lot of importance owing to the amount of power improvement and turbine load reduction it caters. Specifically, aerodynamic loading on the downstream turbine(s) is a reason for concern that allows many wind

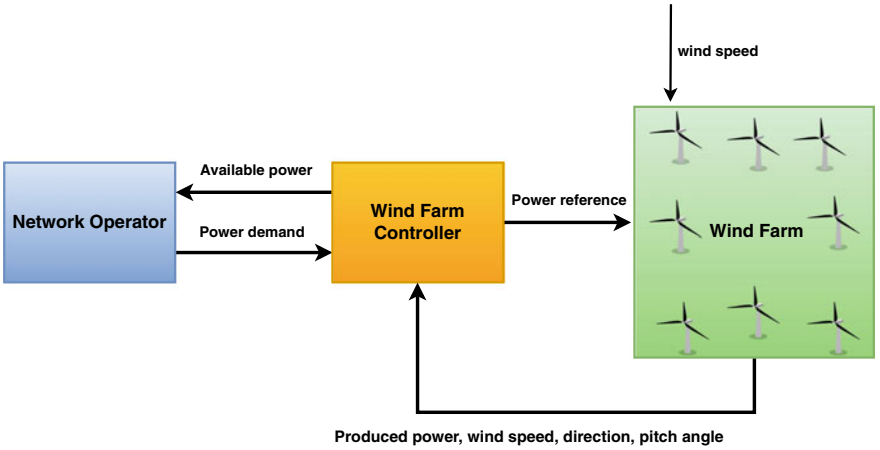

Fig. 1.3 Generic wind farm controller for power maximization

farm operators to use high-fidelity sensor devices like light detection and ranging (LIDAR). Further, for generator-torque control, the aim is to keep a track on the tip-speed ratio and adjusting the reaction torque keeping the blade pitch constant. In case of higher wind speed conditions, above rated speed, the blade-pitch controller acts in order to keep generator torque constant. Figure 1.3 illustrates the layout of a generic wind farm controller aimed to maximize power output when it is allowed to follow a given power reference. Various inputs like power produced, wind speed and direction, and pitch angle are fed to the controller.

1.2 Blade-Pitch Control for Wind Turbines

Among various works in literature, Bossanyi has carried out studies in closed-loop control of wind turbines focusing on pitch and torque control in modern variable-speed wind turbines [5]. Since the market thrust is essentially reliant on variable-speed machines, the control of power produced especially above rated speeds becomes important. Classical proportional–integral control of wind turbines includes the control of blade-pitch angle in order to regulate the aerodynamic power. For a fixed-speed pitch-regulated turbine, the PI control may be expressed as

$$y_\beta = \left(\frac{K_i}{s} + K_p\right) x_p, \tag{1.2}$$

where y_β and x_p are the demanded pitch and arithmetic difference between measured power and rated power. Figure 1.4 illustrates the key components of a PI control for pitch-regulated wind turbines.

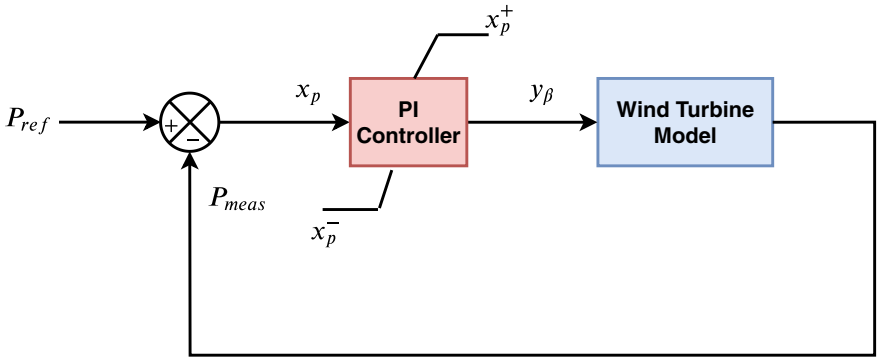

Fig. 1.4 PI control with anti-windup for fixed-speed pitch-regulated wind turbines

In case of PI control with integrating action solely responsible for correcting steady-state error, a large input may cause overshoot which results from actuator saturation [14]. Thus, a windup action is necessary to limit the output from controller and can be expressed as

$$sat(x_p) = \begin{cases} x_p^+, & \text{if } x_p > x_p^+ \\ x_p, & \text{if } x_p^- \leq x_p \leq x_p^+ \\ x_p^-, & \text{if } x_p < x_p^- \end{cases}, \tag{1.3}$$

where x_p^+ and x_p^- are the saturation limits imposed on the controller input x_p. In case of pitch-regulated control, a large error in the turbine power may cause erroneous controller response leading to uncontrollable oscillations which may result in excessive wear and tear of mechanical equipment.

Similar to blade-pitch control in fixed-speed machines, in variable-speed turbines, the error in the rotor speed is given as input to the controller while the torque is held constant. This type of control strategy is used for Region III of wind turbine curve above rated speed. Further, one of the major issues with wind turbine control is the aerodynamic load causing mechanical damage to the rotor blades, turbine hub, and tower. Individual pitch control (IPC) as well as collective pitch control (CPC) is used to mitigate the transient oscillations arising due to turbulent flow. Since a wind turbine consists of rotating and nonrotating parts, IPC uses Coleman transformation where the sensor signals from rotating frame of reference are converted into nonrotating frame of reference. First use of Coleman transformation was put forward by Bossayni where the linear quadratic Gaussian (LQG) control is applied [6]. The control algorithm works fast when it is decoupled in direct and quadrature axis and a reverse transformation is then used to attain pitch demands for three blades. Coleman transformation is given as

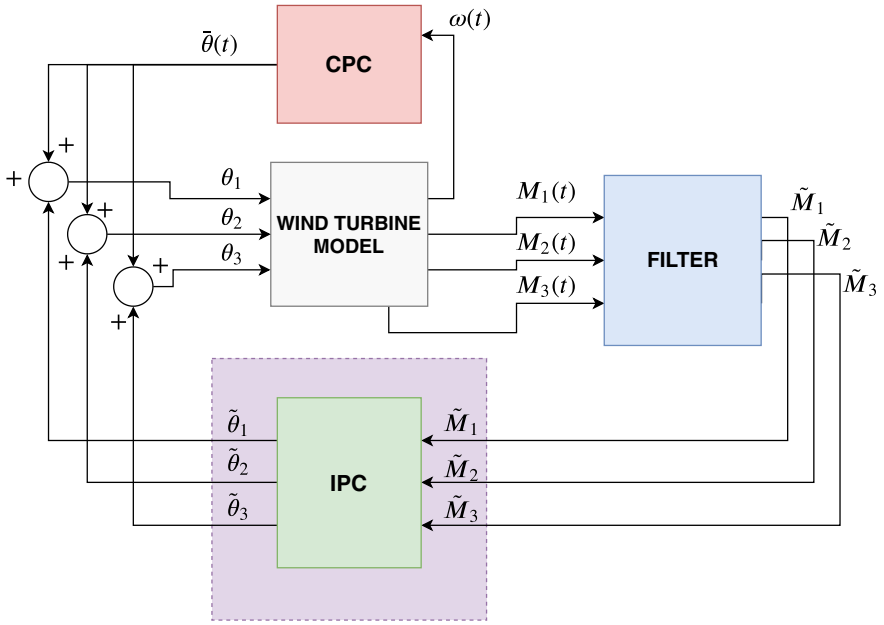

Fig. 1.5 Combined architecture for collective pitch control (CPC) and individual pitch control (IPC) of wind turbine

$$\begin{pmatrix}\theta_d\\ \theta_q\end{pmatrix} = \begin{pmatrix}\cos(\psi) & \cos(\psi+\frac{2\pi}{3}) & \cos(\psi+\frac{4\pi}{3})\\ \sin(\psi) & \sin(\psi+\frac{2\pi}{3}) & \sin(\psi+\frac{4\pi}{3})\end{pmatrix}\begin{pmatrix}\theta_1\\ \theta_2\\ \theta_3\end{pmatrix} \tag{1.4}$$

and inverse Coleman transformation from d-q axis to rotating frame of reference is given as

$$\begin{pmatrix}\theta_1\\ \theta_2\\ \theta_3\end{pmatrix} = \begin{pmatrix}\cos(\psi) & \cos(\psi+\frac{2\pi}{3}) & \cos(\psi+\frac{4\pi}{3})\\ \sin(\psi) & \sin(\psi+\frac{2\pi}{3}) & \sin(\psi+\frac{4\pi}{3})\end{pmatrix}^T\begin{pmatrix}\theta_d\\ \theta_q\end{pmatrix}, \tag{1.5}$$

where θ_d, θ_q refer to the direct and quadrature axes pitch demands in fixed axis, whereas $\theta_1, \theta_2, \theta_3$ are the blade pitch demands in rotating frame of reference, and ψ refers to the azimuth angle of rotor. Figure 1.5 illustrates the architecture for CPC and IPC of a wind turbine. The collective pitch control accounts for regulating rotor speed $\omega(t)$ and IPC accounts for reducing perturbations in the flapwise root bending moments on each turbine blade.

The blade dynamics for a wind turbine for load characterization as proposed by Bossanyi is given as

$$\frac{\dot{M}_i(t)}{dt} + 2\pi f_{blade}\xi_{blade}\dot{M}_i(t) + 4\pi^2 f_{blade}^2 M_i(t) = 4\pi^2 f_{blade}^2 M_{flap,i}(t), \tag{1.6}$$

where f_{blade}, ξ_{blade} are the natural frequency and damping ratio of the blade, $M_i(t)$ is the flapwise blade root bending moment, and $M_{flap,i}$ is the flapwise aerodynamic loading on ith blade [5]. Similarly, tower dynamics can be modeled as a mass–spring–damper system for analyzing fore–aft motion as

$$m_T \ddot{x}_{fa}(t) + \xi_T \dot{x}_{fa}(t) + k_T x_{fa}(t) = F_T(t) = \frac{3}{2h} M_{tilt}(t), \tag{1.7}$$

where m_T, ξ_T, k_T denote tower mass, damping, and stiffness coefficients, respectively, whereas M_{tilt} is the tilt moment of the rotor. In the line of the work carried out by Selvam et al., the individual pitch control technique essentially uses Coleman transformation for minimization of rotor and tilt movements [29]. Apart from LQG-based control, a feedforward controller is also used to filter out the low-frequency influence of wind on rotor vibrations. The results revealed that LQG-based IPC resulted in better fatigue load reduction than conventional PI-based IPC. Furthermore, it is possible to improve the fatigue load reduction by means of LIDAR-based measurement devices that offer excellent preview information of wind speed. The use of LIDAR in wind turbine control is studied by Schlipf et al. where a nonlinear model predictive control is used for reducing the fatigue loads on wind turbine [28]. The performance of this method is compared with baseline controller and results reveal reduction up to 50% without any significant compromise in wind power. Baseline controller implements torque controller in tandem with collective blade-pitch control, while a model predictive controller predicts the future behavior based on the current measurements and an internal model.

In terms of speed regulation, Frost et al. have demonstrated a direct adaptive control of a utility scale wind turbine [12]. According to wind turbine power curve illustrated in Fig. 1.1, if a turbine operates in Region III which is characterized by wind speeds greater than rated speed, generator may result in overheating armature cables and thus causing damage to the power electronics equipment. Furthermore, higher wind speeds also cause damage to the nonrotating parts of the turbine in terms of excessive wear and tear and in some cases cracks in rotor blades and tower. A direct model reference adaptive control is used for rejecting the disturbances for improving the speed regulations and results are compared with conventional PI-based pitch controller. Johnson et al. have discussed several standard and adaptive control techniques for energy maximization in Region II of wind turbine curve [17]. Adaptive control is applied for regions with positive and negative speeds. Further, Moradi et al. have discussed the performance of classical PID control and H_∞ control for a wind turbine in presence of uncertainties like variation of power coefficient, discontinuity in wind speed, and inaccurate wind speed measurement [22]. It is observed that, in case of PID control, the oscillatory response is very high when the plant is subjected to uncertainties while with H_∞ control, a much more smooth response in turbine speed is observed.

1.3 Wake Control for Wind Turbines

Wind turbines placed behind upstream turbines face reduction in power due to wake interactions. This decline in power captured is primarily responsible for the increased use of ancillary devices like battery energy storage system (BESS) in a wind farm. Irregular wind loads cause nonrotating turbine parts to experience fatigue that ultimately result in turbine failure. Wind wakes can be characterized as loss in power production and increase in dynamic loading on downstream turbines. With stochastic wind flow, the variation in power produced can be a critical issue for wind farm operators. Wind farms in United States have been generating 10–15% of less power than their capacity due to wake interactions. Wake interactions need an accurate modeling that aids in the micro-siting process and increase the annual energy production (AEP) of a wind plant. In order to model wind wakes in a wind farm, various kinematic models and 2D/3D models are used. Among kinematic models, Jensen's [16] model, Fradsen's [11] model, Ainslie's [1] model, and a Gaussian wake model put forward by Bastankhah [3] are used for wake characterization. Kinematic model utilizes simple algebraic equations that relate freestream velocity, downstream distance, and wake entrainment factor with wake velocity. On the other hand, 2D/3D models are based on Navier–Stokes equations which, however, are time-consuming. Figure 1.6 illustrates different wake models used for wind resource assessment.

Various experimental studies have been carried out that validate wake models in terms of power captured. Primarily, two methods, namely, axial induction control and yaw angle control are implemented in wind industry. In axial induction control method, the pitch angle of upstream turbines is increased in order to increase the wind speed intended for downstream turbines. In yaw-based control, the yaw angle of upstream turbines is varied in order to deflect wake flow away from the rotor of downstream turbines. It is observed that it leads to significant reduction in dynamic loading. From a wind farm operator's perspective, the objective of maximizing power output and minimizing loading effect is of prime importance. This collective method of improving wind farm performance is called as active wake control (AWC) and is summarized in Fig. 1.7.

Mathematically, such an optimization problem may be expressed as

$$\min_{\theta,\gamma} J = \frac{J_{load}(\theta,\gamma)}{J_{pow}(\theta,\gamma)}, \tag{1.8}$$

where $J_{load}(\theta, \gamma)$ and $J_{pow}(\theta, \gamma)$ refer to the individual optimization functions for loading effect and power capture in a wind farm. Optimization based on multiple objectives involves careful limits on the constraints. In order to optimize the loading effect on wind turbines, the lifetime of each equipment is considered. The lifetime (L_t) of a turbine equipment is related inversely with stress (S_t) acting on it. Mathematically, it can be expressed as

$$L_t = \frac{1}{K S_t^M}, \tag{1.9}$$

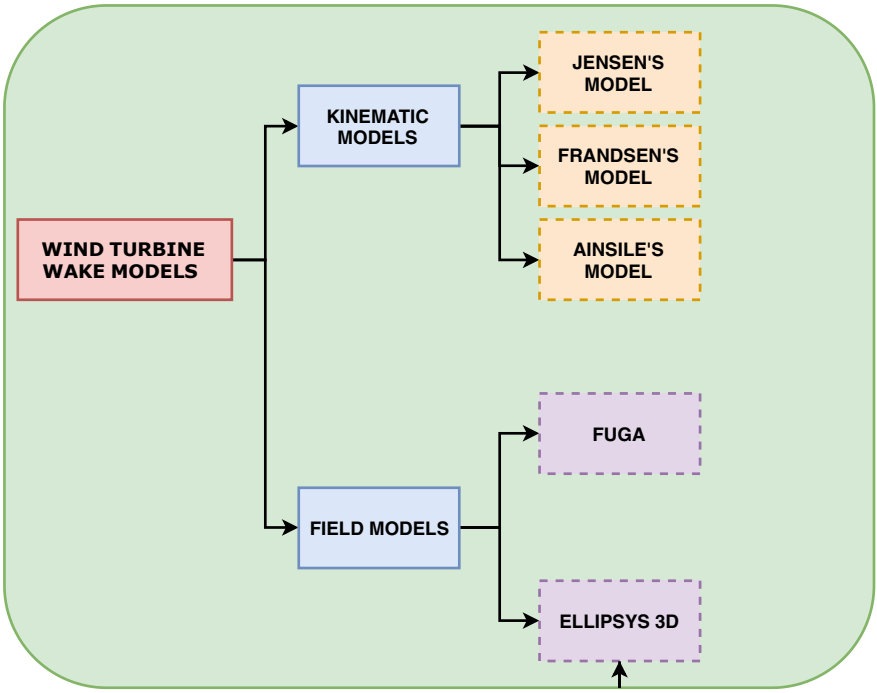

Fig. 1.6 Various wake models for wind turbines

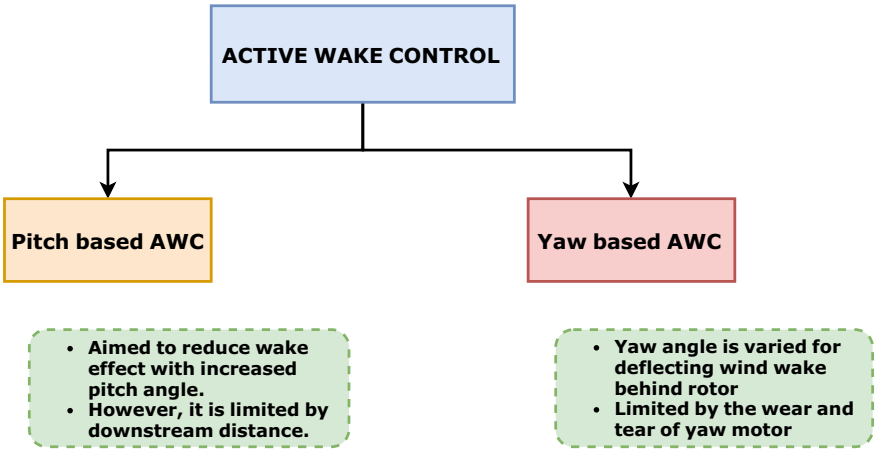

Fig. 1.7 Summary of active wake control in wind farms

where K and M are the constants reflecting material properties. As far as pitch-based active wake control is based, the pitching is carried out only on the leading turbines in a wind farm. The turbines that are not experiencing any wake effect are pitched suitably leading to increased velocity at downstream turbines. Kanev et al. have studied the impact of wake mitigation control strategies for wind farms of different layouts and scales [18]. An active wake control with pitch-based and yaw-based methodology is applied for maximizing power capture in a wind farm. The potential capability is also assessed for lifetime improvement. Results reveal that for pitch-based AWC, only 1–5% of wake losses are recovered due to the limitations posed by downstream distance. Further, Van Dijk et al. have presented a methodology that involves yaw misalignment for power optimization on a 3×3 wind farm [9]. Power increase of 2.8% was seen in the conditions of differential wind loading that also saw a decrement of 8.2 and 12.5% of flapwise and edgewise loading on turbine blade. The problem formulation is based on a constrained minimization which may be expressed as

$$\min_{\gamma} c(\gamma) = -\lambda\Big(\sum_{i=1}^{N} P_i(\gamma)\Big) + \frac{1-\lambda}{2N}\sum_{i=1}^{N}\Big(\Delta\bar{M}_{f,i}(\gamma) + \Delta\bar{M}_{e,i}(\gamma)\Big), \quad (1.10)$$

where γ is the yaw angle, $P_i(\gamma)$ is the power produced by ith turbine, N are the total number of turbines, and $\Delta\bar{M}_{f,i}(\gamma)$, $\Delta\bar{M}_{e,i}(\gamma)$ are the flapwise and edgewise loading on the turbine blade. Lauresen et al. have discussed a model predictive control for minimizing the load on the turbine in a wind farm [20]. The performance of MPC controller is compared with classical PI control. Different scenarios relating the demanded power and produced power are tested that validate the methodology for power maximization while minimizing wake effect simultaneously. Further, in terms of influence of wake on energy production, Nikoli et al. have presented an adaptive neuro-fuzzy inference system based methodology [24]. Experimental analysis is carried out for wind speeds 6, 8, and 10 m/s. Results revealed that ANFIS is a reliable soft computing technique for predicting the power deficit losses as well as wind speed deficit for a wind farm. It is also observed that wind direction has a significant influence on the power deficit ratio and must be considered while carrying out micro-siting.

With the onset of renewable energy systems, the grid integration of wind energy systems has increased drastically. This integration also questioned the reliability and security of power system at large. Due to numerous advantages offered by wind energy systems in form of pollution-free power, the investment has also increased particularly in offshore platform. In case of offshore wind farms, the abundant wind resource has also played a major role in attracting heavy investments in European countries in particular. However, the intermittency, whether in onshore platform or offshore platform, jeopardizes the capacity requirements for reserves power sources, and hence it must be optimized.

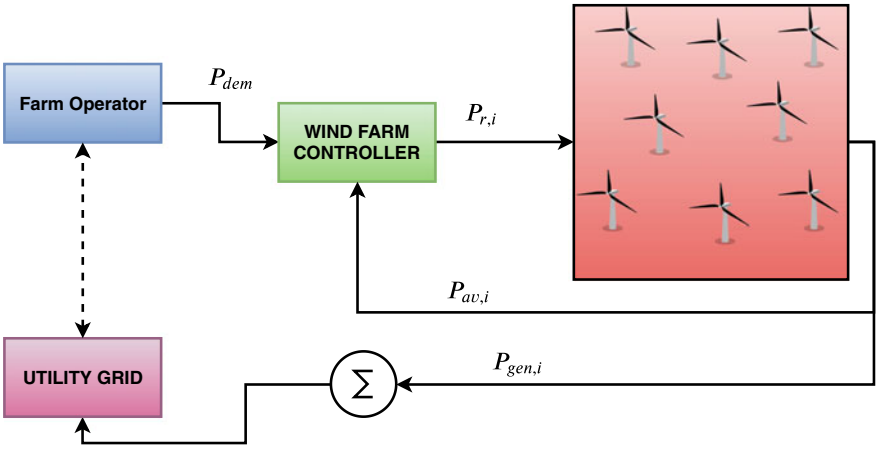

Fig. 1.8 Schematic for wind power controller aimed at reserve power maximization

Since wind is stochastic, generation from wind power plants keeps on varying which calls for the need of reserve power capacity. Wind power plants (WPPs) can have battery energy storage systems as their reserve but are often critiqued due to their high initial investment cost. Since wind resource is abundant and power potential is enormous, WPPs can also serve the purpose of providing ancillary support to modern-day grids. This fast acting support can be in form of frequency regulation. Control of WPPs in conventional terms focuses on power maximization with minimum cost. However, in a study carried out by Siniscalchi-Minna et al., the power reserve is optimized keeping in mind the generation capability of each turbine unit in a wind farm [30]. Frequency support can be provided by WPPs by delivering real power for a long duration in order to thrive frequency to its nominal value. A de-loading mode of operation where each turbine unit operates at around 70–80% of its rated value is implemented. However, this frequency support faces challenges posed by the ever-changing aerodynamic conditions in Prandtl layer, where wind turbines operate. Figure 1.8 illustrates the control methodology adopted for reserve power maximization.

Consider a scenario where the generated wind power P_{gen} is higher than power demand P_{dem}, in such condition(s), the remaining power is termed as reserve power P_{res}. The total available power is sum of wind powers produced by each turbine. In presence of wind wakes, the upstream turbines are forced to produce less wind power in order to maximize the power captured at downstream turbines. This can be done by either yawing or tilting an upstream wind turbine. Siniscalchi-Minna et al. discuss reserve power maximization, a linear programming problem (LPP) is constructed to minimize the difference between demanded power and set-point reference power. Mathematically, this can be expressed as

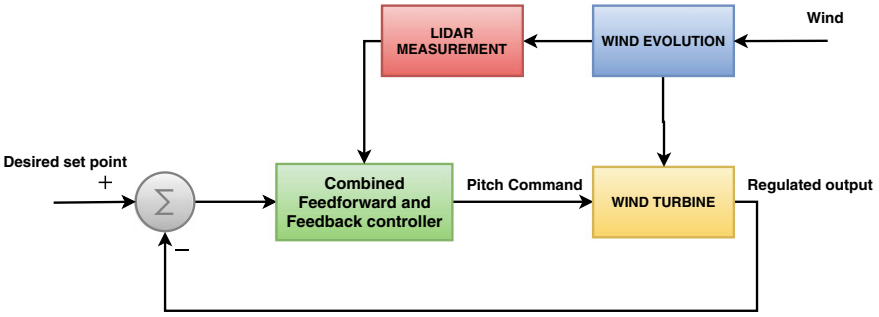

Fig. 1.9 Block diagram showing LIDAR use in wind turbine control

$$\min \quad w^T \varepsilon \tag{1.11}$$

$$\text{subject to} \quad P_{dem} = \sum_{i=1}^{N} P_{r,i}, \tag{1.12}$$

$$|P_{dem} - \sum_{j=1}^{N} P_{r,j}| \leq \varepsilon_i, \tag{1.13}$$

$$P_{min,i} \leq P_{r,i} \leq P_{av,i}, \tag{1.14}$$

where $\varepsilon = [\varepsilon_1, \ldots, \varepsilon_N]^T$ and $w = [w_1, \ldots, w_N]^T$ are the weights and $P_{min,i}$ represents the minimum power contribution from the ith turbine while $P_{r,i}$ is the reference power set point for turbines. In order to validate this methodology, a 12-turbine wind farm layout is considered and three cases are discussed. Results revealed that based on the proposed strategy the downstream turbines were able to contribute to the reserve power need. Further, it is observed that a significant amount of reserve power is optimized for different wind directions, and the authors have stated a possible expansion of the proposed scheme to evaluate the mechanical loads in wind farms.

Control objective for such a dynamic phenomenon involves use of accurate wind measurement devices like LIDAR. In recent years, the use of LIDAR in control of wind turbines as well as wind farms has increased. Wind speed measurements in front of a wind turbine can be used as part of feedforward- or preview-based controllers to help mitigate dynamic structural loads caused by turbulent wind conditions. Various studies have shown that improvements in turbine load performance can be achieved with prior knowledge of incoming wind flow. Figure 1.9 shows the block diagram of LIDAR-based control of wind turbine. LIDAR detects the wind speed ahead in time which helps the controller to act accordingly.

Commercially available LIDAR technologies include continuous wave (CW) LIDAR and pulsed LIDAR. A LIDAR system estimates the wind speed component in radial direction which is analogous to the freestream wind speed v_0 assuming the wind speed component in y- and z-directions is zero. Since LIDAR works on the principle of laser beam transmission, any change in laser direction will lead to directional bias error that contributes to erroneous wind speed measurement. Mathematically, the line-of-sight velocity estimated by LIDAR is given as

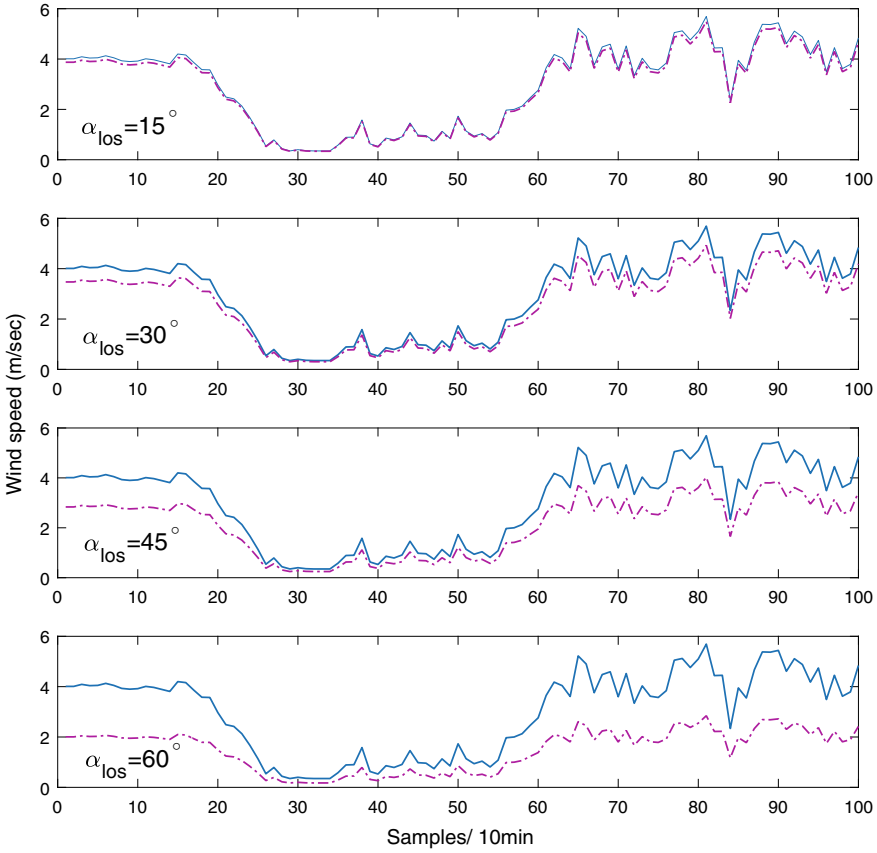

Fig. 1.10 LIDAR estimate of wind speed for different line-of-sight angles. Blue line (solid) represents incoming wind speed and violet (dashed) represents LIDAR estimate

$$v_{los} = \sqrt{v_x^2 + v_y^2 + v_z^2}\cos\alpha_{los}, \tag{1.15}$$

where v_x, v_y, v_z are the wind speed components in x-, y-, z-directions, respectively, and α_{los} is the angle formed between LIDAR beam and incoming wind speed component. Assuming zero directional bias error, the LIDAR estimate $\hat{v}_x$ of wind speed is given as

$$\hat{v}_x = \frac{v_{los}}{\cos\alpha_{los}}. \tag{1.16}$$

Figure 1.10 illustrates the wind speed estimated by LIDAR for different line-of-sight angles. It is observed that for $\alpha_{los} = 15°$, the error in wind speed estimation is minimum and increases significantly upon increasing line-of-sight angle.

LIDAR-based control in wind farm has been in limelight for recent years. Rezaei et al. have discussed an alternative to classical feedforward controller [27]. A LIDAR-

based controller that incorporates preview wind speed measurement is used for generator speed regulation. An uncertain wind speed model is used that is based on LIDAR measurements. Numerical simulations are carried out in presence of uncertainties and results reveal that LIDAR-based control outperforms CART3 controller by 62% in terms of root mean square error for speed regulation. Raach et al. have described a closed-loop wake steering method to simulate the LIDAR information for wind turbines [25]. Wake center for upstream wind turbine is estimated and is controlled for achieving desired yaw angle. The LIDAR data is also used on SOWFA simulator. Howland et al. have carried out a site-specific wake steering control for power maximization [15]. In order to statistically validate the control scheme, Kolmogorov–Smirnov test was performed with null hypothesis stating the power production from baseline controller and experimental analysis from yaw measurements have similar distributions. Results reveal that K–S test is insignificant for wind sector $320^\circ \pm 5$ and is only useful if smaller bins are used for calculating average power. Bossanyi et al. have explored the possibility of combined axial induction control and wake steering control to minimize power losses and fatigue loads on wind turbines in a wind farm [4]. A fast time-domain simulation model captures turbine and wake dynamic effects, so that wind farm controllers can be tested in time-varying conditions for assessing the performance of the combined power and yaw controller.

Predominately, the losses occurring due to wake are characterized by maximum velocity deficit. The spatial location in terms of (x, y, z) coordinates is the position in the wake field that corresponds to maximum power loss and this point is known as the wake center. Wake center tracking is explored by Cacciola et al., where the hub loads at the downstream turbine are used to collect information related to wind speed deficit and horizontal shear [7]. A minimization problem is used to accurately determine wake center using the hub sensors to provide information with good accuracy. The limitation of this method is the usage of Larsen's model that does not encapsulate yaw misalignment. Barthelmie and Pryor have discussed an automated wake characterization algorithm to identify wake center position under different atmospheric conditions of the day [2]. The wake center position is measured using a Doppler LIDAR for a duration of first 6 months of 2017 and scans reveal that this position changes during night time when stable atmospheric conditions prevail during daytime. Further, an important aspect of power maximization is studied by Raach et al., where the authors have used a H_∞ controller to redirect the wake streamflow for yaw angle control [26]. The system identification toolbox is used for identifying various plant models. Finally, closed-loop performance of the controller is tested under different atmospheric conditions.

1.4 Wind Turbine Micro-Siting

Energy yield from fossil fuels is limited with environmental concerns being raised globally. To deal with this, alternative sources of energy like Solar PV, Wind, Tidal, Biomass, Geothermal, and Hydropower are being preferred. The hidden potential in

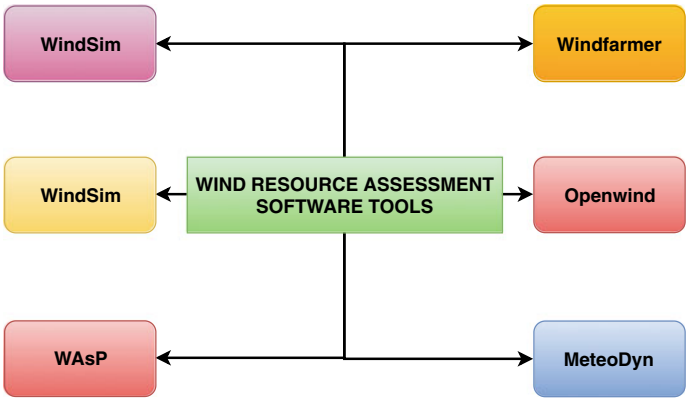

Fig. 1.11 Commonly used wind resource assessment software tools

wind energy is best utilized if installation and commissioning are carried out which are complemented by an accurate wind resource assessment [10]. Thrust factors that affect the energy yield of a wind site include accurate wind speed measurement campaign, local terrain, and accessibility to roadways and orographic conditions. With the advent of LIDAR-based measurement devices, the wind resource assessment (WRA) has significantly improved the annual energy production (AEP) of a wind farm. Often while selecting land for a wind farm project, constraints in form of area, forbidden zones, investment limit, and labor pose challenges for an investor. However, various software packages are available that carry out the wind resource assessment for determining the annual energy yield as illustrated in Fig. 1.11.

The most popular software tool is WAsP, which is based on micro-flow analysis for determining the wind resource for a particular area. However, WAsP is not suitable for carrying out WRA in complex terrain characterized by hilly areas. To tackle this, based on CFD analysis, a latest release of this software is available that calculates the energy yield for complex terrains. On the other hand, WindSim is based on 3D Navier–Stokes equation solver for determining the optimal locations for wind turbines that offer better velocity profile and less turbulence. This tool is essentially used for power maximization. MeteoDyn uses CFD-based simulations to estimate the wind resource under the given area. It uses Katic model for calculating energy yield under wake effect [19]. Windfarmer optimizes a given wind farm layout for maximum return of investment. CFD is used for wake effect and along with that the package also offers studies pertaining to noise and visual impact of turbines in a wind farm. Similarly, Openwind and WindPro are used for optimizing wind farm layout based on Katic model and determine the AEP. It is worthwhile to note that Openwind offers a tool to study the shadow flicker effect in wind turbines that causes tower deflection under high wind speed conditions.

It is observed that apart from the abovementioned thrust factors, the initial investment has had a major role to play while designing a wind farm. While we focus on

onshore wind farms, the electrical infrastructure needed in forms of cables, auxiliary devices, and insulation increases the cost of the overall project. Similarly, with offshore wind farms, the cost incurred to lay out high-voltage DC cables poses a challenge too. Thus, for a proper wind farm design catered to deliver maximum AEP with minimum investment cost, a channelized way of placing wind turbines in a given area must be done. This process of optimal turbine placement is known as micro-siting.

Wind turbine micro-siting is governed by an aerodynamic phenomena called wake effect. The interactions among wind turbines in a wind farm deteriorate the net power capture and losses incurred from this are huge. To minimize the wake interactions, optimization techniques based on a multi-objective perspective of power maximization and cost minimization are chosen. Early works of micro-siting were carried out by Mosseti et al. [23] and Grady et al. [13] which later on became benchmark works for researchers to compare their novel micro-siting techniques. Mosseti et al. have used genetic algorithm to determine optimal wind farm layout for maximizing production capacity. The objective function can be expressed as

$$\min_{N_T} \text{Obj} = \frac{1}{P_{farm}} w_1 + w_2 \frac{cost_{farm}}{P_{farm}}, \tag{1.17}$$

where P_{farm} and $cost_{farm}$ represent the total wind farm power and cost per annum incurred, N_T is the total number of wind turbines in a wind farm, and w_1, w_2 are the weights imposed on objective function. The expressions for P_{farm} and $cost_{farm}$ can be expressed as

$$P_{farm} = T \sum_{i=1}^{N_s} \sum_{j=1}^{N_T} p(s_{ij}) \int_{u_{ci,j}}^{u_{co,j}} P_{WT}(u'_{ij}) p_{ij}(u'_{ij}) du \tag{1.18}$$

$$cost_{farm} = N_T \left(\frac{2}{3} + \frac{1}{3} e^{-0.00174 N_T^2} \right), \tag{1.19}$$

where T is the number of hours in a year, N_s are number of sectors of wind rose, $u_{ci,j}$ and $u_{co,j}$ are the cut-in and cut-off wind speed, and $p(s_{ij})$ is the probability of occurrence of wind in ith direction at the jth turbine. Further, Grady et al. have implemented genetic algorithm for arriving at the optimal wind farm layout but have used a simplistic objective function of form

$$\min \text{obj} = \frac{cost_{farm}}{P_{farm}}. \tag{1.20}$$

Although the efficiency reported by Mosetti et al. is higher than Grady et al., genetic algorithm can be used for optimizing layout of wind farms successfully. Mosetti et al. do not consider enough generations for achieving targeted convergence. MirHassani et al. have considered the effect of uncertain wind conditions on optimal

wind farm layout [21]. A mixed integer linear programming (MILP) technique is used and turbines with different hub heights are considered. Results reveal that compared to Chen et al. [8], the increment in power production is approximately 3.1%.

1.5 Hybrid Wind Farms: Paradigms and Challenges

Modern-day electricity grids operate on the concept of hybrid interconnection where multiple power sources contribute their power to the point of common coupling. With renewable energy sources (RES) becoming more popular day by day, wind and solar technologies have been installed in large quantities to meet energy demands of remote and rural areas. The essence of a hybrid renewable energy system relies on the load demand which is stochastic in its nature. Consider a hybrid system comprised of wind, solar, and battery sources. When the load demand is less, excess of power from wind and solar is used to charge the battery system without violating battery state of charge limits. In case when load demand is more than combined generation of wind and solar, the power stored in battery is used to compensate the deficit power.

Hybrid renewable energy systems typically consist of battery backup in order to cater events of deficit power. In the present context, the concept of hybrid wind farms in particular is focused on multi-wind farms that interact with each other in the events of power deficit or excess. The decision-making and control of such hybrid wind farms equipped with BESS is a challenging task. Hybrid wind farms deal with wind resource which is variable and in need of accurate forecast techniques. An accurate wind forecasting technique ensures power reliability to the grid and lessens the BESS duty. For a wind farm operator, the main objective is to maximize power output from the wind farm and minimize the mechanical loads acting in turbulent conditions. The decision-making techniques evaluated in this book are based on a series of alternatives that aim to minimize the penalty incurred to a wind farm operator. A multi wind farm topology is selected where the decision is to be made for choosing the best strategy for hybrid operation of wind farm. Figure 1.12 illustrates a schematic of hybrid renewable energy system feeding AC loads.

Control aspects for a hybrid wind farm are based on pitch and yaw angle based methods where the controller aims to maximize the power output from a wind farm. In the present context, a hybrid wind farm is considered with an objective to manage the wake effects. Control-oriented techniques based on precise wind speed measurements have carried out three different types of wind farm layouts. Adaptive PI control and classical PI control methods are adopted and LIDAR simulations are used to track the wake flow behind the upstream turbine in a wind farm. The potential power maximization capability of wind farms is evaluated based on yaw correction achieved by controller. Further, for BESS the operating cost incurred along with their lifetime is analyzed under different wake scenarios.

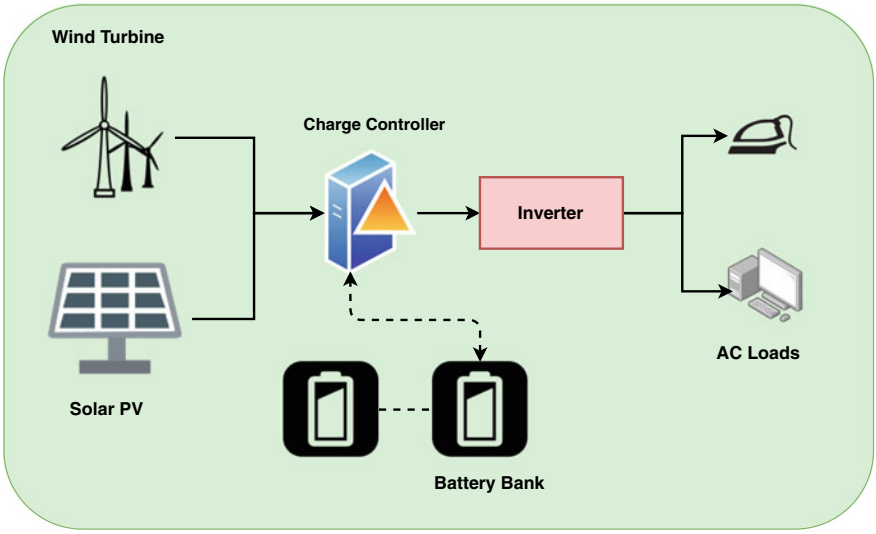

Fig. 1.12 Hybrid renewable energy system

References

1. Ainslie J (1988) Calculating the flowfield in the wake of wind turbines. J Wind Eng Ind Aerodyn 27(1–3):213–224
2. Barthelmie RJ, Pryor SC (2019) Automated wind turbine wake characterization in complex terrain. Atmos Meas Tech Discuss, 1–31
3. Bastankhah M, Porté-Agel F (2014) A new analytical model for wind-turbine wakes. Renew Energy 70:116–123
4. Bossanyi E (2018) Combining induction control and wake steering for wind farm energy and fatigue loads optimisation. J Phys: Conf Ser 1037:032011
5. Bossanyi EA (2000) The design of closed loop controllers for wind turbines. Wind Energy 3(3):149–163
6. Bossanyi EA (2003) Individual blade pitch control for load reduction. Wind Energy 6(2):119–128. https://doi.org/10.1002/we.76
7. Cacciola S, Bertelè M, Schreiber J, Bottasso C (2016) Wake center position tracking using downstream wind turbine hub loads. J Phys: Conf Ser 753:032036
8. Chen Y, Li H, Jin K, Song Q (2013) Wind farm layout optimization using genetic algorithm with different hub height wind turbines. Energy Convers Manag 70:56–65
9. van Dijk MT, van Wingerden JW, Ashuri T, Li Y (2017) Wind farm multi-objective wake redirection for optimizing power production and loads. Energy 121:561–569
10. Durak M, Şen Z (2002) Wind power potential in turkey and akhisar case study. Renew Energy 25(3):463–472
11. Frandsen S, Barthelmie R, Pryor S, Rathmann O, Larsen S, Højstrup J, Thøgersen M (2006) Analytical modelling of wind speed deficit in large offshore wind farms. Wind Energy 9(1–2):39–53
12. Frost SA, Balas MJ, Wright AD (2009) Direct adaptive control of a utility-scale wind turbine for speed regulation. Int J Robust Nonlinear Control 19(1):59–71
13. Grady S, Hussaini M, Abdullah M (2005) Placement of wind turbines using genetic algorithms. Renew Energy 30(2):259–270

14. Hippe P (2006) Windup in control. Springer, Berlin
15. Howland MF, Lele SK, Dabiri JO (2019) Wind farm power optimization through wake steering. Proc Natl Acad Sci 116(29):14495–14500
16. Jensen N (1983) A note on wind generator interaction
17. Johnson KE, Pao LY, Balas MJ, Fingersh LJ (2006) Control of variable-speed wind turbines: standard and adaptive techniques for maximizing energy capture. IEEE Control Syst 26(3):70–81
18. Kanev S, Savenije F, Engels W (2018) Active wake control: an approach to optimize the lifetime operation of wind farms. Wind Energy 21(7):488–501
19. Katic I, Højstrup J, Jensen N (1987) A simple model for cluster efficiency, A. Raguzzi, pp 407–410
20. Laursen TK, Sivabalan S, Borchersen AB, Larsen JA (2014) Wake-effect minimising optimal control of wind farms, with load reduction. IFAC Proc Vol 47(3):6770–6775
21. MirHassani S, Yarahmadi A (2017) Wind farm layout optimization under uncertainty. Renew Energy 107:288–297
22. Moradi H, Vossoughi G (2015) Robust control of the variable speed wind turbines in the presence of uncertainties: a comparison between H_∞ and PID controllers. Energy 90:1508–1521
23. Mosetti G, Poloni C, Diviacco B (1994) Optimization of wind turbine positioning in large windfarms by means of a genetic algorithm. J Wind Eng Ind Aerodyn 51(1):105–116
24. Nikolić V, Shamshirband S, Petković D, Mohammadi K, Ćojbašić Ž, Altameem TA, Gani A (2015) Wind wake influence estimation on energy production of wind farm by adaptive neuro-fuzzy methodology. Energy 80:361–372
25. Raach S, Schlipf D, Cheng PW (2016) Lidar-based wake tracking for closed-loop wind farm control. J Phys: Conf Ser 753:052009
26. Raach S, van Wingerden JW, Boersma S, Schlipf D, Cheng PW (2017) $\mathscr{H}_\infty$ controller design for closed-loop wake redirection. In: 2017 American control conference (ACC). IEEE
27. Rezaei V (2014) LIDAR-based robust wind-scheduled control of wind turbines. In: 2014 American control conference. IEEE
28. Schlipf D, Schlipf DJ, Kühn M (2012) Nonlinear model predictive control of wind turbines using LIDAR. Wind Energy 16(7):1107–1129
29. Selvam K, Kanev S, van Wingerden JW, van Engelen T, Verhaegen M (2009) Feedback-feedforward individual pitch control for wind turbine load reduction. Int J Robust Nonlinear Control 19(1):72–91
30. Siniscalchi-Minna S, Bianchi FD, De-Prada-Gil M, Ocampo-Martinez C (2019) A wind farm control strategy for power reserve maximization. Renew Energy 131:37–44

Chapter 2
Multi-criteria Decision-Making: An Overview

Decision-making on day-to-day basis is a common human practice that essentially requires one to choose a best alternative among many. Modern-day decision-making has evolved over the years with early developments dealing with multi-objective optimization approach in the field of operations research. The inception of decision-making is explained lucidly by Benjamin Franklin based on his work on moral algebra. He gives an example of his stand on an important issue where he writes arguments that support his views and arguments that do not. Based on his own understanding, he crosses out the arguments that hold equal importance. Once he reaches a stage where all the arguments on one side are crossed out, he chose the side with leftover arguments. This anecdote describes the importance of weights in decision-making process. Since 1950s, Multi-criteria decision-making (MCDM) has been practiced actively by theoretical and applied scientists to test the potential capability of mathematical modeling of decision-making problem.

Figure 2.1 illustrates the thrust applications of MCDM.

Similar to MCDM, multi-objective optimization approach that models an optimization problem with multiple objectives is also deployed for solving real-time scenarios. Such scenarios are often governed by constraints that reflect the economies of scale. In the field of finance and economics, MCDM is widely used to make decisions related to investments where apart from financial variables, intangible variables like social, cultural, and political effects are also to be considered [6]. Hallerbach et al. discussed the relevance of MCDM methods in finance sector where the firm management's aim is to maximize the profits incurred by investment from various shareholders [8]. Usually, a firm has more than one shareholder deciding the main objective. With a common objective of wealth maximization considering constraints, the opportunity provided by MCDM methods in finance sector is tremendous.

H. S. Dhiman and D. Deb, *Decision and Control in Hybrid Wind Farms*,
Studies in Systems, Decision and Control 253,
https://doi.org/10.1007/978-981-15-0275-0_2

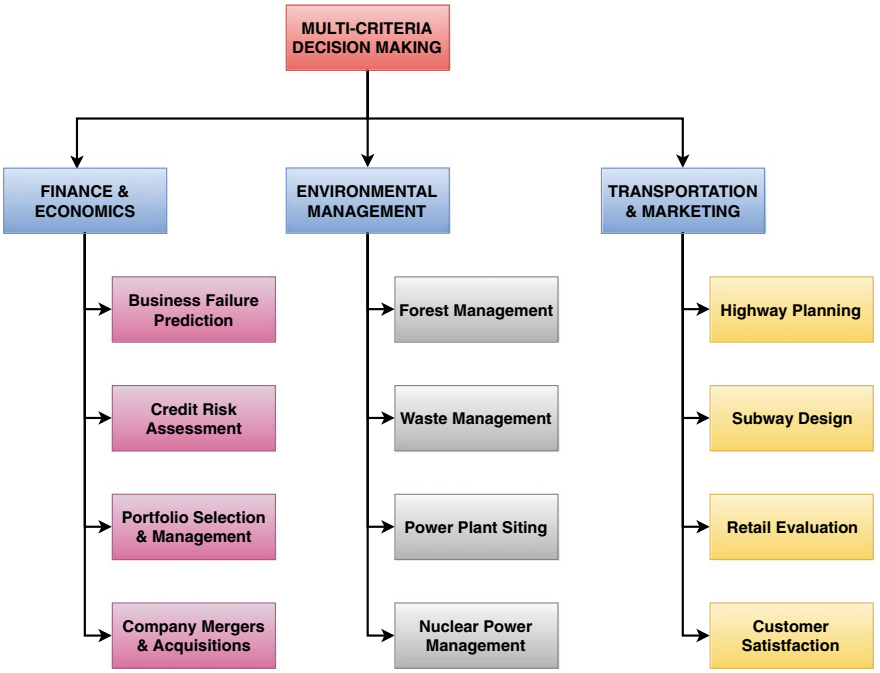

Fig. 2.1 Applications of multi-criteria decision-making

2.1 Terminologies Related to MCDM

Given a multi-criteria decision-making process, several terminologies are used that describe the path to the decision. An MCDM approach is commonly used in the field of supplier selection, renewable energy sector, selecting type of manufacturing material. Following are the terminologies used in an MCDM process:

- Alternative: An alternative can be described as a "choice" that a decision-maker has to make in order to arrive at the best plan of action that eventually supports the designed framework. Alternatives can be of tangible and intangible form. For example, for a supplier selection problem, alternatives can be a list of suppliers with varied nature of material/product under investigation.
- Decision criteria or attributes: Criteria refer to an entity tangible or intangible that directly influences the result of the decision-making process. In an MCDM problem, there may be multiple criteria, each highlighting its importance in terms of weights.
- Criteria weight: It refers to a quantitative numeric value assigned to each criterion for aiding the decision-making process and streamlining beneficial and non-beneficial criteria.

2.2 MCDM: Materials and Methods

The MCDM approach helps the decision-makers in the identification of the best alternative from an array of plausible criteria. An $m \times n$ matrix is identified with matrix element, say h_{ij} such that

$$H = \begin{matrix} \\ A_1 \\ A_2 \\ \vdots \\ A_m \end{matrix} \begin{matrix} \begin{matrix} C_1 & C_2 & \dots & C_n \end{matrix} \\ \begin{pmatrix} h_{11} & h_{12} & \dots & h_{1j} \\ h_{21} & h_{22} & \dots & h_{2j} \\ \vdots & \vdots & & \vdots \\ h_{i1} & \dots & \dots & h_{ij} \end{pmatrix} \end{matrix}$$

describes a performance score representing a semantic relationship between the alternative $i = 1, 2, \dots, m$ w.r.t the criteria $j = 1, 2, \dots, n$.

Figure 2.2 illustrates a generic flowchart to approach a given MCDM problem.

We now discuss the decision-making problem through six methods: (i) simple additive weighting (SAW), (ii) technique for order of preference by similarity to ideal solution (TOPSIS), (iii) complex proportional assessment (COPRAS), (iv) analytic hierarchical process, (v) ELECTRE, and (vi) PROMETHEE methods as illustrated in Fig. 2.3.

2.2.1 Simple Additive Weighting (SAW) Method

Hwang et al. in 1981 presented this method by assigning each performance score of alternative A_i with a specific weight w_i, to obtain a weighted sum of all the criteria for an alternative [9]. The steps involved are enumerated through this flowchart (Fig. 2.4).

The step-by-step procedure is described as follows:

- Step 1: Identify the alternatives $(A_1, A_2, \dots, A_m)$ and criteria $(C_1, C_2, \dots, C_n)$.
- Step 2: Develop a normalized decision matrix:

$$\hat{H}_{ij} = \frac{\min h_{ij}}{h_{ij}} \quad i = 1, 2, \dots, m; \;\; j = 1, 2, \dots, n, \tag{2.1}$$

$$\hat{H}_{ij} = \frac{h_{ij}}{\max h_{ij}} \quad i = 1, 2, \dots, m; \;\; j = 1, 2, \dots, n, \tag{2.2}$$

where (2.1) is used for non-beneficial criteria, and (2.2) for beneficial criteria.

- Step 3: For each criterion, find entropy e_j and divergence values d_j:

$$e_j = -\frac{1}{\log m} \sum_{i=1}^{m} \hat{H}_{ij} \log(\hat{H}_{ij}), \quad d_j = |1 - e_j|, \quad j = 1, 2, \dots, n. \tag{2.3}$$

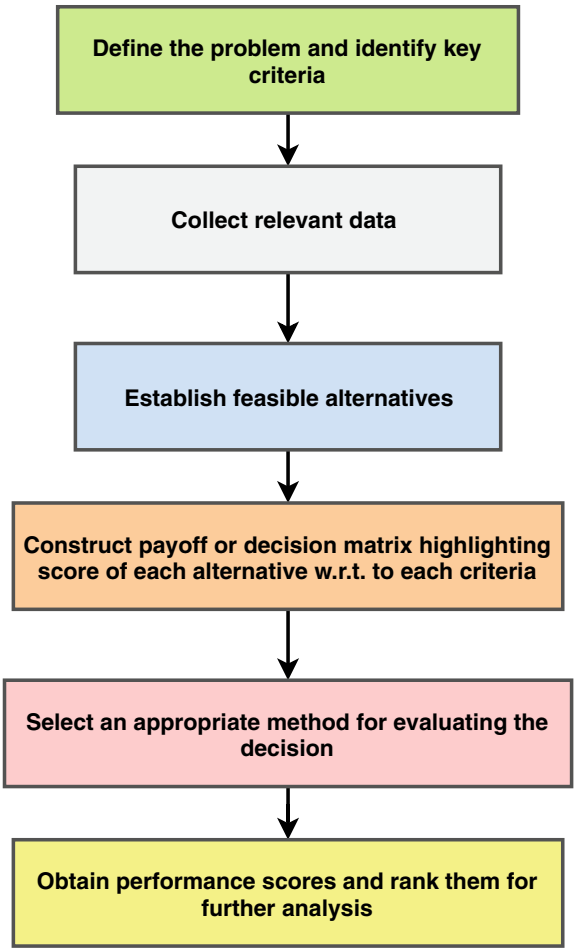

Fig. 2.2 Generic flowchart for multi-criteria decision-making

- Step 4: Determine the weights for the respective criterion:

$$w_j = \frac{d_j}{\sum_{j=1}^{n} d_j}. \tag{2.4}$$

- Step 5: Finally, calculate the priority score for each alternative and arrange according to highest priority:

$$S_i = \sum_{j=1}^{n} w_j h_{ij}. \tag{2.5}$$

In order to demonstrate the SAW method, we consider an example of car selection based on qualitative criteria given quantitative weights. Consider five automobiles, namely, Jeep Compass, MG Hector, Kia Seltos, Tata Harrier, and Hyundai Creta.

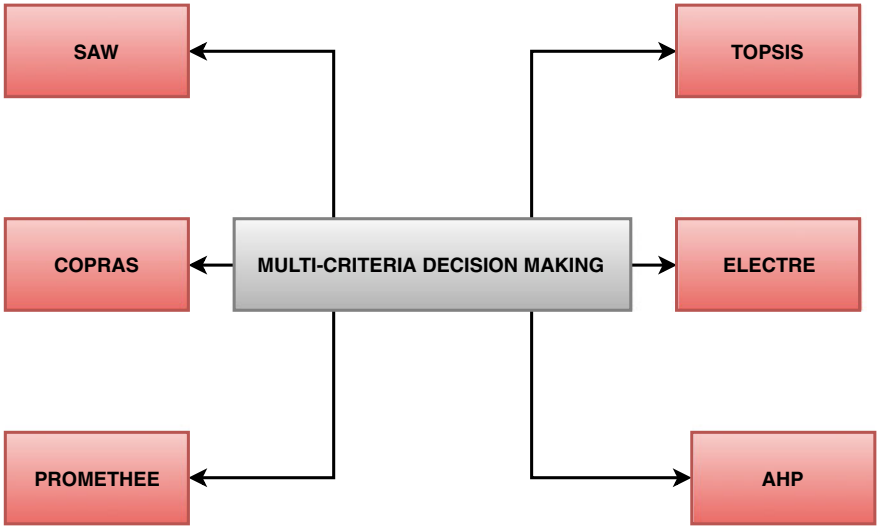

Fig. 2.3 Commonly used multi-criteria decision-making techniques

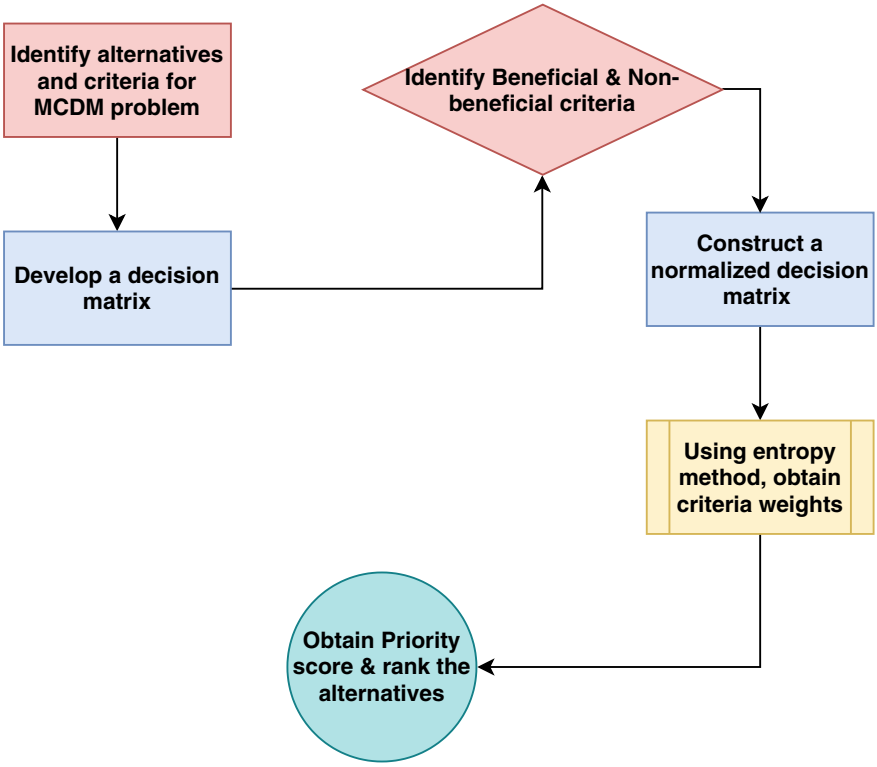

Fig. 2.4 Flowchart for simple additive weighting

These automobiles are evaluated on criteria like style, lifespan, fuel economy, and cost. Out of these, cost criterion is a non-beneficial criterion. Based on a survey carried out by an automobile expert, a decision matrix H_{ij} is constructed which is given as

$$H = \begin{array}{c} \begin{matrix} \text{Style} & \text{Lifespan} & \text{Fuel economy} & \text{Cost} \end{matrix} \\ \begin{pmatrix} 7 & 5 & 5 & 4 \\ 9.5 & 8 & 6 & 6 \\ 10 & 7 & 6 & 6 \\ 9 & 7.5 & 6 & 7 \\ 5 & 7 & 6.5 & 4 \end{pmatrix} \end{array} \begin{matrix} \text{Jeep Compass} \\ \text{MG Hector} \\ \text{Kia Seltos} \\ \text{Tata Harrier} \\ \text{Hyundai Creta.} \end{matrix}$$

Further, based on (2.1) and (2.2), a normalized decision matrix is obtained as

$$\hat{H} = \begin{pmatrix} 0.7000 & 0.6250 & 0.7692 & 0.5714 \\ 0.9500 & 1.0000 & 0.9231 & 0.8571 \\ 1.0000 & 0.8750 & 0.9231 & 0.8571 \\ 0.9000 & 0.9375 & 0.9231 & 1.0000 \\ 0.5000 & 0.8750 & 1.0000 & 0.5714 \end{pmatrix}.$$

Next, we determine the criteria weights using entropy method as described by (2.3)–(2.4) and are given as $w = \{0.2299, 0.2700, 0.3135, 0.1865\}$. The performance scores are determined using (2.5) and are depicted in Table 2.1.

The most preferred automobile is MG Hector followed by Tata Harrier, Kia Seltos, Hyundai Creta, and Jeep Compass. It is therefore possible to explore a potential choice based on a mathematical model.

2.2.2 *Technique for Order of Preference by Similarity to Ideal Solution*

The technique for order of preference by similarity to ideal solution (TOPSIS) ascertains the ideal choice by determining the shortest Euclidean distance to the positive ideal solution and the longest distance to the negative ideal solution [5].

Table 2.1 Performance scores based on SAW method

Alternative	Performance score	Ranking
Jeep Compass	0.6775	5
MG Hector	0.9377	1
Kia Seltos	0.9155	3
Tata Harrier	0.9360	2
Hyundai Creta	0.7714	4

Lourenzutti et al. have identified a method to incorporate the factors considered by multiple decision-makers, and the same has been tested for three different cases [11]. Yang et al. discussed TOPSIS and Shanon entropy methods for flood vulnerability assessment for a Hainan province in China [14]. Various flood vulnerability indicators are assessed by TOPSIS method, and the nonhomogeneous nature in the indicators is handled by Shanon entropy method. The values of the vulnerability index are calculated by using a hydrodynamic model. In terms of dam site selection, Balioti et al. presented a method based on AHP to find the criteria weights and TOPSIS as a method to find the best site in Greece [1]. A total of five designs for spillways are assessed considering nine criteria. Figure 2.5 illustrates a flowchart highlighting the steps followed for TOPSIS method.

The following steps are used for priority score determination:

- Follow Steps 1–2 as in the case of the SAW method.
- Construct a normalized decision matrix with its elements as

$$\hat{H}_{ij} = \frac{h_{ij}}{\sqrt{\sum_{j=1}^{n} h_{ij}^2}} \quad i = 1, \ldots, m; \; j = 1, \ldots, n. \tag{2.6}$$

- Construct a weighted normalized matrix using the weights for each criterion:

$$\hat{h} = w_j H_{ij} \quad i = 1, \ldots, m; \; j = 1, \ldots, n. \tag{2.7}$$

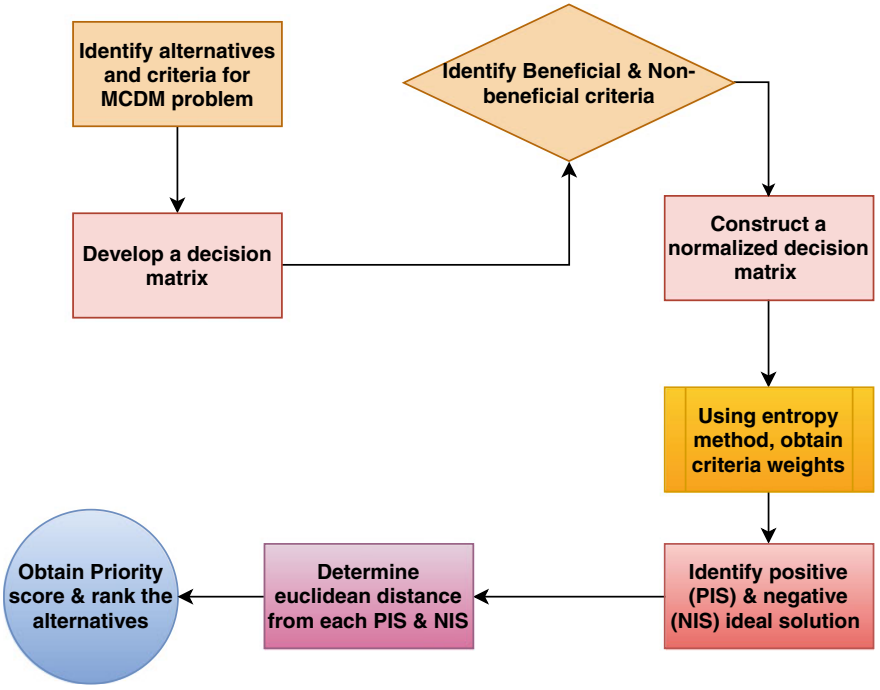

Fig. 2.5 Flowchart for TOPSIS method

- Identify positive and negative ideal solutions S^+ and S^-, respectively, as

$$S_j^+ = \{(\max h_{ij} | j \in t); (\min h_{ij} | j \in n-t) | i = 1, 2, \ldots, m\}, \tag{2.8}$$

$$S_j^- = \{(\min h_{ij} | j \in t); (\max h_{ij} | j \in n-t) | i = 1, 2, \ldots, m\}, \tag{2.9}$$

  where t and $n-t$ represent the number of beneficial and non-beneficial criteria, respectively.
- Evaluate relative closeness of each alternative from the p-norm Euclidean distances D_i^+ and D_i^-, and rank in descending order:

$$G_i = \frac{D_i^-}{D_i^- + D_i^+} \quad i = 1, \ldots, m; \; 0 \leq G_i \leq 1, \tag{2.10}$$

$$D_i^+ = \left\{ \sum_{j=1}^{n} \left(\hat{h}_{ij} - S_j^+ \right)^p \right\}^{1/p}, \; D_i^- = \left\{ \sum_{j=1}^{n} \left(\hat{h}_{ij} - S_j^- \right)^p \right\}^{1/p}, j = 1, \ldots, n. \tag{2.11}$$

TOPSIS method is tested for the same example as done for the SAW method. The normalized decision matrix based on (2.6) is given as

$$\hat{H} = \begin{pmatrix} 0.3767 & 0.3206 & 0.3777 & 0.3234 \\ 0.5113 & 0.5129 & 0.4532 & 0.4851 \\ 0.5382 & 0.4488 & 0.4532 & 0.4851 \\ 0.4844 & 0.4809 & 0.4532 & 0.5659 \\ 0.2691 & 0.4488 & 0.4910 & 0.3234 \end{pmatrix}. \tag{2.12}$$

After calculating the normalized decision matrix, the criteria weights are calculated that highlight their relative importance over another. Based on entropy method used in SAW method, the weights are given as

$$w = \{0.2186, 0.2654, 0.2885, 0.2275\}. \tag{2.13}$$

Next, we evaluate the positive and negative ideal solutions. A positive ideal solution (PIS) supports a particular alternative while the negative ideal solution (NIS) provides an insight into the worst possible one. Using (2.8), (2.9), the PIS and NIS are

$$S^+ = \{0.1177, 0.1361, 0.1416, 0.0736\}, \; S^- = \{0.0588, 0.0851, 0.1090, 0.1287\}.$$

We find the distances D^+, D^- based on (2.11), and since it is a p-norm distance, only positive integer values are to be set. The distances are given as

$$D^+ = \{0.0025, 0.0008, 0.0009, 0.0017, 0.0019\},$$
$$D^- = \{0.0018, 0.0031, 0.0027, 0.0023, 0.0026\}.$$

Table 2.2 Performance scores based on TOPSIS method for car selection problem

Alternative	Performance score	Ranking
Jeep Compass	0.4223	5
MG Hector	0.8051	1
Kia Seltos	0.7552	2
Tata Harrier	0.5716	4
Hyundai Creta	0.5842	3

Finally, we calculate the priority or performance scores for each alternative using (2.10). The priority scores indicate the best choice and worst choice which are purely based on the element values of decision matrix chosen by decision-maker. The priority scores are enlisted below (Table 2.2).

From TOPSIS and SAW method analysis, we observe that Jeep Compass still remains the least preferred choice for automobile given the adopted criteria used.

2.2.3 Complex Proportional Assessment (COPRAS) Method

The complex proportional assessment (COPRAS) method involves a stepwise ranking process to ascertain the performance of each alternative while taking into account different conflicting situations. Zolfani et al. implemented COPRAS and AHP to solve the quality control manager selection problem with knowledge, experience, and educational background as key factors [15]. Bhowmik et al. discussed the problem of selecting an appropriate green energy source for Tripura, India based on the entropy-based COPRAS method [3]. Possible alternatives like solar, hydro, biogas, and biomass are chosen along with a set of beneficial and non-beneficial criteria. Following are the steps for COPRAS method:

- Decision matrix is constructed either based on a survey or a questionnaire.
- Work out the normalized decision matrix and establish the weights based on entropy method as discussed for TOPSIS method.
- Determine weighted normalized matrix $\hat{H}_{ij}$ using (2.6).
- Determine the aggregated weighted scores for beneficial and non-beneficial criteria:

$$R_i^+ = \sum_{j=1}^{q} \hat{h}_{ij}, \; R_i^- = \sum_{j=q+1}^{n} \hat{h}_{ij} \;\; | \; i = 1, 2, \ldots, m, \tag{2.14}$$

where q represents the number of beneficial criteria, and $n - q$ represents the number of non-beneficial criteria.

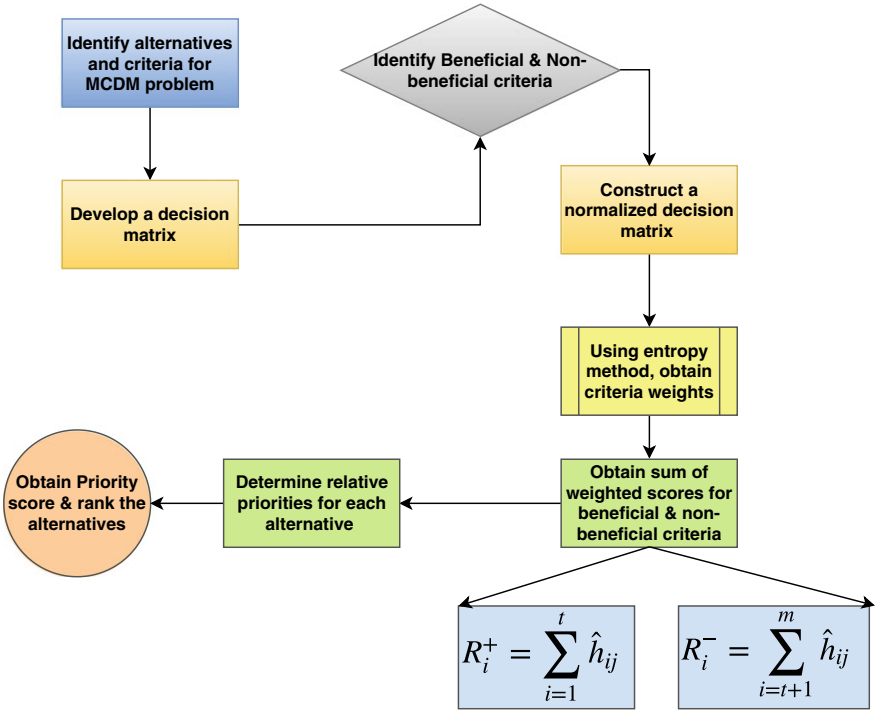

Fig. 2.6 Flowchart for COPRAS method

- Determine relative priorities for each alternative as

$$U_i = R_i^+ + \frac{\sum_{i=1}^{m} R_i^+}{R_i^- \sum_{i=1}^{m} \frac{1}{R_i^-}}. \tag{2.15}$$

- Find the final priority score for each alternative, arranged in descending order:

$$L_i = \frac{U_i}{U_{max}} \times 100\%. \tag{2.16}$$

The steps involved in this method can be enumerated through this flowchart (Fig. 2.6).

As an example, we now solve the MCDM problem discussed for SAW and TOPSIS method and see how the performance results unfold based on COPRAS method. The decision matrix remains the same as well as the normalized decision matrix along with the criteria weights as obtained in the TOPSIS method. The sum of weighted scores for beneficial and non-beneficial criteria is evaluated using (2.14) and is given as follows:

Table 2.3 Performance scores based on COPRAS method

Alternative	Performance score	Ranking
Jeep Compass	0.8708	5
MG Hector	1.000	1
Kia Seltos	0.9760	2
Tata Harrier	0.9428	4
Hyundai Creta	0.9640	3

$$R^{+} = \{0.2764, 0.3787, 0.3675, 0.3643, 0.3196\}, \tag{2.17}$$

$$R^{-} = \{0.0736, 0.1103, 0.1103, 0.1287, 0.0736\}. \tag{2.18}$$

The relative priorities of the alternatives are evaluated using (2.15) and (2.16) and the priority scores are listed in Table 2.3.

Thus, results reveal that as per COPRAS method, MG Hector is the most preferred automobile followed by Kia Seltos, Hyundai Creta, Tata Harrier, and Jeep Compass is the worst possible choice.

2.3 The Analytic Hierarchy Process

Analytic hierarchy process (AHP) was coined by Saaty that is based on decomposing a given MCDM problem into a system of hierarchies [12]. A matrix representing relative importance of the alternatives with respect to each criterion is built. AHP provides a key framework based on designing a decision matrix which highlights the hierarchies depicting environmental scenarios, objectives pertaining to corporate decisions and medical strategies. AHP has been successfully applied to domains like prioritization, resource allocation, and decision-making, and is described as follows:

- Define the decision-making problem and identify key criteria.
- Based on the criteria, set of alternatives, and decision goal, structure the hierarchy of the problem.
- Construct pairwise comparison matrices where the elements of the matrices higher in the priority are compared with those of lower priority.
- Based on the priorities obtained, weigh up the priorities in lower level and repeat this step for every element. Add these priorities to obtain final priorities for the lowest level.

In order to assign relative importance among different criteria quantitatively, the following scales are used in the AHP method as shown in Table 2.4.

Consider an MCDM problem with three alternatives and four criteria. The decision matrix is given by

Table 2.4 Relative importance for AHP method

Scale	Importance
1	Equal importance
3	Moderate importance
5	Strong importance
7	Very strong importance
9	Absolute importance
2, 4, 6, 8	Compromise between 1, 3, 5, 7, 9

Table 2.5 Performance scores based on AHP

Alternatives	Score	Ranking
A_1	0.34	2
A_2	0.35	1
A_3	0.31	3

$$H = \begin{matrix} \\ A_1 \\ A_2 \\ A_3. \end{matrix} \begin{matrix} \begin{matrix} C_1 & C_2 & C_3 & C_4 \end{matrix} \\ \begin{pmatrix} 25 & 20 & 15 & 30 \\ 10 & 30 & 20 & 30 \\ 30 & 10 & 30 & 10 \end{pmatrix} \end{matrix}$$

Consider the weights of the criteria as $w = \{0.2, 0.15, 0.40, 0.25\}$. Next we evaluate $K_j = \sum_{i=1}^{m} h_{ij}$ and divide the respective elements with K_j where $j = 1, 2, \ldots, n$ and a_{ij} are the elements of the matrix. The relative matrix is given as

$$H^* = \begin{matrix} \\ A_1 \\ A_2 \\ A_3. \end{matrix} \begin{matrix} \begin{matrix} C_1 & C_2 & C_3 & C_4 \end{matrix} \\ \begin{pmatrix} 25/65 & 20/55 & 15/65 & 30/65 \\ 10/65 & 30/55 & 20/65 & 30/65 \\ 30/65 & 10/55 & 30/65 & 10/65 \end{pmatrix} \end{matrix}$$

Next, we evaluate the performance score of the alternatives given as

$$B_i = \sum_{j=1}^{n} w_j \hat{h}_{ij}, \quad i = 1, 2, \ldots, m, \tag{2.19}$$

where w_j is the weight assigned to each criterion and $\hat{h}_{ij}$ represents the elements of the H^* matrix. The performance scores are listed in Table 2.5.

Based on the performance scores, the alternatives are ranked as $A_2 \succ A_1 \succ A_3$. AHP is a simplistic method that involves careful study of the alternatives as it considers their pairwise comparison. The common areas where AHP is applied include corporate planning, public policy, and strategic planning.

2.4 ELECTRE Method

Another method used in MCDM approach was ELECTRE method, which stands for *elimination and choice translating reality*, and was first put into use in 1966 [7]. In this approach, the alternatives are compared with each other in a pairwise manner for given criteria. A pairwise comparison between alternatives h and k may be based on a monetary value or a physical entity given as $r(h)$ and $r(k)$. Sometimes a decision-maker may come up with a threshold value like average of $r(h)$ and $r(k)$ or arithmetic difference between them. ELECTRE method comprises two parts, that is, outranking the alternatives and an exploitation procedure to ascertain the decision.

In terms of outranking procedure, a degree of concordance is obtained between two alternatives h and k. Consider a relation hSk which implies preference of h over k provided the majority criteria are consistent with it. If the concordance condition holds, none of the criteria that support hSk should oppose it. Concordance index $C(hSk)$ is determined using

$$C(hSk) = \frac{\sum_{j \in l'} w_j}{\sum_{j \in l} w_j}, \tag{2.20}$$

where l' is the set of criteria satisfying the concordant condition and l is the set of all criteria. Concordance condition $C(hSk) > C^*$ must be satisfied in order to

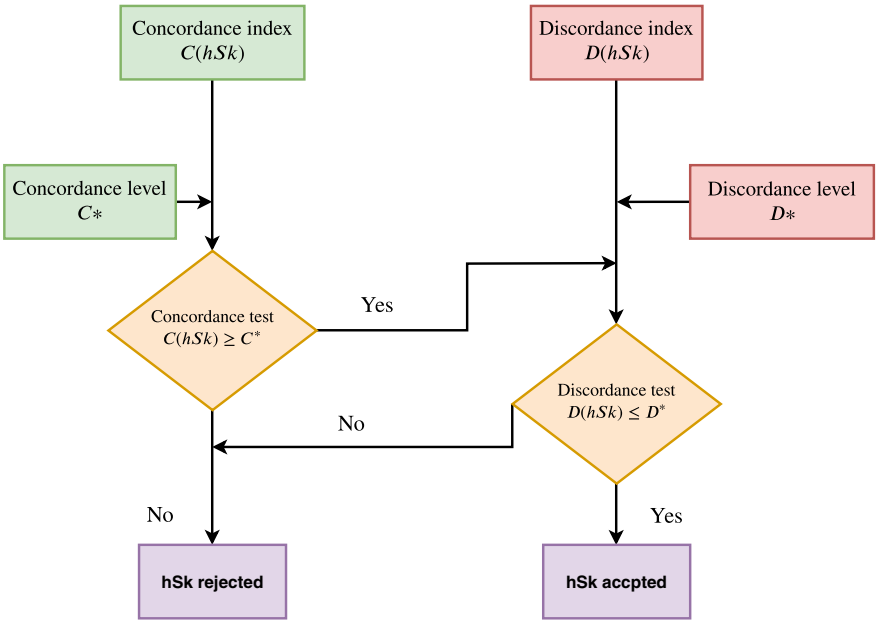

Fig. 2.7 Flowchart for ELECTRE method

proceed further for discordance test. C^* refers to the concordance level. Discordance index determines the possibility of a disagreement between preference of h over k as asserted by concordance test. The discordance index is given by

$$D(hSk) = \max_{j:r_{hj}<r_{kj}} \frac{\{r_{kj} - r_{hj}\}}{d_{max}}, \tag{2.21}$$

where d_{max} represents the maximum difference between performance alternatives. For a given discordance level $D^* \geq D(hSk)$, the preference of h over k is rejected. This procedure is performed for every pair (h, k) to arrive at the best alternative.

Figure 2.7 illustrates the flowchart for ELECTRE method.

2.5 Preference Ranking Organization Method of Enrichment Evaluation (PROMETHEE)

Consider a multi-criteria problem as a set of alternatives

$$\max \ \{c_1(a), c_2(a), \ldots, c_n(a), \ |a \in A\}, \tag{2.22}$$

where A represents a finite set of alternatives $\{a_1, \ldots, a_m\}$ and $\{c_1(a), \ldots, c_n(a)\}$ represents a set of criteria. According to the mathematical problem stated above, there exists no set of alternatives that would maximize all the given criteria. Hence, it is only meaningful to talk about relative comparisons between alternatives. In relation to the preference ranking organization method of enrichment evaluation (PROMETHEE) method for decision-making, the principle of dominance is widely used for expressing preference of one alternative over other for given criteria under a certain function evaluation [4]. Mathematically for alternatives $(a_1, a_2) \in A$, this can be expressed as

$$\begin{cases} \forall j : g_j(a_1) \geq g_j(a_2), \iff a_1 P a_2 \\ \forall j : g_j(a_1) = g_j(a_2), \iff a_1 I a_2 \\ \exists l : g_l(a_1) > g_l(a_2), \\ \exists l : g_k(a_1) < g_k(a_2), \iff a_1 R a_2 \end{cases} \tag{2.23}$$

where P, I, *and* R refer to *preference, indifferent,* and *incomparable*. An alternative is considered better than others if it is better than on all criteria. Similarly, if an alternative performs better for criterion l but underperforms for a criterion k, in that case the two alternatives are said to be incomparable. The stepwise procedure of PROMETHEE algorithm is pictorially depicted in Fig. 2.8 and is enumerated below:

- Construct a pairwise comparison matrix between alternatives based on the qualitative and quantitative data available.

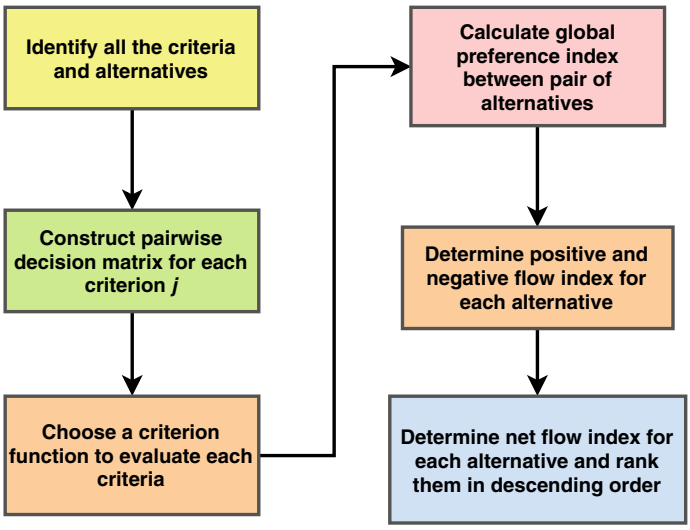

Fig. 2.8 Flowchart for PROMETHEE method

- Based on the application, identify a suitable preference function which determines the preference of alternative a_1 over a_2 and so on. The preference values are either "1" or "0" where former indicates strong preference and latter means indifferent preference. Various function like usual criterion, U-shape criterion, V-shape criterion, and Gaussian criterion are used.
- Calculate global preference index, $\prod(a_1, a_2)$ between alternatives a_1 and a_2 as

$$\prod(a_1, a_2) = \sum_{j=1}^{n} w_j P_j(a_1, a_2), \tag{2.24}$$

where w_j is the weight corresponding to criteria j; $P_j(a_1, a_2)$ is the preference function value between alternatives a_1 and a_2.

- Based on the global preference indices, calculate positive flow $(\eta^+(a_i))$ and negative flow $(\eta^-(a_i))$. The positive flow is indicative of preference of an alternative over others while the negative flow determines the quantitative index showing by how much a particular alternative is outranked by others. The positive and negative flows are given as

$$\eta^+(a) = \frac{1}{1-n} \sum \prod(a_1, a_2), \ \eta^-(a) = \frac{1}{1-n} \sum \prod(a_2, a_1). \tag{2.25}$$

- Calculate the net flow score for each alternative using

$$\eta(a) = \eta^+(a) - \eta^-(a). \tag{2.26}$$

The alternative with maximum net flow score is considered the best.

Compared to other methods, PROMETHEE has a simplistic approach and finds its application in the field of logistics, transportation, and energy management.

2.6 Sensitivity Analysis in Decision-Making

Decision-making process is often challenged by the variations in input parameters. Decision-makers face scenarios where the processes involved are stochastic in nature. Any new alternative or criteria added or removed from the decision environment can have drastic repercussions on the decision result. Early works in sensitivity analysis are carried out by Wendell where the effect of varying the input parameters after optimizing the problem through linear programming is discussed [13]. Traditional sensitivity analysis methods vary only one parameter at a time, but Wendell describes a tolerance method to vary multiple parameters at the same time. As research progressed, Barron and Smith presented two methods for sensitivity analysis for multi-attribute models based on entropy method and a least square method. Both the methods operate on a pair of alternatives where the best one is evaluated based on the closest set of weights that equates their ranking [2].

Sensitivity analysis carried out on MCDM methods also reflects the uncertainties present in the decision-making process. Uncertainty is defined as an entity that is not fixed or has no crisp status. Uncertainties can be internal or external of which latter holds significant importance. Internal errors are the uncertainties pertaining to structure of the MCDM problem. These errors may arise due to lack of human knowledge or biased opinions adopted during a mass survey. In the present context of hybrid wind farms, the criteria dealing with hybrid wind farm operation may pose some uncertainties in form of wind wakes and sudden change in wind speed and direction. Such difficulties are solved by using a fuzzy-based approach that models the decision-making problem to resolve the complexities faced by decision-maker, thereby increasing the reliability of the method and also the sensitivity to internal changes in model. On the other hand, external uncertainties relate to the situations that deal with external environment of the decision. For example, while selecting the site for construction of a multipurpose shopping arcade, factors like geographic location, amenities offered, and security act as external uncertainties. The effect of sensitivity can be modeled mathematically by using function evaluations that may represent a distance metric from a desired one or a utility. Consider a function $\eta(T(x, \xi), \phi)$, where ξ and ϕ represent the external and internal uncertainties on a decision-making process. The impact of variations in ξ and ϕ is assessed for testing the robustness of the MCDM method. Sometimes, the decision-maker may be provided with specified values of function $\eta(\xi, \phi)$. In such cases, it is mandatory to vary the parameter values outside their range to see how the decision-making results unfold. The commonly used sensitivity analysis method is stochastic multicriteria acceptability analysis (SMAA) that determines an acceptability index for each alternative uncertainties [10]. It is therefore important to incorporate sensitivity analysis into MCDM processes.

This chapter highlights the popular MCDM methods used in everyday life as well as in sectors like finance, economics, and management. Out of these methods, our study on hybrid operation in wind farms deals with SAW, TOPSIS, and COPRAS. Predominately, these methods objectively analyze each alternative with respect to given criteria. However, in methods like AHP and ELECTRE, the pairwise comparison of alternatives with respect to each other is the key step in identifying the best choice which is not relevant to our problem definition of hybrid wind farms. The sole objective AHP process is based on interdependencies among alternatives and criteria which can cause rank reversal. While dealing with TOPSIS and COPRAS method, the evaluation of performance scores becomes simple and is easy to understand while this is not true with ELECTRE method. It is also important to note that in decision-making the assigning weights to the criteria is a crucial task. Techniques like entropy method and moora method are often used for this purpose. The strategies modeled as alternatives are discussed in the next chapter are purely independent to each other. Coincidentally, the randomness in the input model (decision matrix) is also discussed via a suitable form of sensitivity analysis for SAW, TOPSIS, and COPRAS methods.

References

1. Balioti V, Tzimopoulos C, Evangelides C (2018) Multi-criteria decision making using TOPSIS method under fuzzy environment. Application in spillway selection. Proceedings 2(11):637
2. Barron H, Schmidt CP (1988) Sensitivity analysis of additive multiattribute value models. Oper Res 36(1):122–127. https://doi.org/10.1287/opre.36.1.122
3. Bhowmik C, Bhowmik S, Ray A (2018) The effect of normalization tools on green energy sources selection using multi-criteria decision-making approach: a case study in india. J Renew Sustain Energy 10(6):065901
4. Bottero M, D'Alpaos C, Oppio A (2018) Multicriteria evaluation of urban regeneration processes: an application of PROMETHEE method in northern Italy. Adv Oper Res, 1–12. https://doi.org/10.1155/2018/9276075
5. Byun H, Lee K (2005) A decision support system for the selection of a rapid prototyping process using the modified topsis method. Int J Adv Manuf Technol 26(11):1338–1347. https://doi.org/10.1007/s00170-004-2099-2
6. Dymowa L (2011) MCDM with applications in economics and finance. In: Soft computing in economics and finance. Springer, Berlin, pp 107–186. https://doi.org/10.1007/978-3-642-17719-4_4
7. Figueira JR, Greco S, Roy B, Słowiński R (2012) An overview of ELECTRE methods and their recent extensions. J Multi-Criteria Decis Anal 20(1–2):61–85. https://doi.org/10.1002/mcda.1482
8. Hallerbach WG, Spronk J (2002) The relevance of MCDM for financial decisions. J Multi-Criteria Decis Anal 11(4–5):187–195
9. Hwang CL, Yoon K (1981) Methods for multiple attribute decision making. Springer, Berlin, pp 58–191
10. Lahdelma R, Hokkanen J, Salminen P (1998) SMAA - stochastic multiobjective acceptability analysis. Eur J Oper Res 106(1):137–143. https://doi.org/10.1016/s0377-2217(97)00163-x
11. Lourenzutti R, Krohling RA (2016) A generalized TOPSIS method for group decision making with heterogeneous information in a dynamic environment. Inf Sci 330:1–18

12. Saaty TL (1984) The analytic hierarchy process: decision making in complex environments. In: Quantitative assessment in arms control. Springer US, pp 285–308. https://doi.org/10.1007/978-1-4613-2805-6_12
13. Wendell RE (1997) Linear programming 3: the tolerance approach. In: Advances in sensitivity analysis and parametric programming. Springer, US, pp 158–178. https://doi.org/10.1007/978-1-4615-6103-3_5
14. Yang W, Xu K, Lian J, Ma C, Bin L (2018) Integrated flood vulnerability assessment approach based on TOPSIS and shannon entropy methods. Ecol Indic 89:269–280. https://doi.org/10.1016/j.ecolind.2018.02.015
15. Zolfani SH, Rezaeiniya N, Aghdaie MH, Zavadskas EK (2012) Quality control manager selection based on AHP- COPRAS-g methods: a case in iran. Econ Res-Ekon Istraživanja 25(1):72–86. https://doi.org/10.1080/1331677x.2012.11517495

Chapter 3
Decision-Making in Hybrid Wind Farms

Having dominated as primary energy source, fossil fuel consumption has seen a significant spurt in the twentieth century. However, with increased carbon footprints from fossil fuels globally, renewable energy technologies have been reinforced as energy source in developing and developed countries. Increased penetration of wind power in utility grid questions stable power system operation due to random wind speed causing erratic dispatch of generated power. The concern of forecasting challenges among wind practitioners has gathered industrial limelight over the years in order to minimize their financial losses. An accurate wind power forecast ensures system reliability and reduces auxiliary equipment cost. Traditionally, wind forecasting techniques are categorized into two broad models: statistical models and machine learning models. With wind being stochastic on temporal scale, nonlinearity induces forecasting challenges for statistical models. Machine learning models in tandem with signal decomposition techniques (wavelet transform and empirical model decomposition) form the bulwark for accurate forecasting methods.

Hybrid operation of wind farms has seen a lot of interest in recent times wherein the stochastic nature of wind results in market operators choosing an optimal strategy to maximize profit. The current problem deals with three non-beneficial criteria, namely, wind wakes, wind curtailment, and forced outages, to find the best option. Three MCDM methods are applied to find the best alternative, and the results reveal that for all these methods, borrowing deficit power from a neighboring farm is the best. Comparative analyses in terms of data requirement, the effect of dynamic decision matrices, and rank reversal are also presented.

3.1 Introduction

Global scenario in the wind energy sector has led to an increase in job creation with heavy investments in both onshore and offshore platforms. Wind energy integration in utility grid has also brought attention toward its sophisticated and reliable control operations [7]. Wind turbines operating in an atmospheric boundary layer experience

H. S. Dhiman and D. Deb, *Decision and Control in Hybrid Wind Farms*,
Studies in Systems, Decision and Control 253,
https://doi.org/10.1007/978-981-15-0275-0_3

a wide range of physical phenomenon and achieving economies of scale is one of the primary objectives for a wind farm operator. Majority of the losses occurring in a wind farm are due to inaccurate forecasting. To compensate for the deficit power, wind farm operators have to rely on reserve power sources like a system of batteries. Thus, it is essential to approach a wind farm operation with a strategy that focuses on a plan of action to minimize cost incurred.

Multi-criteria decision-making (MCDM) poses a cost-effective solution through its mathematical modeling approach for determining the best available choice. Primarily, MCDM methods are categorized into compensatory and outranking techniques. Compensatory techniques approach toward the best alternative solely based on their positive traits over negative traits which indicative of a trade-off situation. Analytical hierarchical process (AHP) and fuzzy logic decision-making (FLDM) are commonly used compensatory techniques. Thrust applications of compensatory MCDM techniques include water resources engineering, rural water supply evaluation, and desalination plants, while outranking techniques follow a series of logical decision-making rules based on weights assigned to a set of criteria. Some of the popular outranking methods include the COPRAS, the TOPSIS, the weighted sum and product method, Elimination Et Choix Traduisant la Realite Method (ELECTRE), and the preference ranking organization method for enrichment evaluation (PROMETHEE) [15]. ELECTRE method involves a lot of computational complexity and is not preferred for MCDM problems. Similarly, with PROMETHEE, the rank reversal of the alternatives may question the decision process along with the weights assigned which otherwise are qualitative in nature [9].

One of the most common ways to design an MCDM problem is to conduct mass surveys and questionnaire which has helped thrust applications in the field of science and technology. Renewable energy sources, energy resource planning, utility planning, and building energy management along with transportation energy management are the key areas where MCDM is applied [5]. As discussed by Georgiou et al., AHP and PROMETHEE methods seem to arrive at optimal decisions for an efficient energy configuration for a reverse osmosis desalination plant. Five such topologies as alternatives are ranked considering social, environmental, and economic impact [4]. Kundakc et al. used two outranking techniques, namely, measuring attractiveness by a categorical-based evaluation technique (MACBETH) and evaluation based on distance from average solution (EDAS) to choose the best boiler for a dyehouse in the textile industry [11]. Lee et al. explored MCDM approach to select wind turbine model for installation of a wind farm using interpretive structural modeling (ISM) and the fuzzy analytical hierarchical process (FAHP) [12]. A binary matrix representing relationship between each criterion and its sub-criterion is developed. In the field of offshore wind energy platform, the potential power production scenario in Egypt is analyzed by Mahdy et al. Based on the geographical information system (GIS)-AHP method, factors like water depth, wind flow, and distance from shore are considered for formulating the MCDM problem [14]. Kolios et al. explored the problem of selecting turbine structures for offshore wind farm platform where inputs are varied while designing the decision matrix. Several factors like depth compatibility environmental impact, maintenance cost and cost of installation are

considered as criteria for assessing the alternatives [10]. In Saudi Arabia, the problem of selecting appropriate renewable energy source is studied by Garni et al. with several factors like political, environmental and sociocultural impact, considered as criteria. AHP method is used, solar PV technology followed by solar thermal technology is found as a best choice of alternative [3]. Decision-making process involves mathematical steps as discussed in previous chapter. One such step is normalization of decision matrix. Jahan et al. discussed normalization techniques and their impact on the decision-making procedure [8].

Decision-making process is based on evaluating the alternatives based on a quantitative value which can be ordered in a descending manner. Thus, decision-makers depend solely on the information available from mass surveys and questionnaire to model it into a structured decision problem which can be impartially assessed over given set of criteria. The criteria weights in an MCDM problem cannot be assigned randomly as it may ill-condition the decision matrix which may lead to non-optimal decisions. Based on the prospects that an MCDM problem offers, this chapter highlights some of the MCDM techniques to be applied to the hybrid wind farms. The major contribution of this chapter includes formulation of an optimal hybrid wind farm strategy where aerodynamic phenomena like wind curtailment, wind wakes, and forced outage are considered to affect the choice of an operational strategy. The operational strategy is modeled in form of penalty incurred to a wind farm operator. This requires an accurate wind forecasting scheme to be considered for evaluating the penalty cost. This chapter is structured as follows: Sect. 3.2 discusses the preliminaries of a hybrid operation of a wind farm. The alternatives are described with each involving a penalty cost to be incurred. Results and discussions are explored in Sect. 3.3. We also present a comparative outcome of the MCDM methods considered for this study in Sect. 3.4.

3.2 Problem Formulation

Wind resource available in an abundant form ensures a strong wind power density and is key to a reliable wind farm operation. For maximum power capture, it is beneficial for a wind site to have a terrain that does not escalate the turbulent eddies in atmospheric boundary layer which otherwise can lead to reduced annual energy production. Automation and cutting-edge technologies have ensured the production costs within acceptable limits for a wind farm [2]. It is also observed that apart from the rough terrain and complexities posed by micro-siting, lack of accessibility to the natural resources can be a determining factor in overall project cost for a wind farm.

The concept of a hybrid wind farm as discussed in Chap. 1 deals with accurate wind forecasting schemes. A common practice includes wind power schedules to be available ahead in time to ensure guaranteed power transmission to utility grid. The inherent stochasticity in wind speed causes errors in forecasting which is responsible for deficit or surplus power. Currently, the excess or deficit wind power is taken care by reserve power sources known as battery energy storage system (BESS). Since in

an event of large excess or deficit wind power involving BESS to charge or discharge power, respectively, determination of BESS capacity should be done beforehand. Patel et al. presented methodologies for hybrid wind power generation [17] and we extend these to solve the MCDM problem. The alternatives are listed as follows:

- Alternative 1 (A_1): In this situation, the forecasted wind power is compared with actual wind power and then based on the deficit in each dispatch window the total cost is evaluated. Assuming $\hat{p}_i$ to be the forecasted wind power and p_i to be the actual one, for k_a such instances, the cost is given as

$$F_1 = \beta_w \sum_{i=1}^{k_a} \left(\hat{p}_i - p_i \right), \tag{3.1}$$

  where β_w is cost paid in \$ per 1 kW of deficit wind power. It is worthwhile to note that in case of $p_i > \hat{p}_i$, the operator decides not to pay any penalty.
- Alternative 2 (A_2): Here, the farm operator pays the penalty via combination of two strategies. The deficit in forecasted wind power and actual wind power is calculated and a threshold limit for battery P_b^{th} is calculated in events of deficit power exceeding battery threshold limit. For m_s such events, the wind farm operator pays penalty cost given as

$$F_2 = \zeta_s \sum_{i=1}^{m_s} \left(p_{bi}^{th} - \hat{p}_i + p_i \right), \tag{3.2}$$

  where ζ_s represents penalty paid in \$ for per kW of exceeding threshold limit.
- Alternative 3 (A_3): Consider a situation where the wind farms in neighborhood have excess of wind power. The wind farm dealing with deficit power may borrow power and pay an equivalent penalty. Let p_{2i}, $\hat{p}_{2i}$, p_{3i}, and $\hat{p}_{3i}$ be the actual and forecasted wind powers for wind farms 2 and 3, respectively; in this case, the wind farm operator of farm 1 pays a penalty for l_z given as

$$F_3 = \begin{cases} \alpha_z \sum_{i=1}^{l_z} (p_{2i} - \hat{p}_{2i}), & \text{if} \quad p_{2i} > \hat{p}_{2i}, \\ \alpha_z \sum_{i=1}^{l_z} (p_{3i} - \hat{p}_{3i}), & \text{if} \quad p_{3i} > \hat{p}_{3i}, \\ \delta_z \sum_{i=1}^{l_z} (\hat{p}_i - p_i), \end{cases} \tag{3.3}$$

  where α_z and δ_z are the penalty cost and cost of discharging the battery units to compensate 1 kW of deficit power, respectively. It is worthwhile to note that the penalty cost of battery unit is higher than A_1 and A_2.

- Alternative 4 (A_4): Here the wind farm operator pays penalty where the entire deficit wind power faced by a wind farm is supplied by a set of batteries. The cost expression for u_l such instances is given as

$$F_4 = \delta_x \sum_{i=1}^{u_l} (\hat{p}_i - p_i), \tag{3.4}$$

where δ_x is the cost in \$ for per 1 kW of deficit power supplied by a set of batteries.

Next, we discuss different criteria based on which our MCDM problem is to be assessed. One of the most common aerodynamic phenomena in atmospheric boundary layer is wind wakes. The power loss caused in a wind farm due to wakes is subjected to a set of alternatives. Wind curtailment is another phenomena which the farm operators deal with due to limitations posed by generator system. Wind curtailment also impacts the economic operation of wind farms and more specifically the effect is discussed for thermal generators by Henriot [6]. Curtailment can be helpful in scenarios where a system of batteries are not capable to deliver bulk power. Forced outage is another criteria that affect the hybrid operation of wind farms. It occurs when a wind turbine unit(s) is stalled from its normal operation and is withdrawn from wind farm. This may be due to a regular scheduled maintenance for turbine blades and internal mechanisms.

Quality of landscape is one of the reasons on which the lifetime of a wind farm is dependent. Qualitative and quantitative analysis of landscape has been done actively over the years and it is observed that various sociocultural and economic impacts have affected the surrounding area to the wind farm. Cost action report, namely, "Renewable Energy and Landscape quality" has been brought out to map a relationship between the landscape quality and renewable energy sources [18]. It is interesting to note that the landscape quality of a wind farm is directly related to the set of alternatives discussed. For example, in events where the wind farm operator pays penalty by discharging a system of batteries, the lead discharge can deplete the ecosystem surrounded by the wind farm. However, the landscape quality can be improved by manufacturing batteries that are made up of eco-friendly material.

In the present case, the wind farms considered are with equal number of wind turbines. With different number of turbines, the impact of the alternatives on the landscape quality will be different. As discussed earlier, the lead emissions from battery deteriorate the ecosystem, and with higher number of battery units this effect will be more pronounced. Noise emitted from wind turbine units is also a cause of concern among wind farm operators. Aerodynamic and mechanical noises are commonly observed in a wind farm. Wake generated behind the turbine hub is responsible for aerodynamic noise, while the wear and tear caused in generator and shaft section lead to mechanical noise. Empirical models relating turbine parameters and noise are often used to assess the noise impact on the surroundings of a wind farm. Lowson [13] relates the emitted noise (in dB) to turbine diameter as

$$L_{WA} = 44 \log_{10} R_x + 72, \tag{3.5}$$

Table 3.1 Criteria for the MCDM approach

Label	Criteria	Consequences
C_1	Wind wakes	Leads to power loss
C_2	Wind curtailment	Excess wind speed to be curtailed
C_3	Forced outage	Reduction in farm output

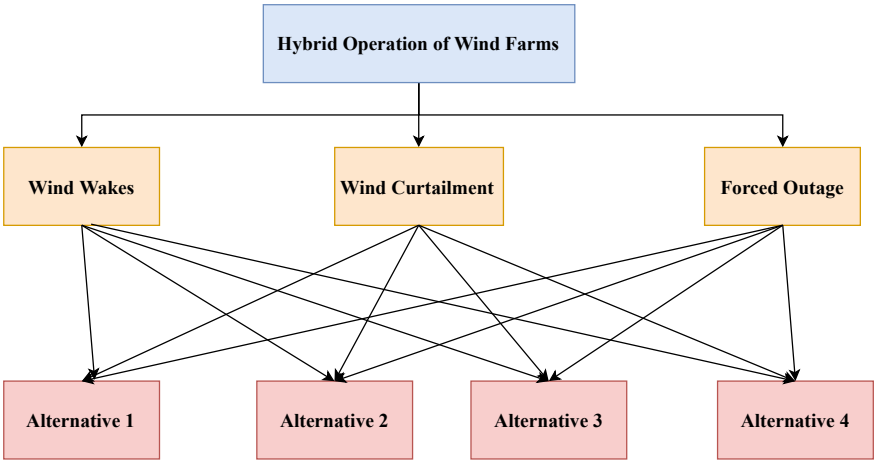

Fig. 3.1 MCDM technique applied to hybrid operation of wind farms

for rotor radius R_x. The logarithmic relationship is indicative of the fact that wind farms with a large diameter turbine can pose significant noise emissions. Table 3.1 depicts the criteria used for assessing alternatives in the MCDM problem. Figure 3.1 illustrates different criteria involved in the MCDM problem.

3.3 Results and Discussions

In this section, we discuss the multi-criteria decision-making approach for hybrid wind farms. To begin with, three wind farms, Bishop and Clerks (Farm X), Paxton (Farm Y), and Blandford (Farm Z) are selected. Wind speed datasets pertaining to two different years are acquired from Wind Energy Center, University of Massachusetts, MA. Using cup anemometer, the wind speed is measured at heights of 15, 78, and 60 m from ground for Farm X, Farm Y, and Farm Z, respectively. To determine the forecasted powers at same hub height, the wind speed for Farm X and Farm Y is transformed to a hub height of 60 m using the standard wind law for elevation [20]. Datasets D1 and D2 for three wind farms are collected for the duration of January 2011 and January 2013 [1] with descriptive statistics listed in Table 3.2. The wind

Table 3.2 Statistical parameters for wind speed Datasets D1 and D2

Statistic	D1 (January 2011)			D2 (January 2013)		
	Farm X	Farm Y	Farm Z	Farm X	Farm Y	Farm Z
Mean	8.3364	8.3612	5.189	10.146	9.4411	6.1096
Std. Dev.	3.2224	3.0543	2.4075	4.2897	2.8944	2.1752
Skewness	–0.0943	–0.1040	0.9670	–0.3428	–0.3219	0.2102

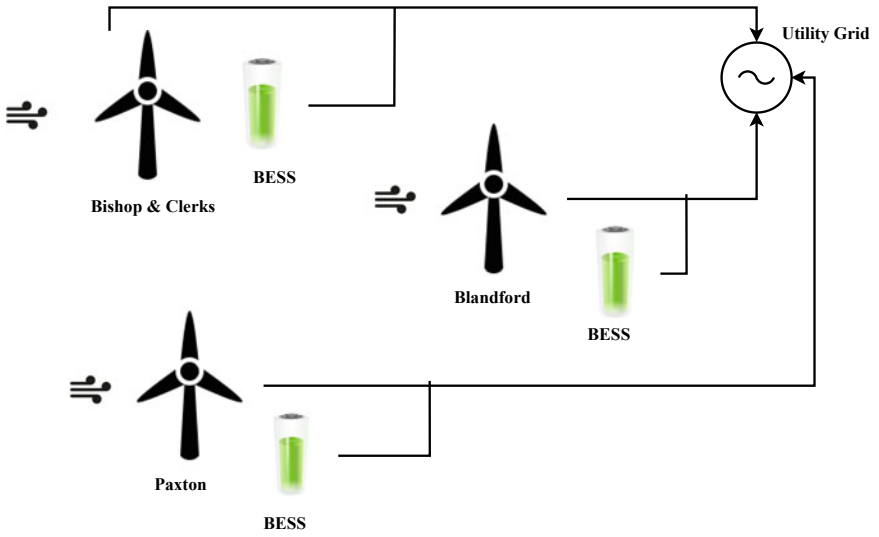

Fig. 3.2 A hybrid wind farm topology depicting Bishop and Clerks, Paxton and Blandford

farms are considered to have a rotor diameter of 77 m and wind direction is directly facing the wind turbines.

A schematic representation of the three wind farms along with battery units is pictorially depicted in Fig. 3.2. First, the penalty cost incurred by the wind farm X, that is, Bishop and Clerks, is calculated. For this, the wind power is forecasted and is compared with actual wind power. Penalty cost for all the alternatives as discussed is then determined.

Figure 3.3 pictorially depicts the wind speed plots for two datasets. The alternatives discussed here are assessed based on a cumulative score. The first part deals with computing the penalty cost for all the alternatives by calculating the deficit power for the wind farm. Second part deals with the non-tangible effect which is calculated from the performance scores of the MCDM methods like SAW, TOPSIS, and COPRAS. The cost obtained in first step is normalized with respect to minimum penalty cost incurred and then is multiplied with performance score to obtain the cumulative priority score for each alternative.

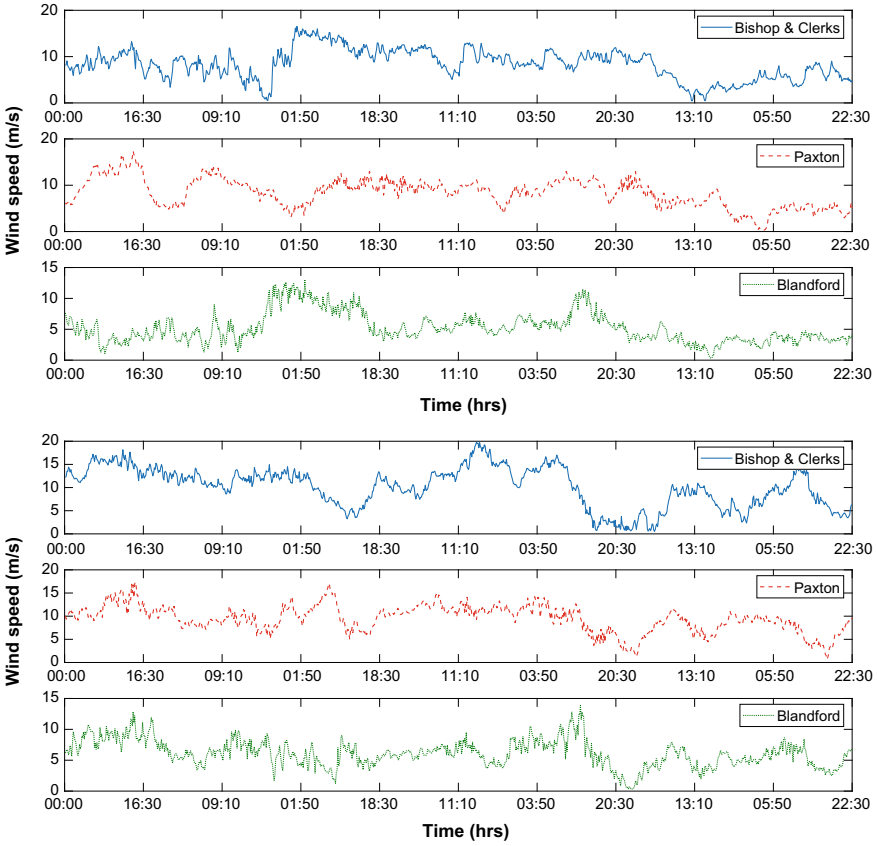

Fig. 3.3 Wind speed pattern for three wind farms in Massachusetts

Least square support vector regression is implemented to predict wind speed which then is later translated into wind power. A dataset with 1000 samples is segmented into training (800) and (200). Based on the forecasted wind speed, we then calculate the forecasted wind power. In order to determine whether a BESS will charge or discharge in any event, the forecasted and actual wind powers are compared. For example, consider Dataset D1 where Fig. 3.4 illustrates the magnitude of charging and discharging powers at each instant. As put forward by Nguyen et al., the BESS capacity can be determined by calculating aggregated sum of charging and discharging powers [16]. The same principle is used here to determine the BESS capacity. Optimal BESS capacity aids its sizing and is also indicative of space requirements for a wind farm operator.

For Datasets D1 and D2, the BESS capacity is enlisted in Table 3.3.

In order to determine a penalty cost for particular alternative, the sum of deficit power in each forecast window is calculated. For each alternative, the cost to dispatch

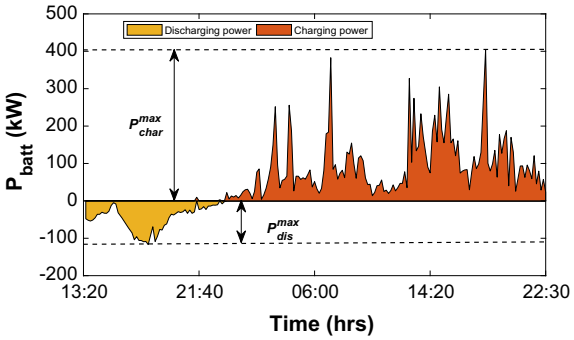

Fig. 3.4 Discharging and charging powers for Bishop and Clerks, Jan 2011

Table 3.3 BESS capacity for two datasets

Dataset	BESS capacity (MW)	Threshold limit (kW)
D1	15	110
D2	50	955

Table 3.4 Penalty cost and normalized cost score for Datasets D1 and D2. PC, penalty cost; NCS, normalized cost score

Alternatives	D1		D2	
	PC ($)	NCS	PC ($)	NCS
A_1	1971.2	1.1665	6514.2	1.3238
A_2	1689.8	1.0000	4920.8	1.0000
A_3	3916.5	2.3177	13587	2.7612
A_4	2252.8	1.3332	7444.8	1.5129

1 kW of deficit power is taken as $\beta_w = \$\ 0.5$, $\zeta_s = \$\ 0.75$, $\alpha_z = \$\ 0.4$, and $\delta_x = \$\ 0.8$. It is worthwhile to note that for alternative A_4 the cost to dispatch 1 kW of deficit power is taken as maximum due to erratic charging and discharging as it can deplete battery life and leads to high maintenance cost. Using the principle of min-max described by Nguyen et al., the BESS threshold limits of 955 and 110 kW are determined for Datasets D2 and D1. For Datasets D1 and D2, the penalty cost ($) along with the normalized cost score (NCS) is depicted in Table 3.4.

In order to determine the intangible effect in form of performance scores, we consider four alternatives and three criteria for the hybrid wind farm operation. Table 3.5 depicts a logical relationship between criteria and different alternatives. In the present context, the criteria discussed are non-beneficial, and hence rather than assigning conventional indices to the alternatives we assign highest score to the least preferred and lowest score to the most preferred alternative. Consider wind wakes as a criteria to evaluate the four alternatives. The power losses in a wind farm due

Table 3.5 Performance scores for the decision matrix [19]

Importance	Performance score as per AHP	Performance score in current work
Equally preferred (EP)	1	9
Equally to moderately preferred (EMP)	2	8
Moderately preferred (MP)	3	7
Moderately to strongly preferred (MSP)	4	6
Strongly preferred (SP)	5	5
Strongly to very strongly preferred (SVP)	6	4
Very strongly preferred (VP)	7	3
Very strongly to extremely preferred (VEP)	8	2
Extremely preferred (XP)	9	1

to wakes can be best handled if alternatives A_2 and A_3 are practiced. Due to large penalty cost for battery discharging, alternative A_4 is not preferred and is given a score accordingly. For the case of wind curtailment, the power which is curtailed can be best dealt if it is supplied to the neighboring wind farm in case of deficit scenario. While for forced outages, it would be an abrupt decision to deliver power via a system of batteries as it could cause deep discharge and would incur high operational cost.

Let us now discuss the reasoning behind assigning element values for each alternative with respect to given criteria in a decision matrix. When it comes to wind wakes, the power losses are high and can be best dealt with alternative A_3 so a score of 2 is assigned to it. For alternatives A_1 and A_2, a score of 8 and 3 is assigned, respectively, due to the large penalty cost incurred to wind farm operator owing to poor forecasting scheme. Similarly, for alternative A_4, discharging a large amount of power will make the farm operator pay more and is not suitable for battery health. Hence, a score of 9 is given to it. For the case of wind curtailment, alternatives A_1 and A_2 are assigned scores of 5 and 4, respectively, while alternative A_4 is given a score of 7 due to high operational cost. Forced outage means taking out wind turbine(s) units out of wind farm which then means that the only legitimate strategy for a wind farm operator could be to deliver power or borrow power from neighboring wind farms and pay an equivalent penalty for it.

As per Saaty, a matrix H is constructed and based on our MCDM problem a matrix H' is given as

Table 3.6 Ranking for alternatives based on the simple additive weighting (SAW) method

Alternatives	D1		D2		Ranking
	PS	CPS	PS	CPS	
A_1	0.3120	0.3640	0.3120	0.4130	3
A_2	0.5021	0.5021	0.5021	0.5021	2
A_3	1.0000	2.3177	1.0000	2.7612	1
A_4	0.2529	0.3372	0.2529	0.3826	4

$$H = \begin{array}{c} \begin{matrix} C_1 & C_2 & C_3 \end{matrix} \\ \begin{pmatrix} 2 & 3 & 1 \\ 7 & 6 & 4 \\ 8 & 7 & 9 \\ 1 & 3 & 2 \end{pmatrix} \end{array} \begin{matrix} A_1 \\ A_2 \\ A_3 \\ A_4 \end{matrix}, \quad H' = \begin{array}{c} \begin{matrix} C_1 & C_2 & C_3 \end{matrix} \\ \begin{pmatrix} 8 & 5 & 9 \\ 3 & 4 & 6 \\ 2 & 3 & 1 \\ 9 & 7 & 8 \end{pmatrix} \end{array} \begin{matrix} A_1 \\ A_2 \\ A_3 \\ A_4. \end{matrix}$$

We solve the decision-making problem having designed a decision matrix. For simple additive weighting (SAW) method, the normalized decision matrix is determined using (2.1) and (2.2). Further, as described in Sect. 2.2.1, the weights for the criteria are calculated. For the SAW method, the normalized matrix is given as

$$\hat{H} = \begin{bmatrix} 0.2500 & 0.6000 & 0.1111 \\ 0.6667 & 0.7500 & 0.1667 \\ 1.0000 & 1.0000 & 1.0000 \\ 0.2222 & 0.4286 & 0.1250 \end{bmatrix}. \tag{3.6}$$

Using (2.3)–(2.4), based on entropy method, the weights are as follows

$$w = \{0.2864, 0.3296, 0.3840\}. \tag{3.7}$$

Table 3.6 enlists the cumulative priority score for the SAW method. The priority scores are determined using the sum of product of weight vector and normalized matrix.

Alternatives are ranked as $A_3 \succ A_2 \succ A_1 \succ A_4$ based on the SAW method. It is observed that paying penalty cost when the deficit power is borrowed from the neighboring wind farm is the best alternative followed by A_2 which is a mix of two strategies. We attempt to find the best alternative using COPRAS method. With the same decision matrix H', using (2.6) the normalization is done and is expressed as

$$\hat{H} = \begin{bmatrix} 0.6364 & 0.5025 & 0.6671 \\ 0.2387 & 0.4020 & 0.4447 \\ 0.1591 & 0.3015 & 0.0741 \\ 0.7160 & 0.7035 & 0.5930 \end{bmatrix}. \tag{3.8}$$

Table 3.7 Ranking based on CPS for the complex proportional assessment (COPRAS) method

Alternatives	D1		D2		Ranking	
	PS	CPS	PS	CPS	D1	D2
A_1	0.2153	0.2511	0.2153	0.2850	4	4
A_2	0.3857	0.3857	0.3857	0.3857	2	2
A_3	1.0000	2.3177	1.0000	2.7612	1	1
A_4	0.2079	0.2772	0.2079	0.3145	3	3

As discussed in Sect. 2.2.1, based on entropy method, the weight vector is

$$w = \{0.4142, 0.1201, 0.4658\}. \tag{3.9}$$

Using (2.15) and (2.16), the aggregated sum of the criteria is evaluated. Table 3.7 depicts the priority score along with cumulative priority score for COPRAS method.

According to the CPS, the alternatives are ranked as $A_3 \succ A_2 \succ A_4 \succ A_1$. We observe that A_3 remains the best choice for the two datasets. Here, it is also important to note that these decision results may vary as we move from one dataset to another. The essence of this approach is based on the accuracy of forecasted wind powers. The decision-making is then solved using TOPSIS method where the matrix is normalized using (2.6). Entropy method is used to calculate the weights. The normalized decision matrix and weights are given as

$$\hat{H} = \begin{bmatrix} 0.6364 & 0.5025 & 0.6671 \\ 0.2387 & 0.4020 & 0.4447 \\ 0.1591 & 0.3015 & 0.0741 \\ 0.7160 & 0.7035 & 0.5930 \end{bmatrix}, \quad w = \{0.4142, 0.1201, 0.4658\}. \tag{3.10}$$

Using (2.8) and (2.9), the positive (PIS) and negative ideal solutions (NIS) are given as

$$S^+ = \{0.0659,\ 0.0362,\ 0.0345\}, \quad S^- = \{0.2965,\ 0.0845,\ 0.3107\}.$$

The Euclidean distance which is indicative of the best and worst possible alternative is calculated and for the p-norm distance we take $p = 2$. The distances are given as

$$D^+ = \{0.0580,\ 0.0155,\ 0,\ 0.0570\}, \tag{3.11}$$

$$D^- = \{0.0008,\ 0.0256,\ 0.0659,\ 0.0006\}. \tag{3.12}$$

Table 3.8 depicts the ranking for the alternatives based on cumulative priority scores for the two Datasets D1 and D2.

Alternatives are ranked as $A_3 \succ A_2 \succ A_1 \succ A_4$ for the TOPSIS method. Once again it is validated that A_3 is the best alternative among the four strategies. Paying

Table 3.8 Ranking using the TOPSIS method

Alternatives	D1		D2		Ranking
	PS	CPS	PS	CPS	
A_1	0.0142	0.0166	0.0142	0.0188	3
A_2	0.5323	0.5323	0.5323	0.5323	2
A_3	1.0000	2.3177	1.0000	2.7612	1
A_4	0.0104	0.0139	0.0104	0.0157	4

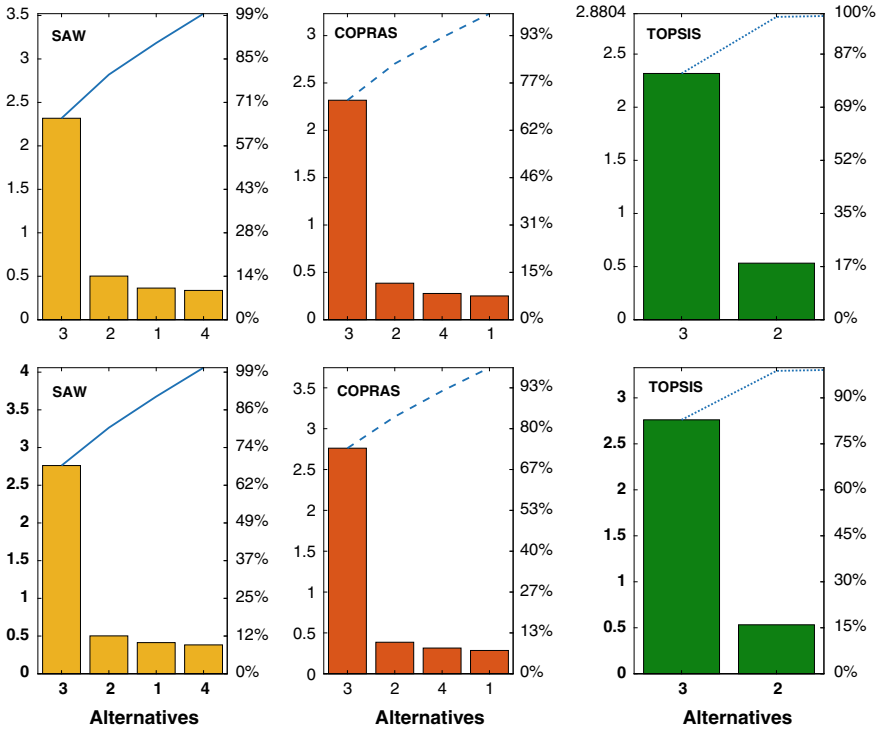

Fig. 3.5 Pareto charts for alternatives for Datasets D1 and D2

penalty for the deficit wind power by borrowing power from neighboring wind speed is an optimal way to make sure wind farm operation is reliable and secure.

Based on the tangible effect and intangible effect, the cumulative priority scores are used as a metric for arriving at the best alternative. Figure 3.5 illustrates the Pareto charts for the alternatives for the two datasets.

3.4 Comparative Analysis of MCDM Methods

Till now we have discussed three MCDM methods for the decision-making process. With each method possessing its own advantages and disadvantages, for a decision-maker it is extremely difficult to select one method out of the bunch. We have evaluated SAW, TOPSIS, and COPRAS methods for hybrid wind farm operation and have chosen four alternatives with three criteria, while it is still possible to have a situation where a new alternative(s) or criteria can be added or removed from the decision-making process. Mathematically, the number of data T required in the decision matrix to be considered in each MCDM method is given as

$$T = (H + 1)\, S, \tag{3.13}$$

where H represents the number of alternatives and S is the number of criteria. It is observed that for the MCDM problem dealing with hybrid operation of wind farms, the methods discussed need a minimum of 15 judgments. This is indicative of the fact that the methods work with same level of inputs.

The problem of rank reversal in decision-making problems is very common. Methods like PROMETHEE and AHP suffer from rank reversal and may skew the decision. In some critical situations of finance and management, such rank reversal may jeopardize the functioning or a crucial decision ultimately resulting in business risk. Wang et al. discussed several scenarios where methods like AHP, SAW, and TOPSIS face the issue of rank reversal [21]. It is also observed that rank reversal can occur due to the addition of indifferent criteria or alternatives. From the SAW method analysis, it is observed that alternative A_3 is the most preferred while A_4 is the least preferred alternative. In order to test the rank reversal phenomenon in the discussed MCDM methods, let us eliminate the least preferred alternative A_4 and test the performance scores again. The same procedure is repeated for COPRAS and TOPSIS method and it is found that alternative A_3 dominates the decision space followed by A_2. This analysis affirms the fact that given the datasets and the structure of the MCDM problem and under all given constraints, the methods are insusceptible to any indifferent alternative or criteria. Table 3.9 showcases the new ranks for SAW, TOPSIS, and COPRAS methods when they are tested for rank reversal, thus assuring the decision-maker of their robustness under dynamic situations.

Table 3.9 Ranking under dynamic decision matrices in the SAW, TOPSIS, and COPRAS methods

Alternatives	Initial	A_4	A_1	A_2
	Rank			
A_4	4			
A_1	3	3		
A_2	2	2	2	
A_3	1	1	1	1

3.5 Decision-Making for Wind Farms in Hills

We now discuss the problem of decision-making for wind farms sites situated in hills. Since it is difficult to locate three wind farm sites in hills which at close proximity, we assume three wind farms with datasets from hilly regions. Consider wind farms XX, YY, and ZZ with their wind speed data pertaining to sites Challicum hills (Australia), Longyuan hills (Tibet), and Ngong hills (Kenya). The wind farms are analyzed for the best alternative as previously assessed for onshore wind farm sites. The wind speed data for May 2019 is taken with a 10 min interval. Figure 3.6 illustrates the wind speed time-series plots for three hilly wind sites.

First, the normalized cost score for each alternative is determined using the predicted and actual wind powers. Wind power is forecasted using LSSVR where the dataset is segmented into training (800) and testing (200). The cost for compensating 1kW of deficit wind power is taken as $\beta_w = \$\,0.5$, $\alpha_z = \$\,0.4$, $\zeta_s = \$\,0.75$, and $\delta_x = \$\,0.8$. The normalized cost score is determined by normalizing the total cost incurred as penalty for all the four alternatives and is depicted in Table 3.10.

Next, we evaluate the priority score for all the alternatives based on SAW, TOPSIS, and COPRAS methods. Since the decision matrix here remains same, the priority

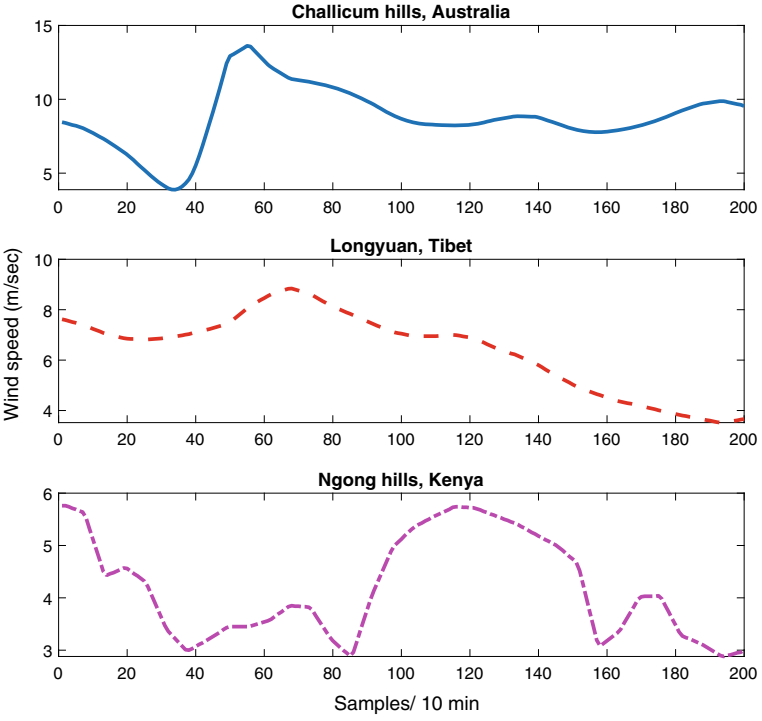

Fig. 3.6 Wind speed time series for hilly wind sites

Table 3.10 Penalty cost and normalized cost score for Hilly wind sites. PC, penalty cost; NCS, normalized cost score

Alternatives	Hilly wind site	
	PC ($)	NCS
A_1	52831	1.000
A_2	84530	1.600
A_3	59945	1.134
A_4	84530	1.600

Table 3.11 Ranking for hilly wind sites using SAW, TOPSIS, and COPRAS methods

Alternatives	SAW	TOPSIS	COPRAS	Ranking
	CPS	CPS	CPS	
A_1	0.3120	0.2153	0.0142	4
A_2	0.8034	0.6171	0.8517	2
A_3	1.1347	1.1347	1.1347	1
A_4	0.4046	0.3326	0.0166	3

scores for all the alternatives remain unchanged. The cumulative priority scores are tabulated in Table 3.11 for SAW, TOPSIS, and COPRAS methods.

3.6 Decision-Making for Offshore Wind Farms

Deployment of offshore wind energy systems has increased over the years owing to abundant wind resource available in sea. In the present context, the multi-criteria decision-making technique is applied to see how things unfold when it comes to alternatives for an offshore wind farm. To study this, three offshore wind farms, namely, Anholt (Denmark), Horns Rev 2 (Denmark), and Amrumbank (Germany) are selected as illustrated in Fig. 3.7. The total distance between these wind farms is approximately 600 km.

We now approach toward constructing decision matrix H for offshore wind farms. Here, the MCDM approach is carried out for wind farm Anholt (Denmark) considering the effects from neighboring wind farms Horns Rev 2 (Denmark) and Aumrumbank (Germany). First, we evaluate the normalized cost score for each alternative based on the deficit forecasted wind powers.

The wind speed datasets for three wind farms are taken for the month of May 2019 each measured at a 10 min interval and are illustrated in Fig. 3.8.

The wind power for three wind farms is forecasted using LSSVR with a training set (800) and testing set (200). The normalized cost score is depicted in Table 3.12.

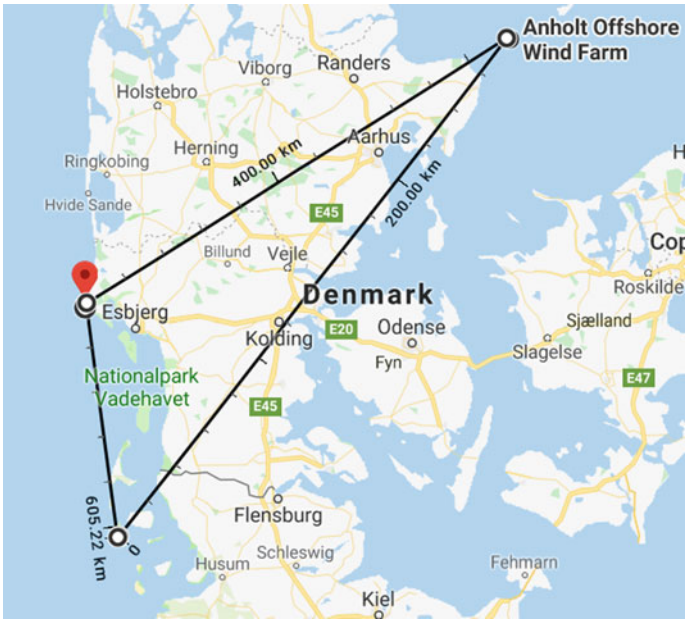

Fig. 3.7 Geographic location of offshore wind farms. *Source* Google Maps

Table 3.12 Penalty cost (PC) and normalized cost score (NCS) for offshore wind farms

Alternatives	D1	
	PC ($)	NCS
A_1	37393	1.000
A_2	59829	1.600
A_3	82919	2.217
A_4	59829	1.600

The decision matrix is based on three criteria, namely, wake effect, wind curtailment, and forced outage. The elements of decision matrix are selected based on their relative importance of each alternative with respect to each criteria as explained in previous sections:

$$H = \begin{array}{c} \begin{matrix} C_1 & C_2 & C_3 \end{matrix} \\ \begin{pmatrix} 2 & 3 & 1 \\ 7 & 6 & 4 \\ 7 & 9 & 9 \\ 1 & 3 & 2 \end{pmatrix} \end{array} \begin{matrix} A_1 \\ A_2 \\ A_3 \\ A_4 \end{matrix}, \quad H' = \begin{array}{c} \begin{matrix} C_1 & C_2 & C_3 \end{matrix} \\ \begin{pmatrix} 8 & 5 & 9 \\ 3 & 4 & 6 \\ 3 & 1 & 1 \\ 9 & 7 & 8 \end{pmatrix} \end{array} \begin{matrix} A_1 \\ A_2 \\ A_3 \\ A_4. \end{matrix}$$

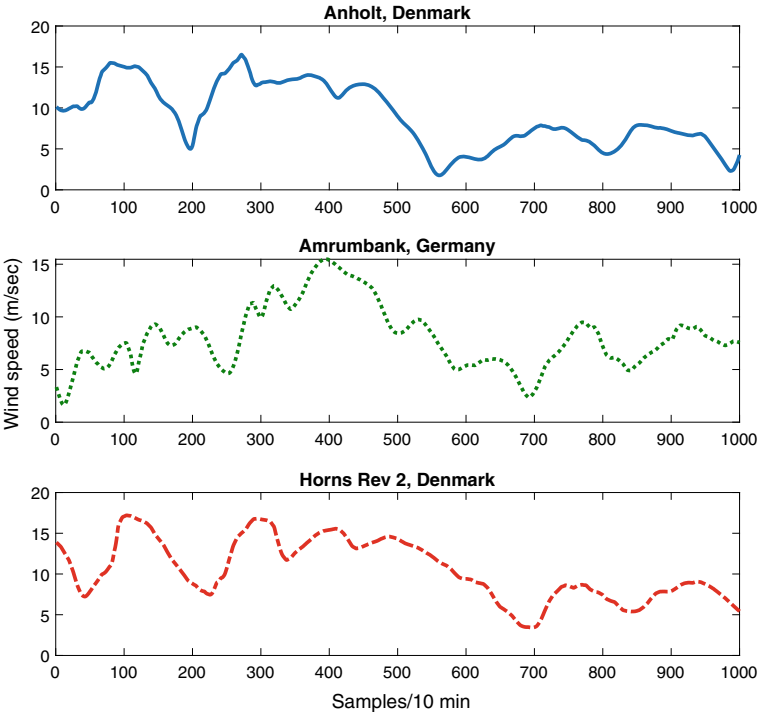

Fig. 3.8 Wind speed time series for offshore wind farms

Based on SAW method, we evaluate the performance scores for alternatives. First, the decision matrix is normalized based on beneficial and non-beneficial criteria and is given as

$$\hat{H} = \begin{array}{c} \begin{matrix} C_1 & C_2 & C_3 \end{matrix} \\ \begin{pmatrix} 0.3750 & 0.2000 & 0.1111 \\ 1.0000 & 0.2500 & 0.1667 \\ 1.0000 & 1.0000 & 1.0000 \\ 0.3333 & 0.1429 & 0.1250 \end{pmatrix} \end{array}.$$

The weights are calculated using entropy method and are given as $w = \{0.3893, 0.2625, 0.3483\}$ and the performance scores are listed in Table 3.13.

Next, we use the TOPSIS method to solve the MCDM problem with the normalized decision matrix calculated as per (2.6), and given as

$$\hat{H} = \begin{bmatrix} 0.6266 & 0.5241 & 0.6671 \\ 0.2350 & 0.4193 & 0.4447 \\ 0.2350 & 0.1048 & 0.0741 \\ 0.7049 & 0.7338 & 0.5930 \end{bmatrix}. \tag{3.14}$$

Table 3.13 Ranking for alternatives based on SAW method for offshore wind farm site

Alternatives	PS	CPS	Ranking
A_1	0.2372	0.2372	4
A_2	0.5129	0.8206	2
A_3	1.0000	2.2175	1
A_4	0.2108	0.3019	3

Table 3.14 Ranking using the TOPSIS method for offshore wind farm site

Alternatives	PS	CPS	Ranking
A_1	0.0610	0.0610	3
A_2	0.5086	0.8137	2
A_3	1.0000	2.2175	1
A_4	0.0082	0.0131	4

Using entropy method stated in Sect. 2.2.1, weights can be determined and are given as

$$w = \{0.2602,\ 0.3437,\ 0.3961\}. \tag{3.15}$$

Positive and negative ideal solutions are worked out using (2.8) and (2.9), and are given as

$$S^+ = \{0.0611,\ 0.0360,\ 0.0294\},\ S^- = \{0.1834,\ 0.2522,\ 0.2642\}.$$

Further, the Euclidean distance from the PIS and NIS is calculated using (2.11), where $p = 2$, and is found as

$$D^+ = \{0.0432,\ 0.0166,\ 0,\ 0.0520\}, \tag{3.16}$$

$$D^- = \{0.0028,\ 0.0172,\ 0.0584,\ 0.0004\}. \tag{3.17}$$

Table 3.14 depicts the ranking for alternatives based on TOPSIS method.

On the lines of same decision matrix, the MCDM problem is approached with COPRAS method. However, for normalization, we use (2.6)

$$\hat{H} = \begin{bmatrix} 0.6266 & 0.5241 & 0.6671 \\ 0.2350 & 0.4193 & 0.4447 \\ 0.2350 & 0.1048 & 0.0741 \\ 0.7049 & 0.7338 & 0.5930 \end{bmatrix}. \tag{3.18}$$

Based on entropy method described in (Sect. 2.2.1), the weights are given as

$$w = \{0.2602,\ 0.3437,\ 0.3961\}. \tag{3.19}$$

Table 3.15 Ranking strategies for offshore wind farm site based on COPRAS method

Alternatives	PS	CPS	Ranking
A_1	0.2083	0.2083	4
A_2	0.0172	0.5307	2
A_3	1.0000	2.2175	1
A_4	0.1887	0.3019	3

Using Eqs. (2.14)–(2.16), the performance scores are computed and final ranks are calculated based on CPS as listed in Table 3.15.

This chapter deals with multi-criteria methods for solving the decision-making problem for hybrid operation of wind farms. The proposed approach is based on identifying the criteria that affect the hybrid operation. In our definition of hybrid wind farms, we have a farm along with a system of batteries that function in events of deficit wind power. Two datasets for wind sites near Massachusetts labeled as D1 and D2 are taken for this study. Wind powers are forecasted using least square support vector regression by training a set of 800 samples. The forecasted wind power is then compared with actual wind power and the deficit power is calculated based on error in forecasting. The normalized cost score is obtained for each alternative based on minimization normalization. Three methods, namely, SAW, TOPSIS, and COPRAS are used to find out the performance scores. A cumulative priority score is then used to select the best alternative. TOPSIS, SAW, and COPRAS methods indicated A_3 to be the best alternative, while rank reversal is observed in case of alternatives A_1 and A_4 for COPRAS method. Meanwhile, we also test the proposed approach for hilly and offshore wind farm sites and results reveal that alternative A_3 is the most preferred choice.

References

1. Center WE (2019) Bishop and clerks, nantucket sound | wind energy center. https://www.umass.edu/windenergy/resourcedata/Bishop_and_Clerks. Accessed on 20 Feb 2019)
2. Deng Y, Yu Z, Liu S (2010) A review on scale and siting of wind farms in China. Wind Energy 14(3):463–470
3. Garni HA, Kassem A, Awasthi A, Komljenovic D, Al-Haddad K (2016) A multicriteria decision making approach for evaluating renewable power generation sources in Saudi Arabia. Sustain Energy Technol Assess 16:137–150
4. Georgiou D, Mohammed ES, Rozakis S (2015) Multi-criteria decision making on the energy supply configuration of autonomous desalination units. Renew Energy 75:459–467
5. Haralambopoulos D, Polatidis H (2003) Renewable energy projects: structuring a multi-criteria group decision-making framework. Renew Energy 28(6):961–973
6. Henriot A (2015) Economic curtailment of intermittent renewable energy sources. Energy Econ 49:370–379
7. ho Hur S (2018) Modelling and control of a wind turbine and farm. Energy 156:360–370. https://doi.org/10.1016/j.energy.2018.05.071

8. Jahan A, Edwards KL (2015) A state-of-the-art survey on the influence of normalization techniques in ranking: improving the materials selection process in engineering design. Mater Des 1980–2015(65):335–342
9. Keyser WD, Peeters P (1996) A note on the use of PROMETHEE multicriteria methods. Eur J Oper Res 89(3):457–461
10. Kolios A, Rodriguez-Tsouroukdissian A, Salonitis K (2016) Multi-criteria decision analysis of offshore wind turbines support structures under stochastic inputs. Ships Offshore Struct 11(1):38–49
11. Kundakcı N (2018) An integrated method using MACBETH and EDAS methods for evaluating steam boiler alternatives. J Multi-Criteria Decis Anal
12. Lee AH, Hung MC, Kang HY, Pearn W (2012) A wind turbine evaluation model under a multi-criteria decision making environment. Energy Convers Manag 64:289–300
13. Lowson MV (1993) Assessment and prediction of wind turbine noise. Technical report, United Kingdom. http://inis.iaea.org/search/search.aspx?orig_q=RN:25009728, eTSU-W–13/00284/REP
14. Mahdy M, Bahaj AS (2018) Multi criteria decision analysis for offshore wind energy potential in Egypt. Renew Energy 118:278–289
15. Majumder M (2015) Impact of urbanization on water shortage in face of climatic aberrations. Springer, Singapore
16. Nguyen CL, Lee HH, Chun TW (2015) Cost-optimized battery capacity and short-term power dispatch control for wind farm. IEEE Trans Ind Appl 51(1):595–606
17. Patel P, Shandilya A, Deb D (2017) Optimized hybrid wind power generation with forecasting algorithms and battery life considerations. In: 2017 IEEE power and energy conference at Illinois (PECI). IEEE
18. Roth M (2018) Renewable energy and landscape quality. Jovis Verlag, Berlin
19. Saaty R (1987) The analytic hierarchy process- what it is and how it is used. Math. Model. 9(3):161–176
20. Tennekes H (1973) The logarithmic wind profile. J Atmos Sci 30(2):234–238
21. Wang YM, Luo Y (2009) On rank reversal in decision analysis. Math Comput Model 49(5–6):1221–1229. https://doi.org/10.1016/j.mcm.2008.06.019

Chapter 4
Fuzzy-Based Decision-Making in Hybrid Wind Farms

Growing energy demands have heightened the concern for renewables in recent times. A hybrid wind farm operation is often taken into consideration while interconnecting large power systems with the decision being dependent on the wind farm operator. The choice of best strategy results in an optimal market scenario. The current work deals with multi-criteria decision-making for hybrid wind farms. A tangible and non-tangible effect of wind phenomenon is considered to obtain the cumulative priority of each alternative based on a set of criteria.

As already explained so far, decision-making is the process of ascertaining the best possible option among feasible alternatives in an environment where goals, limitations, and outcomes of actions taken are imprecisely available and in such conditions, fuzzy set theory can be used to deal with imprecision in the decision-making. Owing to stochastic nature of wind, fuzzy-based TOPSIS and COPRAS methods are candidate methods to be implemented to ascertain the best solution. Further, uncertainties in decision-making are considered to evaluate the rank reversal phenomenon among the set of alternatives. Results indicate that paying penalty for deficit power borrowed from neighboring wind farm is the best option.

4.1 Introduction

Uncertainties in wind speed affect energy assessment, economic study of wind farms, micro-siting, and wind speed prediction. Fuzzy logic and probability distribution technique are extensively used to bridge any shortfall caused due to such randomness. Fuzzy logic finds its application in modeling energy planning activities and deals with real-time application by assigning semantic values. Various methods exist that express the said uncertainty in terms of membership function of triangular, trapezoidal, and Gaussian type. Jafarian et al. have explored the annual wind energy output for 25 different sites in the Netherlands based on fuzzy modeling and ANN [11].

H. S. Dhiman and D. Deb, *Decision and Control in Hybrid Wind Farms*,
Studies in Systems, Decision and Control 253,
https://doi.org/10.1007/978-981-15-0275-0_4

The wind energy estimated using fuzzy technique and ANN is compared with the conventional methods like random number generation, Kiranoudis method, and one-two-three equation method. The proposed method is validated for two turbine models (S47 and E82). In terms of forecasting, Wang et al. have presented a hybrid approach using fuzzy time series model for Hainan wind farm of China [18]. The model is divided into two parts. First, the outliers are determined based on initial ARMA model, and second, the wind forecast is carried out using a neural network based on a backpropagation principle. Fuzzy logic is also applied in order to mitigate fluctuations in electromagnetic torque in wind energy conversion systems (WECS). Bezza et al. describe an MPPT fuzzy controller for reducing the effect of wind fluctuations on a 10 W doubly-fed induction generator (DFIG). The rotor side converter (RSC) of DFIG is controlled using a fuzzy logic controller [3].

In terms of optimization, Benlarbi et al. have demonstrated a fuzzy logic-based optimization method to maximize the overall efficiency of PV water pumping system. Fuzzy logic is used to tune the duty ratio of chopper-driven water pump connected via an induction motor [2]. Decision-making is an important market procedure with transmission and distribution operators trying to maximize their profits by implementing optimal strategy. Multi-criteria decision-making (MCDM) which has been in limelight recently, allows decision-makers to choose the best possible alternative. Among the MCDM methods, analytical hierarchical process (AHP), technique for order or preference by similarity to ideal solution (TOPSIS), and complex proportional assessment (COPRAS) are popular choices that are often practiced by decision-makers globally, as has been seen in the last chapter.

Fuzzy-based analytic network process (FANP) method has been applied by Shafiee to assess the risk connected to offshore wind farms [17]. Such a wind farm with a total of 30 2 MW wind turbines is studied and four methodologies that mitigate the operational risk are studied to identify the best alternative. The results from FANP are compared with AHP. Further, Chen et al. have demonstrated a fuzzy AHP method to select the best plan or strategy for environment-watershed in Taiwan [7]. Fuzzy logic is used to assign weights to criteria in terms of linguistic scale. Wang Chen et al. have presented fuzzy AHP and fuzzy TOPSIS methods to evaluate the green supplier selection problem given the environmental and economic factors [6]. Chamodrakas et al. have discussed the supplier selection problem for electronic marketplaces using fuzzy preference programming where the initial screening of the alternatives is done through hard limits on selection attributes [4].

Multi-criteria decision-making is also used to select suitable wind turbines as explored by Lee et al. using interpretive structural modeling (ISM) and fuzzy analytical hierarchical process (FAHP) [12]. For each criterion, a sub-criterion is identified, and a binary matrix indicating relationship between them is created. Ghosh et al. have carried out a study on vulnerability assessment of wetlands in Kolkata using fuzzy MCDM techniques [8]. Results reveal that 60% of area lies between medium to high wetland conversion zones and thus helps the municipal authority to evaluate vulnerable zones nearby. Zhao et al. have described an integrated fuzzy MCDM approach to select the best battery energy storage system (BESS) considering risks associated with technological, social, environmental factors [20]. Empirical analysis

shows that lithium-ion battery is more preferred followed by sodium sulfide battery. Further, fuzzy Delphi and fuzzy AHP methods are applied to select an appropriate lubricant regenerative technology. In this work, fuzzy Delphi is used to extract the critical factors of regenerative technology through rigorous interviews and questionnaires and fuzzy AHP method is used to rank the alternatives [10]. Further, Hsu et al. have applied a combined fuzzy AHP and fuzzy VIKOR method to evaluate the service gaps for a case study of cinema in Taiwan where managerial strategies are empirically assessed [9]. Results revealed that considering customer choices and perceptions, managers can suitably improve the gaps in service quality in a fuzzy environment. Samanlioglu et al. have demonstrated a fuzzy AHP and fuzzy TOPSIS MCDM approach to select IT personnel for a Turkish diary [16]. A group of three decision-makers is involved in assessing the alternatives for which fuzzy TOPSIS is implemented with the criteria weights as given by fuzzy AHP. The main highlight of this chapter lies in formulating the hybrid operation of wind farms along with identifying a set of criteria with tangible and non-tangible effect of dynamic wind phenomenon. Finally, fuzzy TOPSIS and fuzzy COPRAS methods are applied to address the hybrid operation of wind farms and in case of dynamic decision matrices, rank reversal phenomenon is studied and is validated for wind farm application. This chapter is organized as follows: Sect. 4.2 discusses the fuzzy basics along with fuzzy MCDM techniques: fuzzy TOPSIS and fuzzy COPRAS, for hybrid operation of wind farms. Section 4.3 highlights results and discussions for a problem related to three wind farms.

4.2 Fuzzy MCDM: Materials and Methods

In this section, we present fuzzy-based MCDM approach to solve the said hybrid wind farm problem. A generic flowchart for fuzzy MCDM is illustrated in Fig. 4.1. Owing to random nature of wind, fuzzy logic helps decision-makers to assign linguistic values to the alternatives for a given criteria (beneficial and non-beneficial).

Qualitative importance of criteria is looked at in order to mitigate any bias generated from favorable situations. Next, we discuss fuzzy numbers and basic arithmetic operations useful in MCDM approach.

4.2.1 Fuzzy Numbers: Fundamentals

A fuzzy set $\bar{B}$ in X is defined as

$$\bar{B} = \{x, \mu_B(x)\}, x \in X, \tag{4.1}$$

where $\mu_B(x) : X \rightarrow [0, 1]$ represents a membership function of $\bar{B}$ and $\mu_B(x)$ is the degree of pertinence of x in $\mu_B(x)$. Given $\mu_B(x)$ has a value in between 0 and 1, x

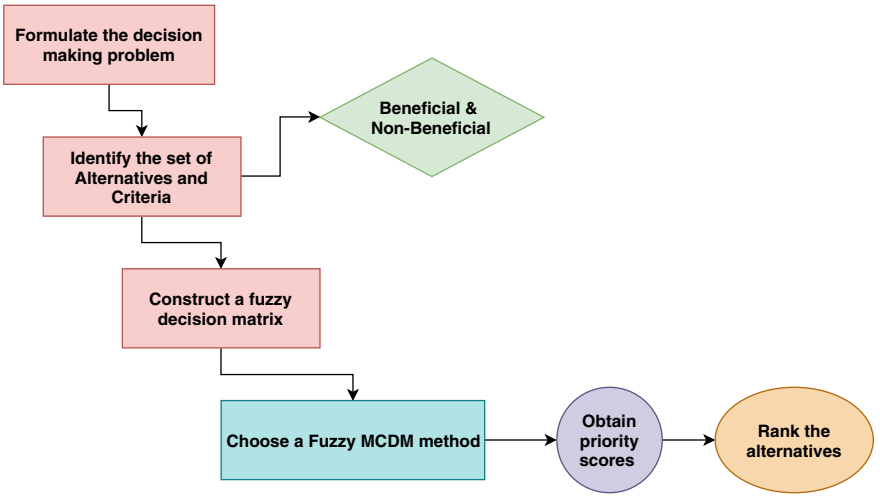

Fig. 4.1 Schematic representation of fuzzy MCDM problem for wind farms

belongs to a fuzzy set $\bar{B}$. Triangular fuzzy numbers (TFNs) are often used to express a degree of uncertainty associated with alternatives [14]. A membership function $\mu_B(x)$ for TFNs $\bar{B} = (e, f, g)$ is given as

$$\mu_B(x) = \begin{cases} 0 & \text{for } x < e \\ \dfrac{x-e}{f-e} & \text{for } e \le x \le f \\ \dfrac{x-g}{g-f} & \text{for } g \le x \le h \\ 0 & \text{for } x > f, \end{cases} \tag{4.2}$$

where (e, f, g) are the real numbers. The arithmetic operations on fuzzy numbers $\bar{B}_1 = (e_1, f_1, g_1)$ and $\bar{B}_2 = (e_2, f_2, g_2)$ are described as

1. Addition: $\bar{B}_1 + \bar{B}_2 = (e_1 + e_2, f_1 + f_2, g_1 + g_2)$.
2. Subtraction: $\bar{B}_1 - \bar{B}_2 = (e_1 - e_2, f_1 - f_2, g_1 - g_2)$.
3. Multiplication: $\bar{B}_1 \times \bar{B}_2 = (e_1 \times e_2, f_1 \times f_2, g_1 \times g_2)$.
4. Division: $\bar{B}_1 \div \bar{B}_2 = (e_1 \div e_2, f_1 \div f_2, g_1 \div g_2)$.
5. Inverse of a TFN: $\bar{B}_1^{-1} = \left(\frac{1}{g_1}, \frac{1}{f_1}, \frac{1}{e_1}\right)$.

4.2.2 Fuzzy TOPSIS

Proposed by Chen, fuzzy TOPSIS is implemented in decision-making processes that lack certainty [5]. TOPSIS method is further extended by assigning linguistic values as performance scores in the decision matrix. Since decision-making varies from person to person, fuzzy TOPSIS method is carried out among k decision-makers for k existing fuzzy decision matrices.

This method is appropriate for solving group decision-making under the fuzzy environment. In this method, the important weights associated with various criteria are given as linguistic variables with the values given as fuzzy numbers. The assessments of criteria are provided in linguistic variables whose values are given as fuzzy numbers. The decision-makers utilize the linguistic variables and their given values to evaluate the importance of the criteria.

The procedure of fuzzy TOPSIS is given as follows:

1. Obtain aggregate weights ($\tilde{w}_{ij}$) of the criteria assessed by k decision-makers and also the aggregate performance score ($\tilde{h}_{ij}$) of alternatives A_i ($i = 1, 2, ...m$) with respect to C_j ($j = 1, 2, ...n$) given by

$$\tilde{w}_{ij} = \frac{1}{k}\left(\tilde{w}_{ij}^1 + \tilde{w}_{ij}^2 + ... + \tilde{w}_{ij}^k\right), \quad \tilde{h}_{ij} = \frac{1}{k}\left(\tilde{h}_{ij}^1 + \tilde{h}_{ij}^2 + ... + \tilde{h}_{ij}^k\right). \tag{4.3}$$

2. Using (4.3), aggregate decision matrix H is given as

$$H = \begin{array}{c} \begin{matrix} C_1 & C_2 & \dots & C_n \end{matrix} \\ \begin{pmatrix} \tilde{h}_{11} & \tilde{h}_{12} & \dots & \tilde{h}_{1j} \\ \tilde{h}_{21} & \tilde{h}_{22} & \dots & \tilde{h}_{2j} \\ \vdots & \vdots & & \vdots \\ \tilde{h}_{i1} & \dots & \dots & \tilde{h}_{ij} \end{pmatrix} \end{array} \begin{matrix} A_1 \\ A_2 \\ \vdots \\ A_m. \end{matrix}$$

3. A normalized fuzzy decision matrix D with its elements $\tilde{d}_{ij}$ for beneficial criteria and non-beneficial criteria is given as

$$\tilde{d}_{ij} = \left(\frac{e_{ij}}{g_j^+}, \frac{f_{ij}}{g_j^+}, \frac{g_{ij}}{g_j^+}\right) \; ; g_j^+ = \textbf{max} \; g_{ij}, \tag{4.4}$$

$$\tilde{d}_{ij} = \left(\frac{e_j^-}{g_{ij}}, \frac{e_j^-}{f_{ij}}, \frac{e_j^-}{e_{ij}}\right) \; ; e_j^- = \textbf{min} \; e_{ij}. \tag{4.5}$$

   The normalization is done so as to preserve the property that the ranges of normalized triangular fuzzy numbers belong to [0, 1].

4. Obtain the weighted normalized decision matrix given weights $\tilde{w}_{ij}$ for each criterion

$$\tilde{H} = [\tilde{h}_{ij}]_{m \times n} = \tilde{w}_{ij} \times \tilde{d}_{ij}. \tag{4.6}$$

5. Now, obtain fuzzy positive (FPNIS) and negative ideal solution (FNIS) as

$$G^+ = \{\tilde{h}_1^+, \tilde{h}_2^+, ..., \tilde{h}_m^+\},\ G^- = \{\tilde{h}_1^-, \tilde{h}_2^-, ..., \tilde{h}_m^-\}. \tag{4.7}$$

6. Use euclidean distances z_j^+ and z_j^- for each alternative from their respective FPIS and FNIS:

$$z_i^+ = \sum_{j=1}^{n} z_p(\tilde{h}_{ij}, \tilde{h}_j^+),\ \ z_i^- = \sum_{j=1}^{n} z_p(\tilde{h}_{ij}, \tilde{h}_j^-), \tag{4.8}$$

$$z_p(x, y) = \sqrt{\frac{1}{3}(e_x - e_y)^2 + (f_x - f_y)^2 + (g_x - g_y)^2}, \tag{4.9}$$

and $x = (e_x, f_x, g_x)$ and $y = (e_y, f_y, g_y)$ as the two TFNs and $z_p(x, y)$ as the euclidean distance according to vertex method, we obtain priority score (O_i) for each alternative and rank them in descending order:

$$O_i = \frac{z_i^-}{z_i^- + z_i^+}. \tag{4.10}$$

4.2.3 Fuzzy COPRAS

Complex proportional assessment (COPRAS) method has been successfully employed to study decision-making process since 1994 Zavadskas et al. implemented the same to solve problems related to construction management and economics [19]. However, due to uncertainties present in the decision-making process, a fuzzy COPRAS method that essentially thrives on COPRAS methodology is adopted to solve the MCDM problem. Bekar et al. have presented a fuzzy COPRAS method to assess the performance measures in productive maintenance [1]. In this paper, a comparative analysis between COPRAS method with grey relations and fuzzy COPRAS is carried out. Further, Nourianfar et al. have explored the selection problem in supply chain management using fuzzy COPRAS method [13]. Here, the criteria weights are assigned with trapezoidal fuzzy numbers (TrFNs) and supplier selection problem is solved based on four criteria: (i) product quality, (ii) relationship closeness, (iii) delivery performance, and (iv) price. Now, we discuss the steps followed to solve MCDM problem using fuzzy COPRAS method.

1. Formulate the MCDM problem based on a set of alternatives $(A_i; i = 1, 2, ..., m)$ and criteria $(C_j; j = 1, 2, ..., n)$ and construct a fuzzy decision matrix.
2. Obtain the normalized fuzzy decision matrix using (4.4) and (4.5) as in fuzzy TOPSIS method.
3. For each alternative A_i, obtain aggregate beneficial and non-beneficial indices T_i^+ and T_i^- as

$$\tilde{T}_i^+ = \left\{ \sum_{j=1}^{t} \tilde{h}_{ij}^e, \sum_{j=1}^{t} \tilde{h}_{ij}^f, \sum_{j=1}^{t} \tilde{h}_{ij}^g \right\}, \tilde{T}_i^- = \left\{ \sum_{j=t+1}^{n} \tilde{h}_{ij}^e, \sum_{j=t+1}^{n} \tilde{h}_{ij}^f, \sum_{j=t+1}^{n} \tilde{h}_{ij}^g \right\}, \tag{4.11}$$

where $j = 1, 2, ...t$ are the beneficial criteria and $j = t+1, t+2, \ldots, n$ are the non-beneficial criteria.

4. Using (4.12), determine the crisp values $U(\tilde{B})$ for each alternative A_i from the fuzzy numbers ($\tilde{B} = (e, f, g)$) obtained in the previous step:

$$U(\tilde{B}) = 2e(1-\alpha) + \frac{g-f}{2}(1-\alpha)^2, \tag{4.12}$$

where $\alpha \in [0, 1]$ is the alpha-cut of fuzzy set $\bar{B}$ in X such that $\bar{B}^\alpha = \{x \in X : \mu_B(x) > \alpha\}$.

5. Obtain the priority scores and rank them in the order of descending degree:

$$XC_i = \frac{U_i}{U_{max}} \times 100\%. \tag{4.13}$$

The current fuzzy TOPSIS and fuzzy COPRAS methods are applied to solve the problem of hybrid wind farm operation where a set of four alternatives are assessed based on three criteria. The fuzzy decision matrix is constructed based on linguistic scores assigned to an alternative with respect to each criterion. Since all the criteria in our MCDM problem are non-beneficial, we define the linguistic scores where the least preferred alternative is assigned the highest score and vice versa. Table 4.1 describes the linguistic scores (LS) used to construct the fuzzy decision matrix.

Since wake effect results in large power loss in a wind farm, compensating the losses via paying penalty will not benefit economically to a farm operator. In such cases, paying an equivalent penalty for borrowed power is a better option. The same methodology of borrowing power is best suited for wind curtailment situation as it is not economical to discharge power in a large magnitude. While in the case of forced outages, it is evident that removal of a turbine unit(s) leads to a sudden reduction in

Table 4.1 Performance scores for decision matrix [15]

Importance	LS as per AHP	LS in this work
Equally preferred (EP)	(1, 1, 3)	(7, 9, 9)
Moderately preferred (MP)	(1, 3, 5)	(5, 7, 9)
Strongly preferred (SP)	(3, 5, 7)	(3, 5, 7)
Very strongly preferred (VSP)	(5, 7, 9)	(1, 3, 5)
Extremely preferred (XP)	(7, 9, 9)	(1, 1, 3)

Table 4.2 Linguistic scores for criteria weights

Importance	LS
Very low (VL)	(1, 1, 3)
Low (L)	(1, 3, 5)
Average (AVG)	(3, 5, 7)
High (H)	(5, 7, 9)
Very high (VH)	(7, 9, 9)

total wind farm capacity, however, such drastic scenarios can be treated economically by using alternative A_2 as discussed in Chap. 3.

As per the linguistic scores stated in Table 4.2, the fuzzy decision matrix (FDM) for our MCDM problem is given as

$$H = \begin{array}{c} \begin{matrix} C_1 & C_2 & C_3 \end{matrix} \\ \begin{pmatrix} MP & MP & EP \\ VSP & SP & SP \\ XP & VSP & VSP \\ EP & EP & EP \end{pmatrix} \end{array} \begin{matrix} A_1 \\ A_2 \\ A_3 \\ A_4. \end{matrix}$$

Further, in terms of TFNs, the fuzzy decision matrix is given as

$$H = \begin{array}{c} \begin{matrix} C_1 & C_2 & C_3 \end{matrix} \\ \begin{pmatrix} (5,7,9) & (5,7,9) & (7,9,9) \\ (1,3,5) & (3,5,7) & (3,5,7) \\ (1,1,3) & (1,3,5) & (1,3,5) \\ (7,9,9) & (7,9,9) & (7,9,9) \end{pmatrix} \end{array} \begin{matrix} A_1 \\ A_2 \\ A_3 \\ A_4. \end{matrix}$$

4.3 Results and Discussions

Next, we present an application of fuzzy TOPSIS method on a hybrid wind farm problem. Three onshore wind farms, Bishop and Clerks, Paxton, and Blandford are selected in order to study the hybrid operation pertaining to four alternatives/methodologies discussed in the last chapter. The wind speed data for all the three sites measured at a hub height of 61 m using a cup anemometer centrally available at Wind energy center, University of Massachusetts. The datasets are labeled X1 (June 2006) and X2 (June 2013) for three wind farms. The wind speed time series for two datasets is illustrated in Figs. 4.2 and 4.3.

For all the three wind farms, we assume a rotor diameter of 120 m and wind direction facing directly the wind turbines. The power produced from the three wind

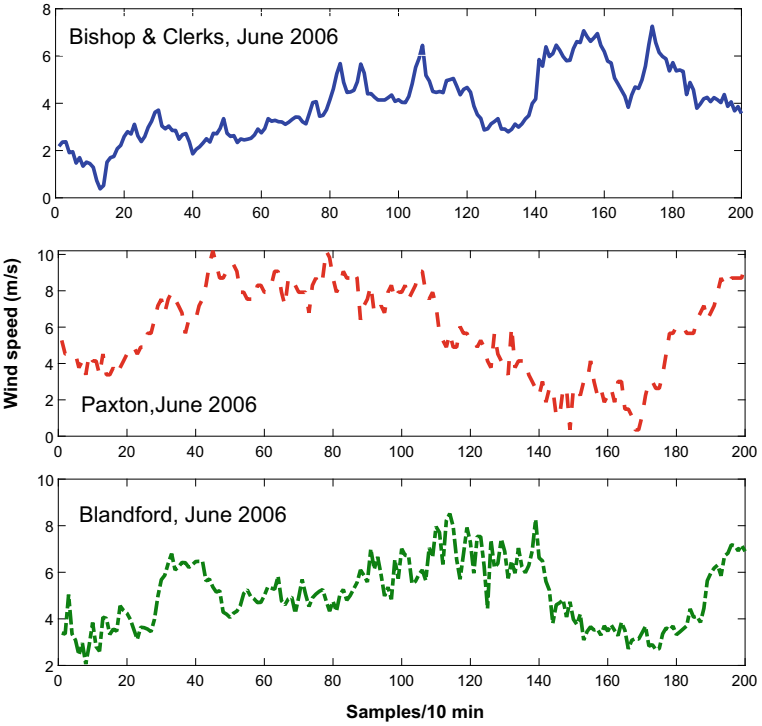

Fig. 4.2 Wind speed pattern for three wind farms in Massachusetts, June 2006

farms is transmitted to the utility grid. Here the decision-making approach is carried out for wind farm Bishop and Clerks. Least square support vector regression (LSSVR) based technique is used for wind speed forecasting and then it is transformed into wind power. The penalty cost is determined for each alternative when the forecasted power exceeds the actual one. The cost for compensating 1 kW of deficit power in each alternative as discussed in the previous chapter is $\beta_w = \$\ 0.5$, $\zeta_s = \$\ 0.75$, $\alpha_z = \$\ 0.4$ and $\delta_x = \$\ 0.8$. Due to consecutive charging and discharging events, the penalty cost for alternative A_4 is highest in order to preserve BESS life. Table 4.3 highlights the penalty cost (PC) (in \$) and normalized cost score for each alternative for two datasets X1 and X2.

Based on minimum normalization technique, the normalized cost scores are determined. In this case, a score of 1 is assigned to the alternative with minimum penalty cost. This reflects the tangible effect incurred to the farm operator from the penalty cost. Likewise, the intangible effect is determined by using the fuzzy MCDM methods. The overall score for the alternatives is worked out by a cumulative priority score (CPS) which is multiplication of priority score (PS) and normalized cost score (NCS). Using fuzzy TOPSIS method, the ranks for the alternatives are computed. The fuzzy decision matrix (FDM) in terms of TFNs normalized according to (4.5)

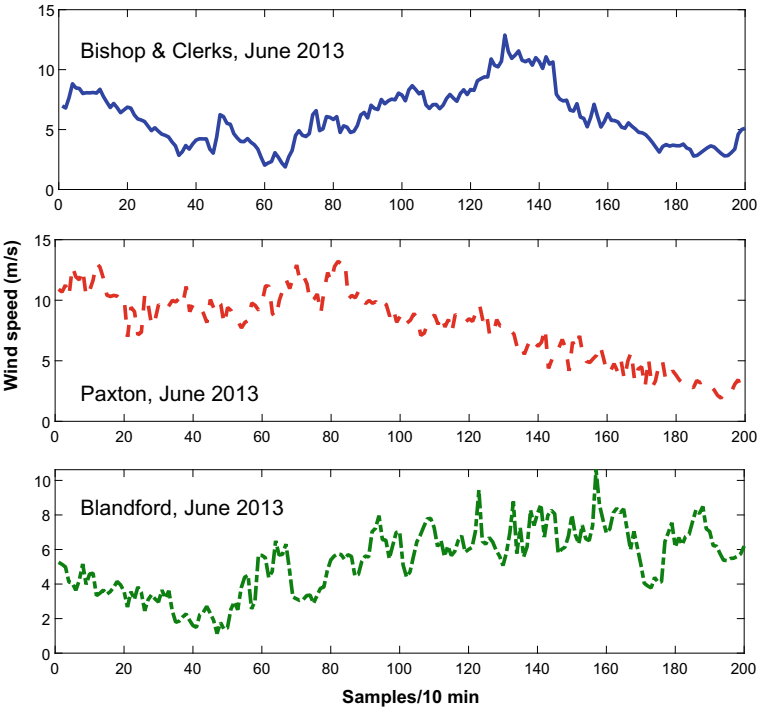

Fig. 4.3 Wind speed pattern for three wind farms in Massachusetts, June 2013

Table 4.3 Penalty cost and normalized cost score for dataset D1 and D2

Alternatives	X1		X2	
	PC ($)	NCS	PC ($)	NCS
A_1	1620.8	0.9880	1551.3	1.0000
A_2	1601.4	1.0000	1921.2	0.8075
A_3	1612.7	0.9930	3392.5	0.4573
A_4	2593.3	0.6175	2482.1	0.6250

is given as

$$H = \begin{array}{c} \begin{matrix} C_1 & C_2 & C_3 \end{matrix} \\ \begin{pmatrix} (5,7,9) & (5,7,9) & (7,9,9) \\ (1,3,5) & (3,5,7) & (3,5,7) \\ (1,1,3) & (1,3,5) & (1,3,5) \\ (7,9,9) & (7,9,9) & (7,9,9) \end{pmatrix} \end{array} \begin{matrix} A_1 \\ A_2 \\ A_3 \\ A_4, \end{matrix}$$

Table 4.4 Euclidean distance and closeness coefficient for each alternative

Alternatives	z^+	z^-	O
A_1	9.9542	0.3933	0.0380
A_2	7.5398	3.3752	0.3095
A_3	0	10.3223	1.0000
A_4	10.3223	0	0.0000

$$D = \begin{matrix} \\ A_1 \\ A_2 \\ A_3 \\ A_4. \end{matrix} \begin{matrix} \begin{matrix} C_1 & C_2 & C_3 \end{matrix} \\ \begin{pmatrix} (0.11, 0.142, 0.2) & (0.11, 0.14, 0.2) & (0.11, 0.11, 0.14) \\ (0.2, 0.33, 1) & (0.14, 0.2, 0.33) & (0.14, 0.2, 0.333) \\ (0.33, 1, 1) & (0.2, 0.33, 1) & (0.2, 0.33, 1) \\ (0.11, 0.11, 0.14) & (0.1, 0.11, 0.14) & (0.11, 0.11, 0.14) \end{pmatrix} \end{matrix}$$

The corresponding weights for criteria are expressed in TFNs as $\tilde{w}_1 = H, \tilde{w}_2 = VH, \tilde{w}_3 = AVG$, which further can be expressed in terms of TFNs as $\tilde{w}_1 = (5, 7, 9), \tilde{w}_2 = (7, 9, 9), \tilde{w}_3 = (3, 5, 7)$. The weighted normalized fuzzy decision matrix is obtained using (4.6) and is given as

$$\tilde{H} = \begin{matrix} \\ A_1 \\ A_2 \\ A_3 \\ A_4. \end{matrix} \begin{matrix} \begin{matrix} C_1 & C_2 & C_3 \end{matrix} \\ \begin{pmatrix} (0.56, 1, 0.6) & (0.78, 1.28, 1) & (1, 1, 1) \\ (1, 0.33, 3) & (1, 1.8, 1.6) & (1.28, 1.8, 2.3) \\ (1.67, 7, 3) & (1.4, 3, 5) & (1.8, 3, 7) \\ (0.55, 0.78, 0.42) & (0.77, 1, 0.71) & (1, 1, 1) \end{pmatrix} \end{matrix}$$

Next, we identify the FPIS and FNIS using (4.7), given as

$$G^+ = \{(1.666, 7, 3), (1.4, 3, 5), (1.8, 3, 7)\} \tag{4.14}$$

$$G^- = \{(0.55, 0.77, 0.42), (0.77, 1, 0.71), (1, 1, 1)\}. \tag{4.15}$$

The euclidean distance between each TFN of weighted normalized fuzzy decision matrix and FPIS and FNIS is provided in Table 4.4.

We observe that the most preferred alternative is A_3 followed by A_2, A_1 and A_4. The cumulative priority scores for datasets X1 and X2 are tabulated in Table 4.5.

Next, we discuss the MCDM results using fuzzy COPRAS method. The weighted fuzzy decision matrix obtained in fuzzy TOPSIS is then evaluated to obtain the aggregate beneficial and non-beneficial indices for each alternative using (4.11). Since all the criteria in our MCDM problem are non-beneficial, we evaluate $\tilde{T}_i^-$ and are given as

$$\tilde{T}_i^- = \{(2.333, 3.2857, 2.6), (3.2857, 5.9333, 7.000), (4.8667, 13, 15), (2.333, 2.778, 2.1429)\}. \tag{4.16}$$

Table 4.5 Cumulative priority score and ranking based on fuzzy TOPSIS method

Alternatives	X1		X2	
	PS	CPS	PS	CPS
A_1	0.0380	0.0376	0.0380	0.0380
A_2	0.3095	0.3095	0.3095	0.2499
A_3	1.0000	0.9930	1.0000	0.4573
A_4	0.0000	0.0000	0.0000	0.0000
Alternatives	Ranking			
	X1		X2	
A_1	3		3	
A_2	2		2	
A_3	1		1	
A_4	4		4	

Table 4.6 Crisp numbers for fuzzy indices ($\tilde{T}_i^-$)

Alpha-cut	A_1	A_2	A_3	A_4
0.1	3.9223	6.3463	9.5700	3.9429
0.2	3.5139	5.5985	8.4267	3.5302
0.3	3.0987	4.8613	7.3033	3.1111
0.4	2.6766	4.1349	6.2000	2.6857
0.5	2.2476	3.4190	5.1167	2.2540
0.6	1.8118	2.7139	4.0533	1.8159
0.7	1.3691	2.0194	3.0100	1.3714
0.8	0.9196	1.3356	1.9867	0.9206
0.9	0.4632	0.6625	0.9833	0.4635
1.0	0	0	0	0

Next, we convert the fuzzy indices obtained in (4.16) using (4.12) for different alpha-cut values into a crisp number. Table 4.6 highlights the crisp numbers for each alternative A_i.

The crisp numbers highlighted in Table 4.6 are then evaluated for the priority scores (XC) using (4.13). The ranking for alternatives based on cumulative priority scores for $\alpha = 0.5$ is listed in Table 4.7.

From Table 4.7, we observe that for dataset X2, the ranks for alternatives A_1 and A_2 are reversed in terms of cumulative priority score which is due to a higher normalized cost score. Such rank reversal is tested by removing one of the alternatives from the fuzzy decision matrix and then testing further the remainder of the alternatives for the best option. The rank reversal due to dynamic decision matrices is tested under fuzzy TOPSIS and fuzzy COPRAS methods.

Table 4.7 Cumulative priority score and ranking based on fuzzy COPRAS method

Alternatives	X1		X2	
	PS	CPS	PS	CPS
A_1	43.17	42.65	43.17	43.17
A_2	66.69	66.69	66.69	53.85
A_3	100.00	99.300	100.00	45.73
A_4	43.31	26.74	43.31	27.07
Alternatives	Ranking			
	X1		X2	
A_1	3		3	
A_2	2		1	
A_3	1		2	
A_4	4		4	

Table 4.8 Ranking of alternative strategies under dynamic decision matrices in fuzzy TOPSIS (**M1**) and fuzzy COPRAS (**M2**) methods

Alternatives	M1				M2		
	Initial rank	A_4	A_1	A_2	A_4	A_1	A_2
A_4	4	–	–	–	–	–	–
A_1	3	3	–	–	3	–	–
A_2	2	2	2	–	2	2	–
A_3	1	1	1	1	1	1	1

From Table 4.8, the effect of dynamic decision matrices can be seen on the rank of alternatives. In first case, when alternative A_4 is removed, A_3 is still the most preferred alternative followed by A_2 and A_1. Further, in next step, when alternative A_1 is removed, A_3 is ranked superior to A_2 indicating the most preferred strategy is paying penalty for deficit power by borrowing power from neighboring wind farm.

4.4 Fuzzy-Based Decision-Making for Hilly Wind Sites and Offshore Wind Farms

Hilly wind farm sites pose a lot of challenges in form of forecasting wind speed due to the uneven terrain. This causes wind farm operators to optimally select their strategy while paying penalty for the deficit wind power. The problem can be tackled by modeling the decision-making in a fuzzy environment where the elements of the decision matrix are TFNs. We use the datasets chosen in the previous chapter. Wind speed data from Challicum hills (Australia), Longyuan hills (Tibet) and Ngong hills (Kenya) is taken for the month of May 2019. The wind power is forecasted using

Table 4.9 Penalty cost and normalized cost score for hilly wind sites

Alternatives	PC ($)	NCS
A_1	52831	1.000
A_2	84530	1.600
A_3	59945	1.134
A_4	84530	1.600

Table 4.10 Ranking for alternatives based on fuzzy TOPSIS method for hilly wind sites

Alternatives	PS	CPS	Ranking
A_1	0.0380	0.0380	3
A_2	0.3095	0.4952	2
A_3	1.0000	1.1347	1
A_4	0.0000	0.0000	4

LSSVR technique with wind speed data segmented into training (800) and testing (200) set. The penalty cost for all the alternatives is evaluated and a normalized cost score is determined. With reference to the methodology discussed in previous sections, p_{2i}, $\hat{p}_{2i}$ represent the actual and forecasted wind power for Longyuan hills at ith instant. Similarly, p_{3i}, $\hat{p}_{3i}$ represent the actual and forecasted wind power for Ngong hills at ith instant. Table 4.9 depicts the normalized cost scores.

From Table 4.9, we can observe that alternative A_2 and A_4 incur maximum penalty to the wind farm operator. Now we evaluate the priority scores using fuzzy TOPSIS and fuzzy COPRAS methods. The fuzzy decision matrix remains the same for hilly wind sites. As the wind speed gets more pronounced due to hilly terrain, for criteria like wind curtailment and forced outage the best alternative is A_3. It is also worthwhile to note that in hilly areas the wind speed changes drastically, so to deal with such a large amount of wind power, charging and discharging the battery system is not suitable and can incur large penalty cost. The fuzzy decision matrix is

$$H = \begin{array}{c} \begin{matrix} C_1 & C_2 & C_3 \end{matrix} \\ \begin{pmatrix} (5,7,9) & (5,7,9) & (7,9,9) \\ (1,3,5) & (3,5,7) & (3,5,7) \\ (1,1,3) & (1,3,5) & (1,3,5) \\ (7,9,9) & (7,9,9) & (7,9,9) \end{pmatrix} \end{array} \begin{matrix} A_1 \\ A_2 \\ A_3 \\ A_4. \end{matrix}$$

Table 4.10 depicts the cumulative priority scores obtained after multiplying normalized cost scores (Table 4.9) and priority scores (Table 4.4).

Table 4.11 Ranking for alternatives based on fuzzy COPRAS method for hilly wind sites

Alternatives	PS	CPS	Ranking
A_1	43.17	43.17	4
A_2	66.69	106.70	2
A_3	100.00	113.4	1
A_4	43.31	69.29	3

Table 4.12 Penalty cost and normalized cost score for offshore wind farm

Alternatives	PC ($)	NCS
A_1	37393	1.000
A_2	59829	1.600
A_3	82919	2.217
A_4	59829	1.600

Similarly, for fuzzy COPRAS method, the cumulative priority scores for alpha-cut $\alpha = 0.5$ are given by multiplying priority scores (Table 4.7) and normalized cost scores (Table 4.9). The ranking based on cumulative priority scores for fuzzy COPRAS method is depicted in Table 4.11.

Uncertainties in offshore wind farm are mainly related to rapid changes in wind speed. Since the wind resource is abundant, the power capturing capacity varies drastically due to wake effects and curtailment. In the present context, as discussed in the previous chapter, the decision-making for three wind farms, namely, Anholt (Denmark), Amrumbank (Germany), and Horns Rev 2 (Denmark). The geographic location of these wind farms is illustrated in Fig. 3.7. The methodology for arriving at the best choice remains the same. The normalized cost score for all the alternatives is determined based on actual and forecasted wind powers. The normalized cost score is depicted in Table 4.12.

Next, we evaluate the fuzzy decision matrix for the best alternative based on the given criteria. In case of offshore wind farms, the variability in wind speed causes wind operators to take immediate actions like wind curtailment and forced outage of turbine unit(s). Based on this, the fuzzy decision matrix can be expressed as

$$H = \begin{array}{c} \begin{matrix} C_1 & C_2 & C_3 \end{matrix} \\ \begin{pmatrix} (5,7,9) & (5,7,9) & (7,9,9) \\ (1,3,5) & (3,5,7) & (3,5,7) \\ (1,1,3) & (1,1,3) & (1,1,3) \\ (7,9,9) & (7,9,9) & (7,9,9) \end{pmatrix} \end{array} \begin{matrix} A_1 \\ A_2 \\ A_3 \\ A_4. \end{matrix}$$

To start off with, we adopt fuzzy TOPSIS method where the weighted normalized decision matrix is calculated according to (4.6) and is given as

Table 4.13 Euclidean distance and closeness coefficient for each alternative

Alternatives	z^+	z^-	O
A_1	14.692	0.3933	0.0261
A_2	12.35	3.379	0.2148
A_3	0.00	15.06	1.000
A_4	15.06	0	0.000

Table 4.14 Ranking for alternatives based on CPS for fuzzy TOPSIS method for offshore wind farm sites

Alternatives	PS	CPS	Ranking
A_1	0.0261	0.0261	3
A_2	0.2148	0.3436	2
A_3	1.000	2.217	1
A_4	0.000	0.000	4

$$\tilde{H} = \begin{array}{c} \begin{matrix} C_1 & C_2 & C_3 \end{matrix} \\ \begin{pmatrix} (0.556, 1, 0.600) & (0.778, 1.285, 1) & (1, 1, 1) \\ (1, 2.33, 3) & (1, 1.8, 1.667) & (1.285, 1.8, 2.333) \\ (1.667, 7, 3) & (2.333, 9, 5) & (3, 9, 7) \\ (0.5556, 0.778, 0.4286) & (0.778, 1, 0.7143) & (1, 1, 1) \end{pmatrix} \end{array} \begin{matrix} A_1 \\ A_2 \\ A_3 \\ A_4. \end{matrix}$$

Further, the fuzzy positive ideal solution (FPIS) and fuzzy negative ideal solution is calculated using (4.7) and are given as

$$G^+ = \{(1.667, 7, 3), (2.33, 9, 5), (3, 9, 7)\} \tag{4.17}$$

$$G^- = \{(0.555, 0.778, 0.4286), (0.778, 1, 0.7143), (1, 1, 1)\}. \tag{4.18}$$

The priority scores are obtained by calculating the euclidean distance using (4.9) and are depicted in Tables 4.13 and 4.14.

Next, we evaluate the alternatives based on fuzzy COPRAS method. The decision matrix remains the same along with weighted normalized decision matrix. We evaluate the aggregated scores for beneficial and non-beneficial criteria. Since in the present context, all the criteria are non-beneficial, we evaluate $\tilde{T}_i^-$ and are given as

$$\tilde{T}_i^- = \{(2.33333.28572.6000), (3.28575.93337.0000), (7.000025.000015.0000), (2.33332.77782.1429)\}. \tag{4.19}$$

Table 4.15 Crisp numbers for fuzzy indices ($\tilde{T}_i^-$) for offshore wind farm site

alpha-cut	A_1	A_2	A_3	A_4
0.1	3.9223	6.3463	8.5500	3.9429
0.2	3.5139	5.5985	8.0000	3.5302
0.3	3.0987	4.8613	7.3500	3.1111
0.4	2.6766	4.1349	6.6000	2.6857
0.5	2.2476	3.4190	5.7500	2.2540
0.6	1.8118	2.7139	4.8000	1.8159
0.7	1.3691	2.0194	3.7500	1.3714
0.8	0.9196	1.3356	2.6000	0.9206
0.9	0.4632	0.6625	1.3500	0.4635
1.0	0	0	0	0

Table 4.16 Ranking for alternatives based on CPS for fuzzy COPRAS method for offshore sites

Alternatives	PS	CPS	Ranking
A_1	2.2476	2.2476	4
A_2	3.4190	5.4704	2
A_3	5.7500	12.7475	1
A_4	2.2540	3.6064	3

Next, we convert the fuzzy indices obtained in (4.19) using (4.12) for different alpha-cut values into a crisp number. Table 4.15 highlights the crisp numbers for each alternative A_i.

The crisp numbers highlighted in Table 4.15 are then evaluated for the priority scores (XC) using (4.13). The ranking for alternatives based on cumulative priority scores for $\alpha = 0.5$ is listed in Table 4.16.

From Table 4.16, we can observe that A_3 is the most preferred alternative followed by A_2, A_4 and A_1. We also see a rank reversal for alternatives A_1 and A_4 as compared to fuzzy TOPSIS method. In the present work, an MCDM approach for a hybrid operation of three wind farms situated in western Massachusetts is considered. The tangible and non-tangible effect of different dynamic phenomenon is considered to evaluate the best alternative. Fuzzy TOPSIS and fuzzy COPRAS methods are used owing to uncertainties present in wind speed characteristics. Triangular fuzzy numbers are used to assign relative importance of each alternative with respect to each criterion. Based on these two methods, it is found that alternative A_3 is the most preferred choice followed by A_2, A_1 and A_4. Further, in case of dynamic decision matrices, the rank reversal phenomenon is tested for the methods. It is found that A_3 is the most preferred alternative indicating its dominance in case of uncertainties.

References

1. Bekar ET, Cakmakci M, Kahraman C (2016) Fuzzy copras method for performance measurement in total productive maintenance: a comparative analysis. J Bus Econ Manag 17(5):663–684
2. Benlarbi K, Mokrani L, Nait-Said M (2004) A fuzzy global efficiency optimization of a photovoltaic water pumping system. Sol Energy 77(2):203–216
3. Bezza M, Moussaoui B, Fakkar A (2012) Sensorless MPPT fuzzy controller for DFIG wind turbine. Energy Procedia 18:339–348
4. Chamodrakas I, Batis D, Martakos D (2010) Supplier selection in electronic marketplaces using satisficing and fuzzy AHP. Expert Syst Appl 37(1):490–498
5. Chen CT (2000) Extensions of the TOPSIS for group decision-making under fuzzy environment. Fuzzy Sets Syst 114(1):1–9
6. Chen HMW, Chou SY, Luu QD, Yu THK (2016) A fuzzy MCDM approach for green supplier selection from the economic and environmental aspects. Math Probl Eng 2016:1–10
7. Chen VY, Lien HP, Liu CH, Liou JJ, Tzeng GH, Yang LS (2011) Fuzzy MCDM approach for selecting the best environment-watershed plan. Appl Soft Comput 11(1):265–275
8. Ghosh S, Das A (2019) Urban expansion induced vulnerability assessment of east kolkata wetland using fuzzy MCDM method. Remote Sens Appl: Soc Environ 13:191–203
9. Hsu W (2015) A fuzzy multiple-criteria decision-making system for analyzing gaps of service quality. Int J Fuzzy Syst 17(2):256–267
10. Hsu YL, Lee CH, Kreng V (2010) The application of fuzzy delphi method and fuzzy AHP in lubricant regenerative technology selection. Expert Syst Appl 37(1):419–425
11. Jafarian M, Ranjbar A (2010) Fuzzy modeling techniques and artificial neural networks to estimate annual energy output of a wind turbine. Renew Energy 35(9):2008–2014
12. Lee AH, Hung MC, Kang HY, Pearn W (2012) A wind turbine evaluation model under a multi-criteria decision making environment. Energy Convers Manag 64:289–300
13. Nourianfar K, Montazer GA (2013) A fuzzy MCDM approach based on COPRAS method to solve supplier selection problems. In: The 5th conference on information and knowledge technology. IEEE
14. Pedrycz W, Gomide F (2007) Fuzzy systems engineering. Wiley Inc, New York
15. Saaty R (1987) The analytic hierarchy process-what it is and how it is used. Math Model 9(3):161–176
16. Samanlioglu F, Taskaya YE, Gulen UC, Cokcan O (2018) A fuzzy AHP–TOPSIS-based group decision-making approach to IT personnel selection. Int J Fuzzy Syst 20(5):1576–1591
17. Shafiee M (2015) A fuzzy analytic network process model to mitigate the risks associated with offshore wind farms. Expert Syst Appl 42(4):2143–2152
18. Wang J, Xiong S (2014) A hybrid forecasting model based on outlier detection and fuzzy time series – a case study on hainan wind farm of China. Energy 76:526–541
19. Zavadskas EK, Turskis Z, Bagočius V (2015) Multi-criteria selection of a deep-water port in the Eastern Baltic Sea. Appl Soft Comput 26:180–192
20. Zhao H, Guo S, Zhao H (2019) Comprehensive assessment for battery energy storage systems based on fuzzy-MCDM considering risk preferences. Energy 168:450–461

Chapter 5
Control Applications in Hybrid Wind Farms

As understood by now, wind turbines extract energy from the randomly varying wind. However, downstream of the turbine, a wake is created where wind speed is reduced. As per the basic definition in fluid dynamics, a wake is the region of recirculating flow behind a moving or stationary blunt object, caused by viscosity, possibly accompanied by flow separation and turbulence. As the flow further proceeds downstream, this wake spreads and finally recovers toward free stream conditions. Such a wake effect is the aggregated influence on the energy produced in the wind farm resulting from effective wind speed changes caused by the impact of the turbines on each other. Wake effect from an upwind turbine undermines a downwind wind turbine's power generation and therefore the revenues from the wind farm itself. There is therefore a need to design a wake steering control scheme to increase the power production of wind farms. Wake effects also vary with the atmospheric conditions.

Wake management in wind farms is complemented by usage of precision measurement devices like light detection and ranging (LIDAR). Aerodynamics in the Prandtl layer of atmospheric boundary layer imposes uncertainties in wind flow which calls for the need of adaptive control. Wake center tracking by LIDAR simulations is used to model the effective wind speed deficit into effective wake center for multiple wake situations. A wake management scheme based on yaw angle variation is implemented for multiple wind turbines. Uncertainties in the wake flow are taken care by an adaptive PI controller which shifts the wake center behind the upstream turbine. Yaw angle of upstream wind turbines is used as a variable parameter in order to redirect the wake flow behind upstream turbine. Parameters like effective wind velocity, deficit, and air turbulence are calculated and are assessed for comparison. The major contribution of this chapter is a methodology based on transfer function where the LIDAR simulations are used to control wake center at the downstream turbine. The proposed scheme is validated for 2-turbine, 5-turbine, and 15-turbine wind farm layouts.

H. S. Dhiman and D. Deb, *Decision and Control in Hybrid Wind Farms*,
Studies in Systems, Decision and Control 253,
https://doi.org/10.1007/978-981-15-0275-0_5

5.1 Introduction

The reliability of a wind power plant depends on the accuracy and robustness of its control system which not only improves the annual energy production but also safeguards its prolonged lifetime of mechanical and electrical equipment. Turbines are erected in a wind farm in a particular fashion which affects the net power captured. However, due to the inherent wake effect, the downstream turbines contribute lesser power to the utility grid. This also leads to subsequent reduction in wind farm efficiency and calls for an appropriate control strategy to lessen the power losses. Wake mixing, a common aerodynamic phenomenon leads to increased structural loading on nonrotating turbine parts like nacelle and tower [5]. Mathematical models like Jensen's model and Frandsen's model which are of high fidelity are widely being put into use for accurately determining velocity and power deficit. In a wind farm, ambient air turbulence is also coupled with turbulence generated from wake interactions which can deplete the power profile.

Extensive research has been carried out recently on the control-oriented wake models that are designed to modify wake characteristics behind upstream turbine. From industrial point of view, a wind farm operator always chooses to maximize the power capture available from wind resource and minimize the resultant mechanical loading on the nonrotating parts of the turbine [39]. Power fluctuations as a result of dynamic nature of wind cause farm operators to increase the dependence on battery energy storage systems (BESS) which calls for efficient and optimal wind farm control. Primarily, two types of control methods are used in wind farms. Axial induction control focuses on altering the pitch angle of the turbine whenever changes in wind speed are noticed which ultimately improves the power captured and reduces structural loading on turbines. Whereas wake redirection-based control redirects the wake stream behind upstream turbine for improving power capture capability of downstream turbines [10]. This type of control is based on yaw angle correction of upstream turbines.

The main objective for any wind farm operator is to maximize power capture from available wind regime. Some of the industry preferred techniques to increase power capture include pitch angle management and yaw angle control. Further, Schlipf et al. described an improvised collective pitch controller to mitigate load fluctuations, transients in rotor speed during sudden and extreme operating conditions [42] using a PI control strategy to curb rotor speed variations by 70–80%. Industry preferred standard feedback control is compared to feedforward blade pitch control for load reduction and increasing wind turbine lifetime [19]. Simulations are carried out for rated and above rated wind field conditions. The individual feedforward pitch controllers are found to perform slightly better than the individual feedback controllers without reduction in power generated.

In [21], the authors carried out a CFD simulation to redirect wakes away from turbine rotor for improved downstream power capture. SOWFA simulation tool is used to study redirection of turbine wakes for a 5-MW wind turbine model using yaw angle-based and IPC-based strategies. Results reveal that IPC-based redirection

does not lead to significant reduction in loading rather yaw based wake redirection improves power capture profile at the downstream turbine. Antonini et al. tested the CFD models for wind simulations by incorporating the uncertainties in wind direction [2] for three wind farms. Wake predictions are carried out based on RANS SST $k-\omega$ and Reynolds stress model and are significantly accurate owing to precise wind direction measurements. Boersma et al. discussed various control-oriented methods for power maximization of wind farms [7].

Simulation tools like FLORIS and SOWFA are used for estimating the velocity deficit. Further, Gebraad et al. presented a novel dynamic wake model for estimating wake center, effective wind speed, and power production for downstream turbines in a wind farm [22]. Experimental analysis has revealed yaw angle control of the upstream turbine to deflect the wake field behind rotor and enhance the power capturing capabilities of the downstream turbine [24, 26]. Repositioning the downwind turbine can significantly reduce the rotor shadow under upstream turbine as described by Gebraad et al. as it improves velocity profile and increase net power capture [23] from the wind farm. Vali et al. presented an MPAC technique for wind farms which minimizes the wind farm reference error [50]. An adjoint-based MPAC is applied to 2×3 wind farm layout where the wind farm power follows the time-varying reference signal. Yaw angle control for a fixed downstream distance of 3D and 6D in a wind tunnel study is experimentally verified and results reveal a 12% increase in power captured [1]. Maeda et al. carried out an experimental analysis on the effect of terrain changes along with turbulent wind field on the total power production with HAWT placed in a wind tunnel [33].

For a single column wind farm layout, optimization study is carried out based on yaw angle control keeping axial induction factor same at each downstream turbine [13]. An experimental analysis has been carried out by Dou et al. where the wake structure and its properties are studied for a small-scale turbine [16]. Parameters like pitch angle, yaw angle, and tip speed ratio are explored for determining optimal turbine performance. Further, an analytical model for predicting the yaw offset is proposed and validated with experimental results. In [43], LIDAR-assisted measurements in tandem with look-ahead controller is demonstrated for load reduction in wind turbines. Fatigue based on damage equivalent load (DEL) which is equivalent load produced when subjected to the same load throughout lifetime, is calculated. The blade and tower bending moment are reduced by 10% and 20%, respectively. In [41], a robust wind-scheduled control is applied for generator speed regulation. LIDAR provides an indirect control that eliminates the uncertainties in wind speed measurement. However, the accuracy of wind speed measurement plays an important role. The robust controller performance for regulating generator speed is seen effective for speeds above rated value. A more comprehensive LIDAR-based wake tracking is studied [40] wherein LIDAR is used to track wake flow and to set the actuator to the desired set point of yaw angle. The measured line-of-sight (los) wind speed is compared with simulated wind speed for estimating wind field parameters.

Predominately, the losses occurring due to wake are characterized by maximum velocity deficit. The spatial location in terms of (x, y, z) coordinates is the position in the wake field that corresponds to maximum power loss and this point is known as

the wake center. Wake center tracking is explored by Cacciola et al., where the hub loads at the downstream turbine are used to collect information related to wind speed deficit and horizontal shear [9]. A minimization problem is used to accurately determine wake center using the hub sensors to provide information with good accuracy. The limitation of this method is the usage of Larsen's model that does not encapsulate yaw misalignment. Barthelmie and Pryor have discussed an automated wake characterization algorithm to identify wake center position under different atmospheric conditions of the day [3]. The wake center position is measured using a Doppler LIDAR for a duration of first 6 months of 2017 and scans reveal that this position changes during night time when more stable atmospheric conditions prevail as compared to that during the daytime. Further, an important aspect of power maximization is studied by Raach et al., where the authors have used a H_∞ controller to redirect the wake streamflow for yaw angle control [39]. The system identification toolbox is used for identifying various plant models. Finally, the closed-loop performance of the controller is tested under different atmospheric conditions.

Experimental analysis carried out by Howland et al. reveal a significant improvement in wind power capture at the downstream turbines as a result of reduced wake shadow from upstream turbine(s) [24]. Gebraad et al. explored a unique method of repositioning downstream wind turbines for reducing the wake effect and thus increasing their power capture [23]. However, in practical situation, the wind turbine repositioning is limited by the constraints posed by land availability. Fleming et al. discussed individual pitch control (IPC) and tilt induced control for redirecting wake flow behind upstream turbines using a high precision tool called simulator for on/offshore wind farm applications (SOWFA) [21]. In a study carried out by Adaramola et al., a 12% increase in power capture is observed when the wind turbine in the upstream is operated by yawing to dominant wind direction [1]. Meanwhile, it is also important to note that terrain conditions and wake generated turbulence also affect the effective yield of a wind farm. Maeda et al. demonstrated in a study the impact of irregular surface conditions and how the turbulence due to wake interactions affect the performance of a Horizontal axis wind turbines (HAWT) when placed in a wind tunnel section [33]. Dar et al. took a case study of single column wind farm layout to understand the effect of optimizing yaw angle of turbines keeping axial induction factor constant [13].

LIDAR-based wake control for power maximization was first put into use by Raach et al. [40] where the measurements by LIDAR mounted on a downstream turbine are used to send appropriate information to a yaw controller of upstream turbine and is tested for a two-turbine system. In an experimental study carried out by Doubrawa et al., characterization of wake flow is studied [17]. Results of the large eddy simulation (LES) study are found to be in tandem with the LIDAR measurement campaign. Furthermore, Doubrawa et al. extended their work on wake characterization by implementing a stochastic model that determines the wake shape and width [18]. When compared to Reynolds-averaged Navier–Stokes (RANS) model, the proposed model performs better on an LES framework. LIDAR-based campaign is utilized for analyzing the effect of variance in radial velocity on the wake shape and deficit [51]. It is interesting to note that the control action achieved with LIDAR

measurements results in a controlled turbulence, and it is also reported that the length of probe results in major errors in radial velocity variance. With the onset of wind turbine and farm control, the challenge has always revolved around precise and accurate measurement equipment.

For an efficient wind farm performance in terms of minimum wake losses and maximum lifetime of turbines, advanced control schemes are required that can better handle the uncertainties in the aerodynamic flow in a wind farm. To deal with such system uncertainties, adaptive control is widely used [11, 25, 30, 36]. The essence of adaptive control is based on parameter estimation when a system encounters uncertainties and thus achieving desired performance in such random events [14, 15, 35, 37]. The desired value of the variable under observation is compared with the actual one in a feedback loop. The parameter adjustment in adaptive control is a key process that allows the controller to take appropriate action. Gain scheduling is one of the most popular forms of adaptive control which is actively used in process engineering. This chapter highlights a transfer function-based approach for controlling wake center of a turbine and improve the performance of a downstream turbine wake management for a wind farm layout is performed. This chapter is organized as follows: Sect. 5.2 highlights the basics of control scheme for a wind farm layout and Sect. 5.3 throws light on a multi-model and multiple wake scenario. In Sect. 5.4, key parameters like power captured and effective air turbulence are presented for wind farms under wake effect, and in Sect. 5.5, a framework for proposed methodology is validated and simulation results are discussed.

5.2 Closed-Loop Control Methodology

Wind speed measurement using a high precision device like LIDAR and control of the wake center are the main objectives of a closed-loop control. LIDAR stands for Light Detection and Ranging which is primarily used to estimate the wind speed ahead in time by using a system of lasers which is installed at the downstream turbines. Various experimental studies have shown that yawing an upstream turbine depletes its power capture but increases the same for a downstream turbine. The wake management strategy implemented here uses the transfer function for modeling wind turbine and estimating wake center deflection. LIDAR enables the tracking of the deflection of wake center caused by changes in yaw angle alignment. The main function of LIDAR is to get relevant information which tracks the trajectory of wake center in terms of an equivalent deflection which is often expressed in terms of rotor diameter.

Wind turbine uses cup anemometer and wind vane for measuring wind speed and direction, respectively. With the advent of LIDAR, nacelle-based wind speed measurement is being carried out in order to take appropriate control actions which ensures the farm operator has enough time to take crucial decisions in case of emergencies [47]. In wind energy market, continuous wave (CW) and pulsed wave (PW) type of LIDAR systems are available of which former is used owing to its ease of use and market value [44]. A beam of specified frequency is emitted and the

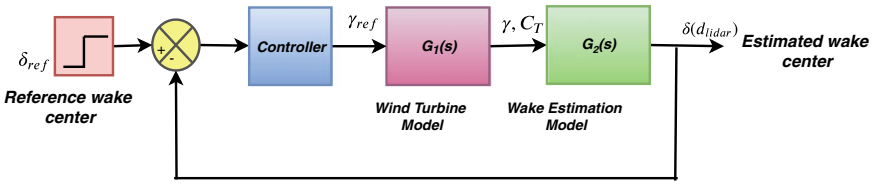

Fig. 5.1 Wake center estimation for a single set of upwind and downwind turbines

back-scattered beam collected by receiver is processed further. Since the operation of an LIDAR is limited to a certain distance, it is important that the wind speeds are measured for a certain preview distance. The line-of-sight velocity is estimated using the time-average wind speed measured after processing it through Doppler spectra. In subsequent subsections, we talk about the key components that comprise a wake redirection control strategy. Primarily, a wind turbine model which inputs a yaw angle and a wake center deflection estimation block for locating the wake center. Figure 5.1 illustrates a systematic arrangement of components of the strategy implemented for wind turbines.

5.2.1 Wind Turbine Model

On the fundamentals of actuator disk theory, for a ith wind turbine in a wind farm, the power extracted is given as

$$P_i = \frac{1}{2}\rho_w A_w C_p u_i^3, \tag{5.1}$$

for air density ρ_w, rotor swept area A_w, power coefficient C_p, and wind speed u_i at the ith turbine [6]. It is also observed that the wind power when captured by an upstream turbine reduces by a certain factor of $\cos^h \gamma$ for a tunable parameter h, and yaw angle γ when operated in a yawed condition. Fleming et al. explored that the tunable parameter h varies in the range $h \in (1.4–2.2)$ [20]. Jonkman et al., further affirmed that the power coefficient which is indicative of aerodynamic efficiency gets modified by a factor $\cos^h \gamma$ for an upstream turbine in a yawed condition [28]. For power capture at a maximum value of $C_p = 0.482$ while accounting for losses due to turbulent wakes, h is chosen as 2. A 2-DOF model for the yaw alignment and nacelle of an upwind turbine is formulated as

$$\ddot{\gamma} + 2D\omega\dot{\gamma} + \omega^2\gamma = \omega^2\gamma_{ref}, \tag{5.2}$$

for undamped eigenfrequency ω, damping factor D, such that the desired yaw angle input γ_{ref} and output γ for a wind turbine are modeled as a transfer function using a system identification block in MATLAB. Output yaw angle γ is determined for a set

of $\gamma_{ref} \in (-25°, 25°)$. With this, the transfer function so obtained has $n_p = 2$ poles and $n_Z = 1$ zero and an accuracy of 99.99%. It is of the following form:

$$G_1(s) = \frac{0.533s + 0.01094}{s^2 + 0.1538s + 0.002736}. \tag{5.3}$$

Qian et al. [38] stated that for an upstream turbine operating in the yaw mode, the power captured is given as

$$P_i = \frac{1}{2}\rho_w A_w C_p u_i^3 \cos^3(\gamma_i). \tag{5.4}$$

An adaptive controller corrects the yaw angle setting for an upstream turbine. Measurements done by LIDAR aim to track the wake center deflection and based on the control action the wake flow is deflected away from the rotor. Power capture by a downstream turbine gets altered as the yaw angle of the upstream turbine is changed. Section 5.4 throws light on the changes in velocity profile when the wind farm is operated in a yawed condition. For the wake management strategy discussed, the turbine model aims to calculate the power captured whenever a control action is initiated by LIDAR measurements.

5.2.2 Wake Center Estimation

Wake center position caused from yaw misalignment has been a center of focus among many researchers to study maximization of power in a wind farm. Empirical relationships between streamwise distance and yaw misalignment have been studied rigorously to accurate locate the position of wake center. In a study carried out by Howland et al., it is found that an error of $\pm 0.02D$ exists between theoretical and experimental estimation of wake center deflection based on a 3D printed porus drag disk model [24]. Empirically, wake center deflection is worked out for an upstream turbine in yawed condition which is also dependent on the longitudinal distance d between two turbines. As per Jimnez et al. [27], the wake center deflection due to yaw misalignment is given as

$$\delta(d) = \frac{\xi_{init}\left(15\left(\frac{2k_d d}{D_0} + 1\right)^4 + \xi_{init}^2\right)}{\frac{30k_d}{D_0}\left(\frac{2k_d d}{D_0} + 1\right)^5} - \frac{\xi_{init} D_0 (15 + \xi_{init}^2)}{30k_d}, \tag{5.5}$$

$$\xi_{init}(\gamma, C_T) = \frac{1}{2}\cos^2(\gamma)\sin(\gamma)C_T, \quad M_\gamma = -2\dot{\gamma}\Omega\cos\psi I_b, \tag{5.6}$$

where ξ_{init} is the initial angle between the wake stream and upstream turbine rotor axis, d is the distance between upstream and downstream turbine, D_0 is the turbine diameter, and k_d is the model parameter subjected to uncertainties. Furthermore,

(5.6) represents the yaw bearing moment caused as a change in yaw angle where $\dot{\gamma}$ represents yaw rate (in rad/sec), Ω represents the angular velocity of rotor, ψ is the azimuth angle of blades and I_b is the moment of inertia of blades [34].

Wake recovery in a wake flow is defined by the parameter k_d to tune which poses a lot of challenges. Wind speed measurement by LIDAR is carried out by a circular scan in a wind field that measures the effective velocity with respect to rotor hub [32]. An appropriate, LIDAR preview distance d_{LIDAR} will lead to accurate measurement of wake center deflection which occurs when an upstream turbine is yawed. In the present context, for a two-turbine wind farm layout, a system identification toolbox is used to determine the transfer function for wake center deflection. Input to the transfer function is the yaw angle misalignment and wake center deflection is the output. Using (5.5), the values of wake center deflection are computed for $\gamma \in (-25°–25°)$. Considering atmospheric conditions, model parameter $k_d = 0.15$ is taken. With accuracy of 93.76%, the transfer function with $n_p = 2$ poles and $n_z = 0$ zeros is given as

$$G_2(s) = \frac{-0.158}{s^2 + 2.56 \times 10^{-12} s + 0.2404}. \tag{5.7}$$

Primary objective of an LIDAR in a wind farm is to acquire precise wind speed measurements that enhance a predictive mode of control. Widespread control structure used in the industry is the PID controllers, primarily because PID controllers can be, in a relative sense, easily implemented, programmed, fine-tuned, and are conceptually straightforward. The proportional gain helps improve the system rise time and response, the integral gain helps modify steady-state errors, and the derivative gain is generally useful in modifying any system overshoot. To maximize the wind farm performance, industry preferred control action based on proportional–integral (PI) technique may be implemented for optimizing the power capture and reduce mechanical loading and tower vibrations. In terms of control error, PI control action can be expressed as

$$f = K_p\left(\tilde{\delta}(\gamma) + \frac{1}{T_i}\int \tilde{\delta}(\gamma)dt\right), \tag{5.8}$$

where $\tilde{\delta}(\gamma)$ is the error in measured and reference wake center deflection and f is the output yaw angle. T_i and K_p represent the time constant and proportional gain, respectively. The best performance for a controller can be achieved by optimally tuning the constants.

5.3 Wake Center Estimation and Adaptive Control

LIDAR-based wake center estimation and control is extendable to a multi-model setup with an upwind and a downwind turbine under different conditions like initial wake stream angle, distance between upwind and downwind turbine, rotor diameter,

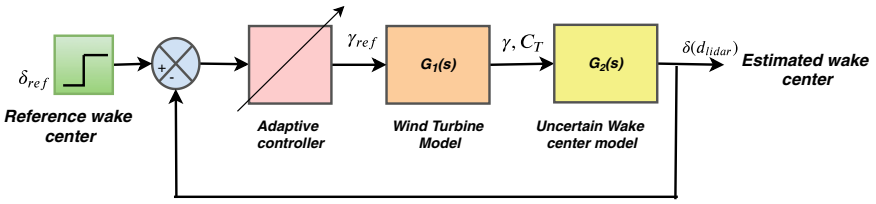

Fig. 5.2 Block diagram representation for wake center estimation

Table 5.1 Estimation accuracies for multi-model transfer function models

LIDAR distance (d_{LIDAR})	Estimation accuracy (%)
$1D_0$	93.76
$1.5D_0$	95.08
$2D_0$	94.94
$2.5D_0$	94.82
$3D_0$	94.71

and model parameter k_d as defined in (5.5). Apart from such factors, the wake development zone, that is, near-wake zone and far-wake zone, also significantly affects wake center estimation [31]. In the present study, a multi-model wake center estimation is studied through a data-driven approach with a constant model parameter k_d, and by varying LIDAR scanning distance d_{LIDAR} in terms of multiples of rotor diameter D_0. Figure 5.2 shows a schematic representation of the proposed strategy for a multi-model scenario.

It is important to note that wind farm operation is accompanied by uncertainties and control objective to track the reference can be difficult in such cases. By varying parameter in a transfer function, the uncertainties can be modeled. In the present case, the uncertainties posed by wake center model can be handled much better by an adaptive controller rather than a classical PI control. Table 5.1 depicts the estimation accuracies of various transfer function models obtained from system identification toolbox in MATLAB.

Wake Center Estimation and Control for Multiple Turbines

Till now, we have described a two-turbine wind farm layout for wake management based on a transfer function methodology. However, large-scale wind farms consist of more than two wind turbines, and the effect of wake interactions among turbines is more pronounced. The wake flow in a large wind farm is also affected by the manner in which turbines are arranged, that is, the layout of the farm. Bastankhah and Porte-Agel devised a Gaussian wake model to describe a wind velocity deficit caused by multiple upstream turbines [4]. Based on various factors like radial distance r from

turbine hub, longitudinal downstream distance x, and thrust coefficient C_T, the model assumes a Gaussian profile. Mathematically, this model can be expressed as

$$u = u_0\left(1 - C(x)e^{\frac{-r^2}{2\sigma^2}}\right), \tag{5.9}$$

$$C(x) = 1 - \sqrt{1 - \frac{C_T}{8(\sigma/D_0)^2}}, \quad \sigma = kx + \epsilon D_0, \tag{5.10}$$

where $C(x)$ represents the maximum normalized velocity deficit caused at a longitudinal distance x and σ is width of the wake which is a function of rotor diameter D_0 and wake growth constant k. Based on quadratic superposition and linear superposition the wake deficit is determined in case of multiple wind turbines. Mathematically, the principle of linear superposition is given as

$$\Delta u_i^{lin} = \sum_{j=1}^{N}\left(1 - \frac{u_j}{u_0}\right), \tag{5.11}$$

where N is the total number of upstream turbines, Δu_i is the velocity deficit for ith due to all upstream turbines on in its wake and Δu_j is the velocity deficit cause due to individual jth upstream turbine.

Katic et al. [29] described a quadratic principle of superposition given as

$$\Delta u_i^{quad} = \sqrt{\sum_{j=1}^{N}(\Delta u_j)^2}. \tag{5.12}$$

A wake management strategy that modifies the yaw angle of the upstream turbines is needed for increasing the power output from downstream turbines. Apart from yaw misalignment, repositioning downstream reduces the shadow under wakes from upstream turbines. However, because of space constraints, the repositioning of turbines is not preferred and thus control of wake center deflection via yaw misalignment is an effective method [12]. Due to the yaw misalignment of upstream turbines, the thrust coefficient offered by the turbines to the incoming wind flow gets altered by a factor of $\cos^3\gamma_j$, where γ_j is the yaw misalignment for the jth upstream turbine in a wind farm.

At ith downstream turbine, the transformed velocity deficit is given as

$$u_i = u_0\left(1 - C_{ij}(x)e^{\frac{-r^2}{2\sigma_{ij}^2}}\right), \quad C_{ij}(x) = 1 - \sqrt{1 - \frac{C_T\cos^3(\gamma_j)}{8(\sigma_{ij}/D_0)^2}}, \tag{5.13}$$

$$\sigma_{ij} = kx_{ij} + \epsilon D_0, \quad \beta = 0.5\left(\frac{1 + \sqrt{1 - C_T}}{\sqrt{1 - C_T}}\right), \tag{5.14}$$

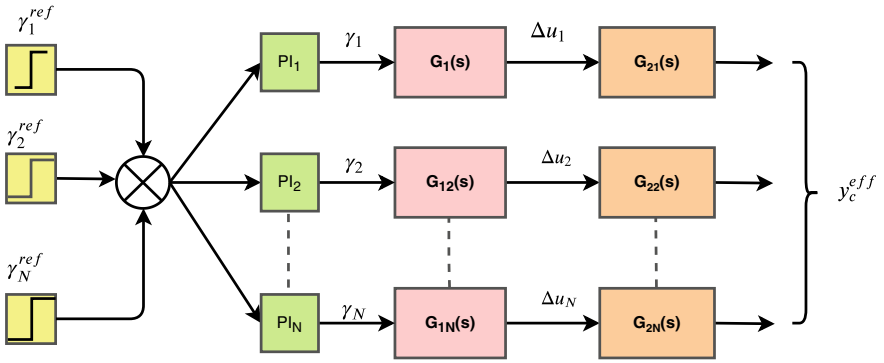

Fig. 5.3 Proposed strategy for multiple wake scenario

where $\epsilon = 0.25\sqrt{\beta}$, and σ_{ij} is the wake width at a distance x_{ij} between jth upwind and ith downwind turbine. Using (5.13), the velocity deficit can be determined for each upstream turbine given the yaw angle misalignment γ_j. Further, for N such upstream turbines, using (5.12), the effective velocity deficit at ith downwind turbine is determined. Figure 5.3 pictorially depicts the schematic block diagram for wake management in case of multiple wind turbines.

For the case of multiple wind turbines, we propose a wake management strategy that takes into account the effective velocity and models the effective wake center faced by a downstream turbine. Such an empirical relationship between wake center position and velocity deficit is given as

$$f(y) = u_m e^{\frac{-(y-\mu_y)^2}{2\sigma_{LIDAR}^2}}, \quad \sigma_{LIDAR} = k d_{LIDAR} + \epsilon D_0, \tag{5.15}$$

where y, μ_y are the hub height and wake center position for a velocity deficit of $f(y)$ given an LIDAR preview distance d_{LIDAR}. Maximum velocity deficit is represented by u_m and is used to estimate the wake center in multiple wake scenario as illustrated in Fig. 5.3. The transfer function models between effective wind velocity deficit and effective wake center can be obtained using the system identification toolbox in MATLAB. Based on the proposed methodology, the transfer function so obtained is of multiple input single output (MISO) form as there are multiple yaw angles from different wind turbines, and there is one effective wake center.

Developed in 1960, Kalman filter (KF) was named after scientist Rudolph Kalman, which aims to estimate the states in presence of noisy measurements or disturbances. State estimation using KF revolves around the recursive processing of noisy data [46] and is extensively used in estimating the state of charge of battery for electric vehicle and energy storage application [48]. Mathematically, KF is modeled as

$$\begin{aligned} \hat{x}_{k+1} &= \mathbf{A}x_k + \mathbf{B}u_k + w_k, \\ \hat{y}_k &= \mathbf{C}x_k + \mathbf{D}u_k + v_k, \end{aligned} \tag{5.16}$$

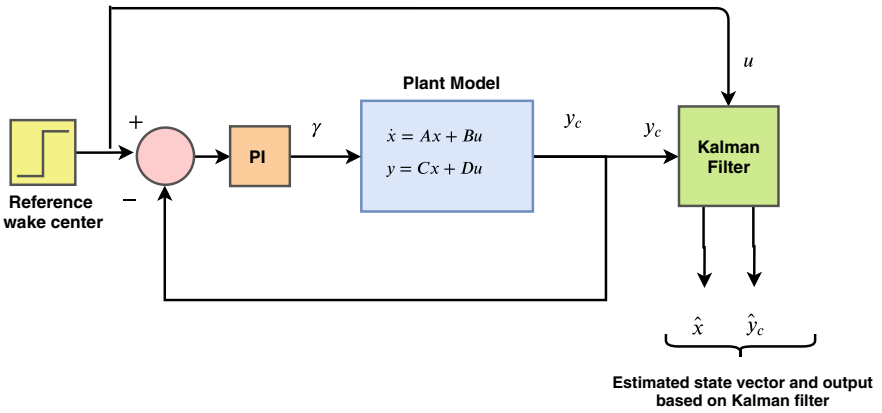

Fig. 5.4 Wake center estimation based on Kalman filter

where **A**, **B**, **C**, **D** are the state-space matrices of the plant; w_k, v_k are process noise and measurement noise at discrete time step k, respectively; and $\hat{x}_{k+1}$ is the update of state vector x_k at time $k+1$. In the present case, KF is used to estimate the wake center for a given set of upstream and downstream turbines. The yaw angle setting acts as an input and wake center as output to the transfer function model so obtained using system identification toolbox (SIT). The block diagram of wake center estimation is illustrated in Fig. 5.4.

Kalman filter takes in state-space matrices **A**, **B**, **C**, **D** and estimates the states and plant output at time $k+1$. The state-space model can be obtained using SIT available in MATLAB.

5.4 Performance Parameters for Waked Wind Farms

A wind farm performance is typically judged by the power profile and the mechanical loading on the downstream turbines. Commonly used models for wake interactions include Jensen's model, Frandsen's model, and Gaussian model. Since wind wakes cause power loss and increase loading on the turbines, it is important for a wind farm operator to quantify the changes in these parameters in terms of % improvement in power captured as well as effective air turbulence. Figure 5.5 illustrates a two-turbine wind farm layout and depicts the deflection in the wind flow behind upstream turbine WT_1 due to a yaw misalignment of γ.

Jensen's model estimates wind speed for a downstream turbine given a radial distance r and longitudinal distance x and is

$$u(x,r) = u_0\left[1 - 2a\left(\frac{r_0}{r_0 + kx}\right)^2\right], \tag{5.17}$$

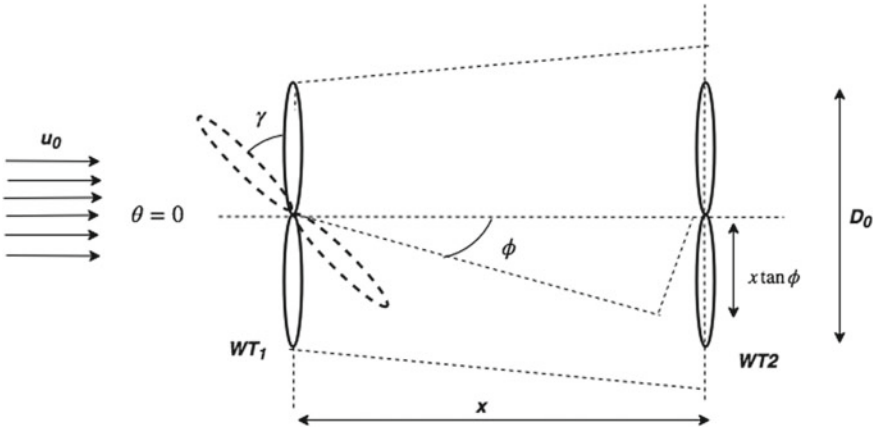

Fig. 5.5 Wake stream deflection in two-turbine wind farm layout

where u_0 is the freestream wind speed, r_0 is the rotor radius, and k is the wake expansion constant. For a given wind direction θ_j and a yaw misalignment of γ_j, the wake stream gets deflected by an angle ϕ_j given as

$$\phi_j = (0.6a_j + 1)\gamma_j + \theta_j, \tag{5.18}$$

where a_j is the axial induction factor for given turbine $j \in X$ (set of all upwind turbines). Now, the velocity profile for a downstream turbine due to a yaw misalignment of upstream turbine is given as

$$u_i(x, r) = \begin{cases} u_0\Big[1 - 2a_j\Big(\dfrac{1}{1 + 2kL\cos(\phi_j)}\Big)^2 \times \cos^2(4.5\phi_j)\Big], & \phi_j \leq 20^\circ \\ u_0, \quad \phi_j > 20^\circ, \end{cases} \tag{5.19}$$

where $L = \frac{x}{D_0} \in [2, 3, 4, 5]$ is the turbine spacing factor expressed as a multiple of turbine diameter. Based on (5.19), an improved velocity profile can be obtained by suitably yawing the upstream turbines by an angle γ_j. The power captured by a yawed upstream turbine is altered by a factor of $\cos^3 \gamma_j$. The net air turbulence faced by a downstream turbine is calculated by introducing a yaw misalignment on an upstream turbine. Using vector sum, the net turbulence due to ambient airflow and wake effect for a downstream turbine is given as

$$I_{eff} = \sqrt{I_a^2 + K^2 \sum_{j=1}^{N} (1 - \sqrt{1 - C_T \cos \gamma_j}) x_j^{-2/3}}, \tag{5.20}$$

where I_a is the ambient turbulence and I_{eff} is net turbulence calculated for a given downstream distance x_j for given N upstream turbines for a wind farm and K = 0.93 is a constant [49].

5.5 Adaptive PID Control Scheme

In spite of several benefits of PID control, a long-standing issue is the need to improve the robustness of PID controllers for reduced sensitivity to gain tuning for uncertainties in the system and time variations, both of which are very prominent issues in the wind farm control problem. Therefore, a variant of PID control like the adaptive PID control which would allow for adaptive modification of the controller gains, needs to be explored under the random wind scenario. If one implements certain rules to change along time, all or some of the parameters the PID controller gains, as per certain input characteristics without modifying the basic PID controller structure, then one essentially has an adaptive PID controller. Wind farm performance is dependent on the effective wind speed seen by the different turbines in presence of wake. That is, the wind farm power output can change with operational and environmental scenarios. For output power stability, the wind farm should be able to operate at controlled conditions. In case of variable load, the conventional PID control can be modified to an adaptive control action for a wind farm.

Transfer function of plant and PID controller, $G_{p2}(s)$ and $G_{c2}(s)$ are given by

$$G_{p2}(s) = \frac{A}{s^2 + a_1\, s + a_0}, \quad G_{c2}(s) = k_p + k_d\, s + \frac{k_i}{s}, \tag{5.21}$$

where A, a_1, and a_0 are constants of transfer function, and k_p, k_i, and k_d are proportional, integral, and differential gains of PID controller.

Let us parametrize $k_d = k$, $k_p = 2k\lambda$ and $k_i = \lambda^2 k$, and a closed-loop transfer function w_{c2} is given by

$$w_{c2} = \frac{A\, G_{c2}(s)}{s^2 + a_1\, s + a_0 + A\, G_{c2}(s)}, \tag{5.22}$$

$$w_{c2}^{-1} = 1 + (s^2 + a_1\, s + a_0)\, A^{-1}\, G_{c2}^{-1}(s). \tag{5.23}$$

The reference input is given by

$$r = w_{c2}^{-1}\, x_d = x_d + ((s^2 + a_1\, s + a_0)\, A^{-1}\, G_c(s)^{-1})\, x_d \tag{5.24}$$

$$= x_d + \ddot{w}_d + a_1\, \dot{w}_d + a_0\, w_d, \tag{5.25}$$

where x_d is the desired output and $w_d = (A^{-1}\, G_{c2}(s)^{-1})\, x_d$. Using (5.25), the block diagram (Fig. 5.6) can be further represented as Fig. 5.7.

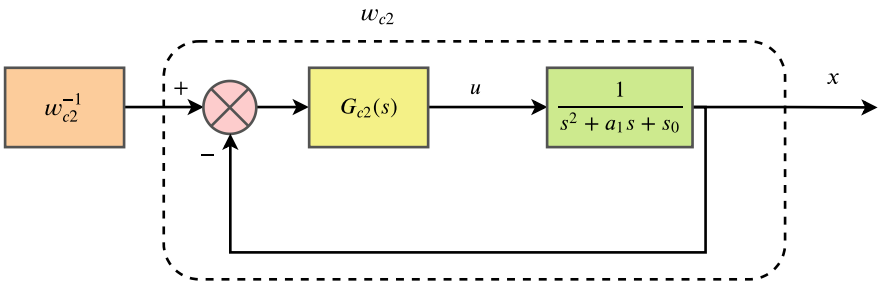

Fig. 5.6 Closed-loop transfer function

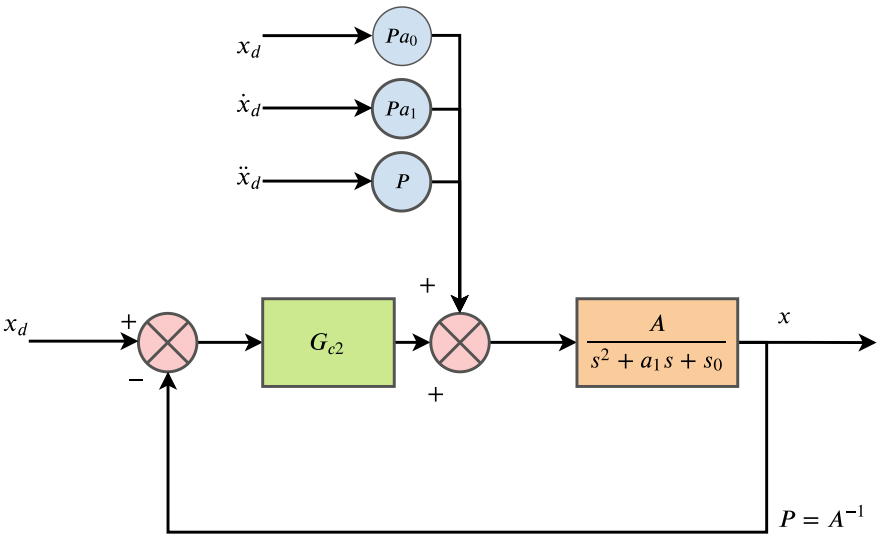

Fig. 5.7 Modified block diagram of closed-loop system

Moving Pa_0 and Pa_1 from forward to feedback path, controller and closed-loop transfer function can be represented as

$$G_{c2}(s) = \frac{(k + 2\lambda P)\, s^2 + (2\lambda k + \lambda^2 P)\, s + \lambda^2 k}{s}, \tag{5.26}$$

$$G_{p2}(s) = \frac{(k + 2\lambda P)\, s^2 + (2\lambda k + \lambda^2 P)\, s + \lambda^2 k}{Ps^3 + (k + 2\lambda P)\, s^2 + (2\lambda k + \lambda^2 P)\, s + \lambda^2 k}. \tag{5.27}$$

Closed-loop transfer function can be given as

$$w_{c2}(s) = \frac{G_{c2}(s)}{Ps^2 + G_{c2}(s)}. \tag{5.28}$$

Now, (5.25) can be represented as

$$r = w_{c2}^{-1}\, x_d = (1 + Ps^2 G_{c2}(s)^{-1})\, x_d = x_d + P\ddot{w}_d. \tag{5.29}$$

Plant input u can be given as

$$\begin{aligned} u &= P\ddot{x_d} + Pa_1\,\dot{x} + Pa_0\,x + G_{c2}(s)e \\ &= P(\ddot{x_d} + 2\lambda e + \lambda^2 e) + Pa_1\dot{x} + Pa_0 x + k\Big(\dot{e} + 2\lambda e + \lambda^2 \int e(u)du\Big). \end{aligned}$$

We define control error $e_1(t)$ and auxiliary error $e_2(t)$ as

$$e_1(t) = \ddot{x}_d + 2\lambda\dot{e} + \lambda^2 e, \quad e_2(t) = \dot{e} + 2\lambda e + \lambda^2 \int e(u)du. \tag{5.30}$$

Using control and auxiliary error, plant input may be given as

$$u = P\ddot{x}_d + P\hat{a}_1\,\dot{x} + P\hat{a}_0\,x + e_2(t). \tag{5.31}$$

Using estimate of $\hat{a_0}$ and $\hat{a_1}$, the adaptive control input u can be given as

$$u = P\ddot{x}_d + Pa_1\,\dot{x} + Pa_0\,x + e_2(t). \tag{5.32}$$

From (5.21), derivative of state can be represented as

$$\ddot{x} = -a_1\,\dot{x} - a_0\,x + P^{-1}\,u. \tag{5.33}$$

Substituting (5.32) in (5.33), we get

$$\begin{aligned} \ddot{x} &= -a_1\dot{x} - a_0 x + P^{-1}(Pe_1(t) + P\hat{a_1}\,\dot{x} + P\hat{a_0} + Pk\,e_2(t)) && (5.34)\\ &= \tilde{a_1}\,\dot{x} + \tilde{a_0}x + e_1(t) + P^{-1}ke_2(t). && (5.35) \end{aligned}$$

From (5.30), we get

$$\dot{e}_2 = \ddot{e} + 2\,\lambda\,\dot{e} + \lambda^2\,e = \ddot{x_d} - \ddot{x} + 2\,\lambda\,\dot{e} + \lambda^2\,e. \tag{5.36}$$

Substituting (5.35) in (5.36), we get

$$\begin{aligned} \dot{e}_2 &= \ddot{x_d} - \tilde{a_1}\,\dot{x} + \tilde{a_0}\,x - e_1(t) - Pke_2 + 2\lambda\dot{e} + \lambda^2 e && (5.37)\\ &= -P^{-1}ke_2 - (\tilde{a_1}\dot{x} + \tilde{a_0}\,x). && (5.38) \end{aligned}$$

Choosing appropriate adaptive laws as

$$\dot{\hat{a}}_1 \;=\; \gamma_3\,\dot{x}\,e_2, \quad \dot{\hat{a}}_2 \;=\; \gamma_4\,x\,e_2, \tag{5.39}$$

for adaptation gains $\gamma_3, \gamma_4 > 0$ and to be appropriately chosen by the control engineer to appropriately handle the desired transient response, and by choosing a Lyapunov candidate function as

$$V_2 = \frac{1}{2}\left(e_2^2 + \frac{\tilde{a_1}^2}{\gamma_3} + \frac{\tilde{a_0}^2}{\gamma_4}\right), \tag{5.40}$$

we find

$$\dot{V}_2 = P^{-1}ke_2^2 < 0. \tag{5.41}$$

Based on the corollary of the Barbalat's Lemma, the stability of the transfer function (5.21), is ensured. Individually, both the fractions of transfer function are stable. Thus, the stability of complete system along with sum of fractions is ensured.

5.6 Results and Discussions

A two-turbine wind farm layout is tested for wake control strategy based on LIDAR simulations. For this purpose, turbines with diameter $D_0 = 80$ m and a hub height of 90 m are taken. Wind turbines WT_1 (upstream) and WT_2 (downstream) are placed at a distance of 400 m apart. Using (5.19), the wind velocity at WT_2 is worked out. Given the atmospheric conditions, the wake expansion constant k can be approximated using the logarithmic law for wind speed profile. Initially, for wind turbine WT_1, the yaw angle is set as $\gamma_1 = 0°$ assuming the wind direction is directly facing the nacelle of WT_1. Deflection caused by yaw angle correction of WT_1 is determined for an LIDAR preview distance $d_{LIDAR} = 1D_0$.

While it is also important to note that the LIDAR operates for a particular range of preview distance and to support this, a range of 0–250 m is assumed in our simulations [45]. Based on the proposed control scheme (Fig. 5.1), wake center for upstream turbine WT_1 is estimated and the controller output sets the required yaw angle setting. The simulation case of 1000 s considers a wind profile where for first 500 s a wind speed of 8 and 10 m/s for the rest 500 s. Considering ambient air turbulence of 10%, turbine model and wake center deflection estimation model are simulated in MATLAB/Simulink given a model parameter $k_d = 0.15$. Model parameter k_d represents how fast a wake flow is recovered behind upstream turbine. The total farm power produced by turbines WT_1 and WT_2 and the wake center estimated by LIDAR simulation is illustrated in Figs. 5.8 and 5.9. The reference wake center is varied from 5 m to –5 m and is compared with the measured value. Further, the error is then processed by adaptive controller to set appropriate value of yaw angle for upstream turbine WT_1. Resulting from this, the wake profile for upstream turbine WT_1 gets modified in form of velocity profile.

For model parameter $k_d = 0.15$, the total wind farm power captured with and without wake redirection is plotted. Compared to Raach et al. [39] which leads to 4.5% increase in total farm power, the proposed wake redirection strategy leads to a power increase of 7.552%. While it is still possible to increase power capture by

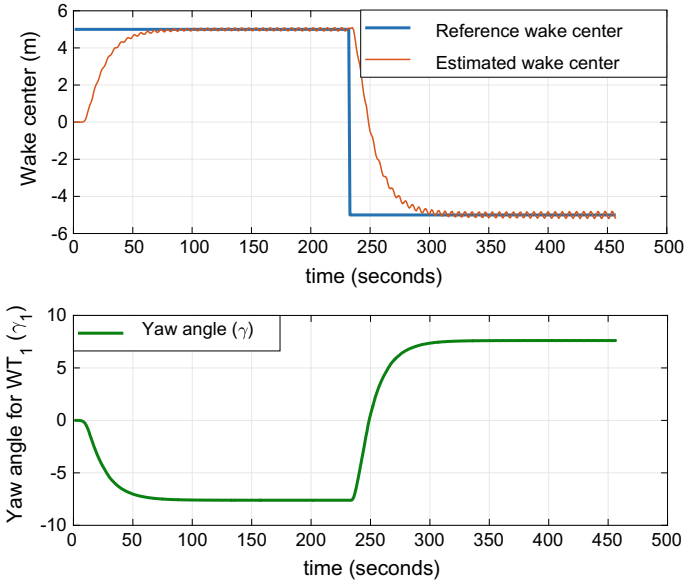

Fig. 5.8 Estimated wake center and yaw angle alignment for model parameter $k_d = 0.15$

repositioning downstream turbine but this is limited by space constraints and thus yaw angle correction is treated as one of the primary methods for wind farm control. The mechanical loading acting on the yaw motor is also important while changing yaw angle. To evaluate this, yaw bearing moment is calculated based on (5.6) due to the proposed control scheme when upstream turbine is operated in yaw mode and is pictorially depicted in Fig. 5.10. The turbine blade mass of 69 tons with a rotor diameter 80 m and azimuth angle $\psi = 0°$ is considered. From Fig. 5.10, we can be that the power spectral density plot has spikes of smaller amplitude which is indicative of a smooth adaptive control achieved. This also states that for a wind turbine yawing beyond limits can cause significant wear and tear to the motor which can be prevented with an adaptive control scheme.

Figure 5.11 pictorially depicts the sensitivity related to input to plant for a two-turbine wind farm layout. The turbine model and wake center estimation model are considered together as a plant as indicated by cascade transfer function $G_1(s)G_2(s)$.

The proposed scheme is also tested for evaluating the effective air turbulence on turbine WT_2. Figure 5.12 illustrates the effective air turbulence acting on WT_2 for different values of yaw angle correction. For a fixed yaw angle, the effective air turbulence on WT_2 decreases as we increase the longitudinal separation between WT_1 and WT_2. This is indicative of the fact that without yawing the upstream turbine, repositioning the downstream turbine can significantly reduce the mechanical loading on the nonrotating parts of the turbine.

The proposed control scheme is then evaluated for multi-model scenario where the LIDAR preview or scanning distance is varied to track the wake center deflection

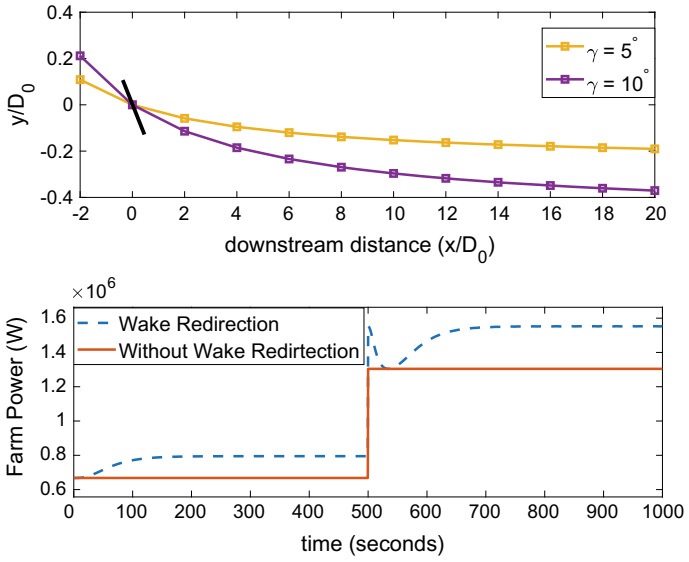

Fig. 5.9 Wake center deflection and wind farm power output

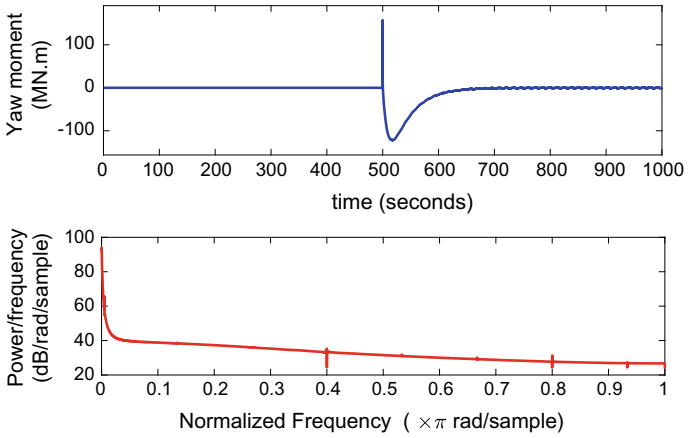

Fig. 5.10 Bearing moment for yaw motor and spectral density

caused by yaw misalignment. It is important to note that the preview distance must be varied until a point that complements the range of LIDAR. Using (5.5), the wake center deflection is determined and a transfer function is estimated using system identification toolbox in MATLAB. The yaw angle is taken as input and wake center deflection as output of the transfer function. Model order with best estimation accuracy is chosen. LIDAR simulations are performed with WT_2 tracking the wake trajectory for different preview distances $d_{LIDAR} = M^L D_0$, where $M^L \in [1, 2, 2.5, 3]$.

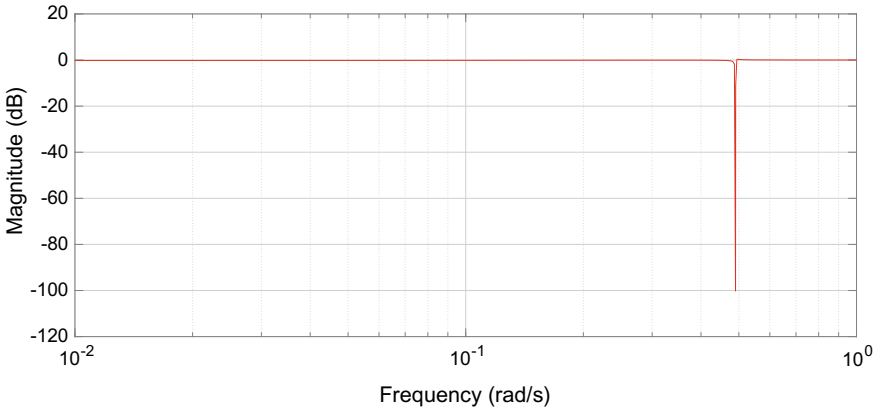

Fig. 5.11 Controller sensitivity for $G_1(s)G_2(s)$ for single wake scenario

Fig. 5.12 Net turbulence for a downstream turbine

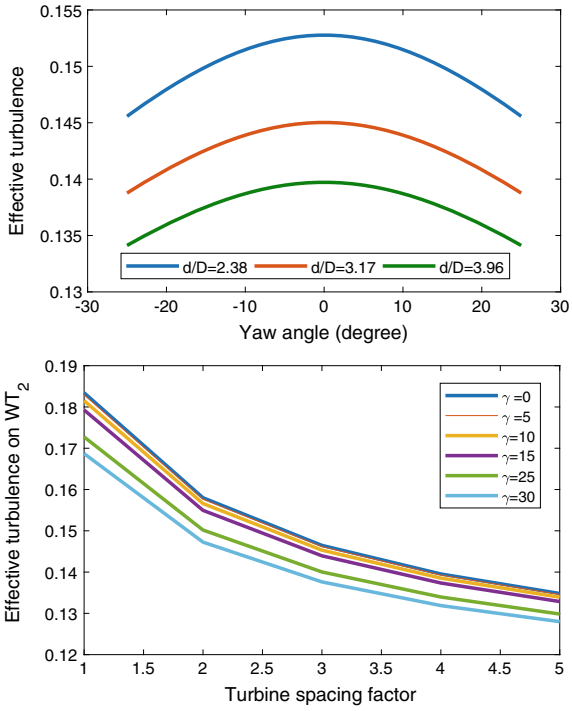

A transfer function model for wake model is obtained for every LIDAR preview distance and the wake center calculated for different models. It is then allowed to track reference wake trajectory to set a desired yaw setting for upstream turbine WT_1 using an adaptive PI controller. For a multi-model approach, the wake center estimation is illustrated in Fig. 5.13.

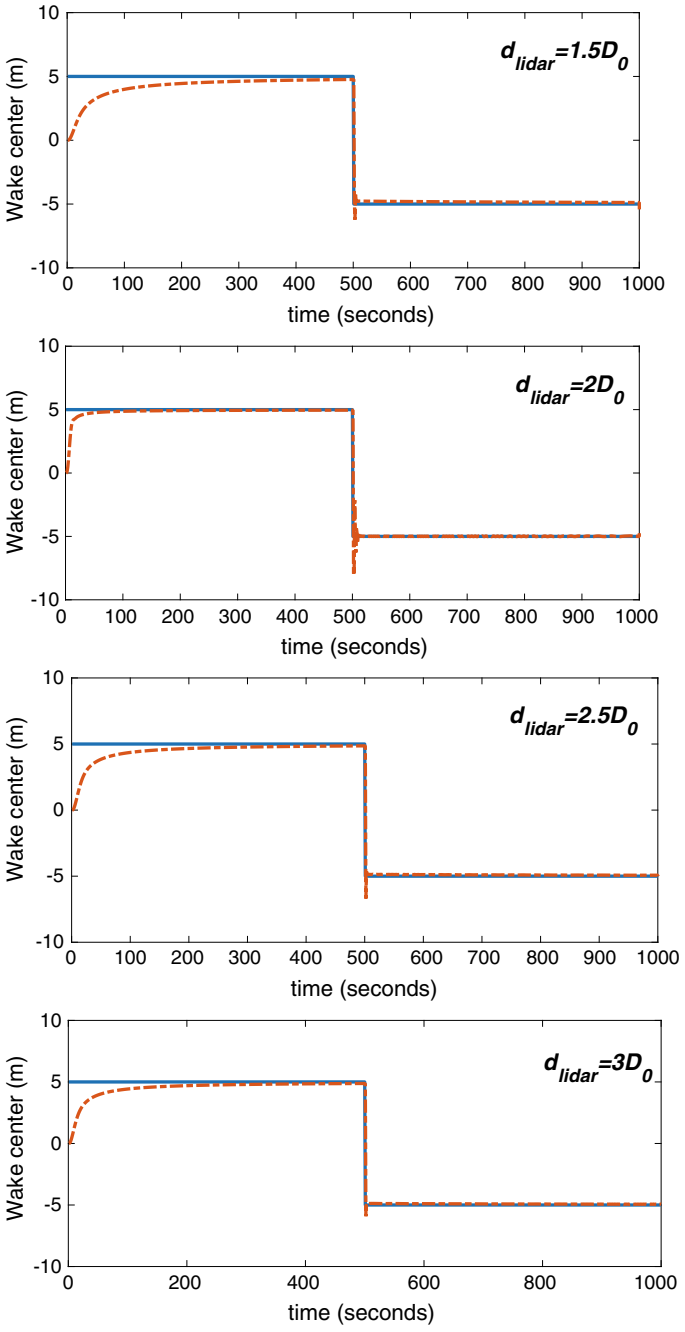

Fig. 5.13 Multi-model approach for two-turbine wind farm. Blue (solid) line represents reference wake center, and orange (dotted) represents estimated wake center deflection

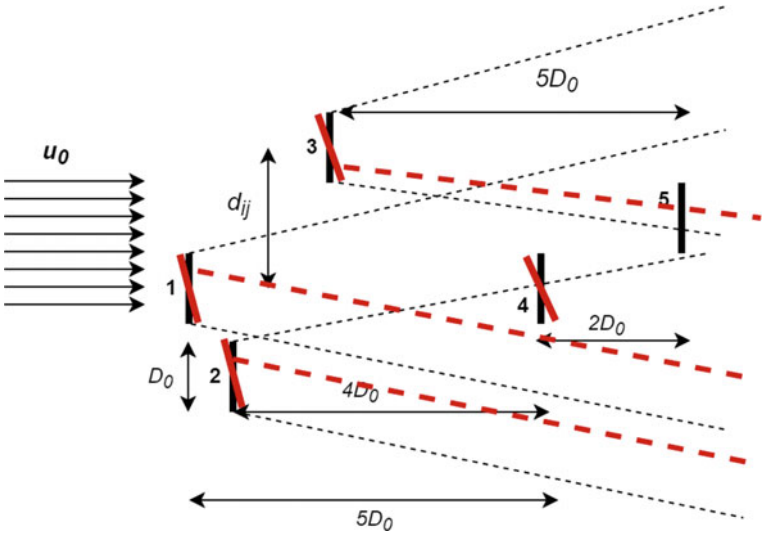

Fig. 5.14 Five-turbine wind farm layout for non-yawed and yawed condition

The model uncertainty which reflects in the form of d_{LIDAR} is considered in this case, and it is observed that for a preview distance of $d_{LIDAR} = 2D_0$, the control is fast and the error between reference and measured value is less. Consider a wind farm layout with five turbines as depicted in Fig. 5.14. Based on the proposed wake management scheme for multiple wind turbines, here we track the effective wake centers faced by turbines WT_4 and WT_5. For example, wind turbine WT_4 observes wake effect from upstream turbines WT_1 and WT_2. Similarly, for wind turbine WT_5 we can observe that wake effect from WT_1, WT_3 and WT_4 is dominant. The longitudinal distances between turbines are illustrated in terms of rotor diameter (D_0). Using (5.13), Gaussian deficit proposed by Bastankhah and Porté-Agel [4], we calculate the effective velocity deficit at downstream turbine location WT_4 and WT_5. In this scenario, the velocity deficit is determined for two cases: (i) non-yawed, when the yaw angles of upstream turbines are left unchanged and (ii) when the yaw angles of upstream turbines are changed.

Table 5.2 depicts parameters related to turbines and the wake model. For determining the effective velocity deficit in yawed condition, yaw angle γ_j for $j \in [1, 2, 3, 4]$ are listed in Table 5.2.

Now, using (5.12) based on quadratic superposition principle, the effective velocity deficit for downstream turbines WT_4 and WT_5 is calculated. Further, using system identification toolbox available in MATLAB, the transfer function model that maps input yaw angle of turbines to the output effective velocity deficit is determined using (5.15). Figure 5.3 is indicative of the multiple wake scenario where each upstream–downstream turbine model is considered as a collective unit for estimating effective wake center. Figure 5.15 illustrates the wake center estimation for WT_1 and WT_2

Table 5.2 Wind turbine parameters for WT_4 and WT_5

Parameter	Value
Rotor radius (r_0)	40 m
Wake expansion factor (k)	0.0075
Wake model parameter (k_d)	0.15
Thrust coefficient (C_T)	0.888
γ_1	$[-5°, 5°]$
γ_2	$[-10°, 10°]$
γ_3	$[-25°, 25°]$
γ_4	$[-15°, 15°]$

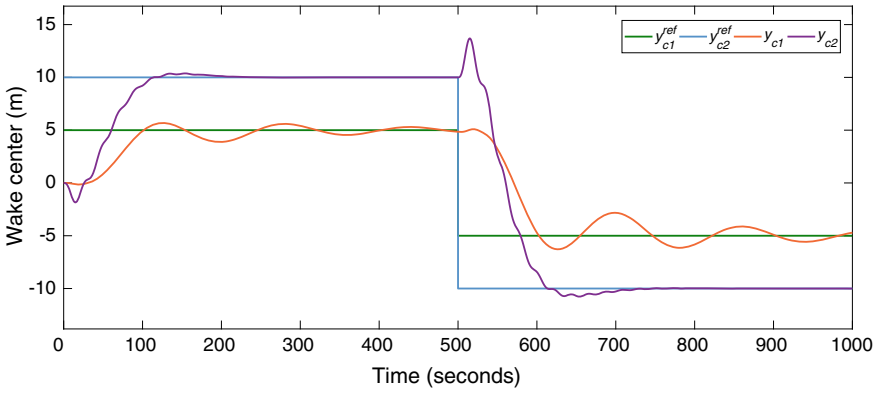

Fig. 5.15 Wake center estimation for upwind turbines WT_1 and WT_2

which are upstream turbines for WT_4. For WT_1 and WT_2, the wake center is estimated and then controlled using adaptive PI controller for desired yaw angle as listed in Table 5.2. With reference to Fig. 5.15, y_{c1}^{ref}, y_{c2}^{ref} are the reference wake centers for WT_1 and WT_2, respectively. Similarly for WT_5, the wake center for upwind turbines WT_1, WT_3, and WT_4 is estimated and controlled using an adaptive PI controller. The upstream turbines aim to follow reference wake centers where the measured output is the effective wake center for the downstream turbines.

Similarly, Fig. 5.16 illustrates the reference and estimated wake centers for WT_1 and WT_4 based on the proposed scheme for multiple wake scenario.

In the present context, LIDAR-based closed-loop adaptive control is studied for a two-turbine and five-turbine wind farm layout. An adaptive control method is implemented for identifying the uncertainties present in the wake center estimation model. The transfer function models for wind turbine and wake center are obtained using system identification toolbox available in MATLAB/Simulink. LIDAR simulations are carried out for two-turbine wind farm layout that track the wake center trajectory. An LIDAR preview distance of $1D_0$ is used and the corrected yaw angle

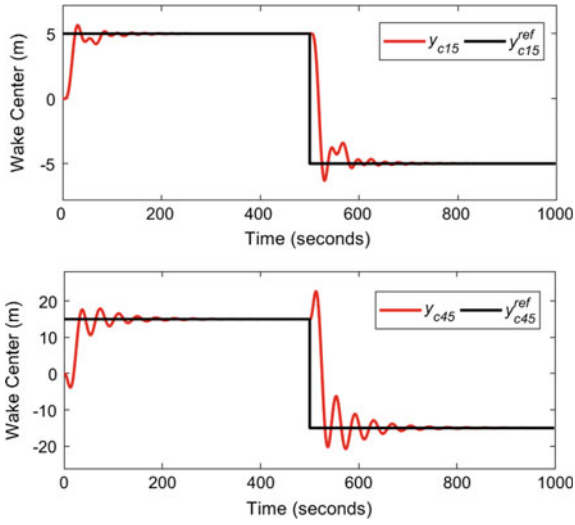

Fig. 5.16 Wake center estimation for upwind turbines WT_1 and WT_4

is then applied to the upstream turbine. Results reveal that a 7.552% increase in total wind farm power. The effect of yaw angle misalignment on the effective air turbulence is also studied and for $\gamma = 0°$, the turbulence acting on a downstream turbine, specifically, WT_2 is maximum thus indicating the need for yaw misalignment. Using adaptive controller, the scenario of multi-model approach is also studied and wake management strategy is verified for different LIDAR preview distances. Further, using a five-turbine layout, a strategy based on effective wake center and effective velocity deficit is modeled as transfer functions and can be used for optimizing power output. The scope of this proposed methodology lies in extension to Ekman layer where eddies dominate the wake flow in form of Coriolis force.

5.7 Case Study for 15-Turbine Wind Farm Layout

Wake center control for multiple wind turbines is tested for a 15-turbine layout where turbine WT_{12} is chosen as turbine of interest as it faces wake effect from the upwind turbines such as WT_2, WT_3, WT_4, WT_5, WT_7, WT_9, and WT_{10}. The distance between each turbine is expressed as a multiple of rotor diameter as illustrated in Fig. 5.17.

The wake centers for individual upstream turbines are controlled by calculating effective velocity deficit in yawed condition. The appropriate yaw angles of WT_j for $j \in [2, 3, 4, 5, 7, 9, 10]$ are $\gamma_2 = 2°$, $\gamma_3 = 2.5°$, $\gamma_4 = 5°$, $\gamma_5 = 7°$, $\gamma_7 = 9°$, $\gamma_9 = 10°$, and $\gamma_{10} = 15°$. The empirical relationship between effective wake center and effective velocity deficit so calculated from (5.15) is then transformed into an overall transfer function with multiple inputs and single output. The wake center of individual

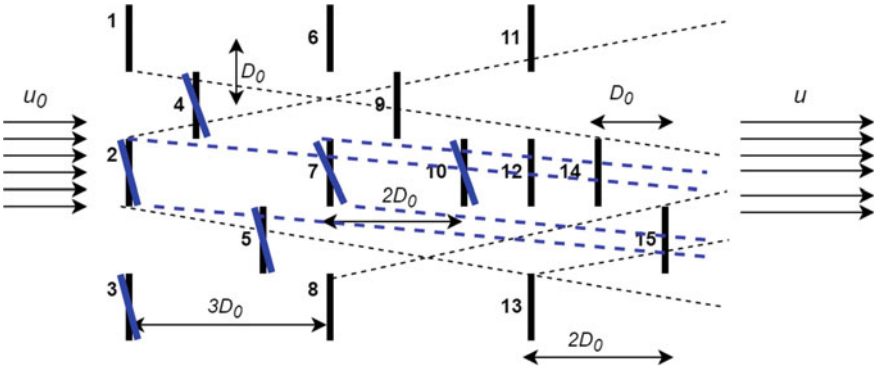

Fig. 5.17 Layout for 15-turbine wind farm in non-yawed (black solid line) and yawed condition (blue solid line)

upstream turbines is controlled for yaw angle based on effective wake center due to all upstream turbines. The LIDAR mounted at nacelle of WT_{12}, scans the effective wind field due to all upstream turbines. The LIDAR scanning distance is taken as $d_{LIDAR} = 2D_0$ for estimating the wake width. Figures 5.18 and 5.19 illustrate the wake center estimated by transfer function and by Kalman filter. The Kalman filter estimates the wake center based on the yaw angle input for multi-input single-output (MISO) system.

Results from Figs. 5.18 and 5.19 reveal that Kalman filter does not track the wake center with high accuracy owing to the nonlinear nature of wind speed, whereas the same is handled with high accuracy by the proposed methodology. The wake center control for the 15-turbine wind farm layout based on the proposed methodology yields in improved power capture and reduced turbulence.

Since wind speed possesses enormous randomness, the Kalman filter-based estimation fails to track the uncertainties posed by wind field dominated by wake effect. This is not to state that recent variants of KF techniques would not perform better, but the fact that the basic variant does not perform as good as the proposed method is significant. In order to evaluate the proposed methodology, the velocity deficit caused due to each upstream turbine for the 15-turbine layout is calculated using the Gaussian wake profile for both, non-yawed and yawed configuration using (5.12).

Figure 5.20 illustrates the effective velocity deficit and during yawed configuration the deficit is found to be 6.15% less than that in non-yawed configuration.

Table 5.3 indicates power captured by each turbine in the 15-turbine farm layout.

Further, Fig. 5.21 represents the normalized velocity at WT_{12} due to each upstream turbine. The plots for WT_2 and WT_3 show that the yaw angle does not have any significant impact on velocity deficit due to the large downstream distance of $6D_0$ to turbine WT_{12}. For WT_7, WT_9, and WT_{10} yawing, the turbine improves the velocity deficit which in turn is reflected in increased power capture. The minimum velocity is found to be at $y/D_0 = 0$ that essentially indicates wake center or the position where maximum power loss occurs.

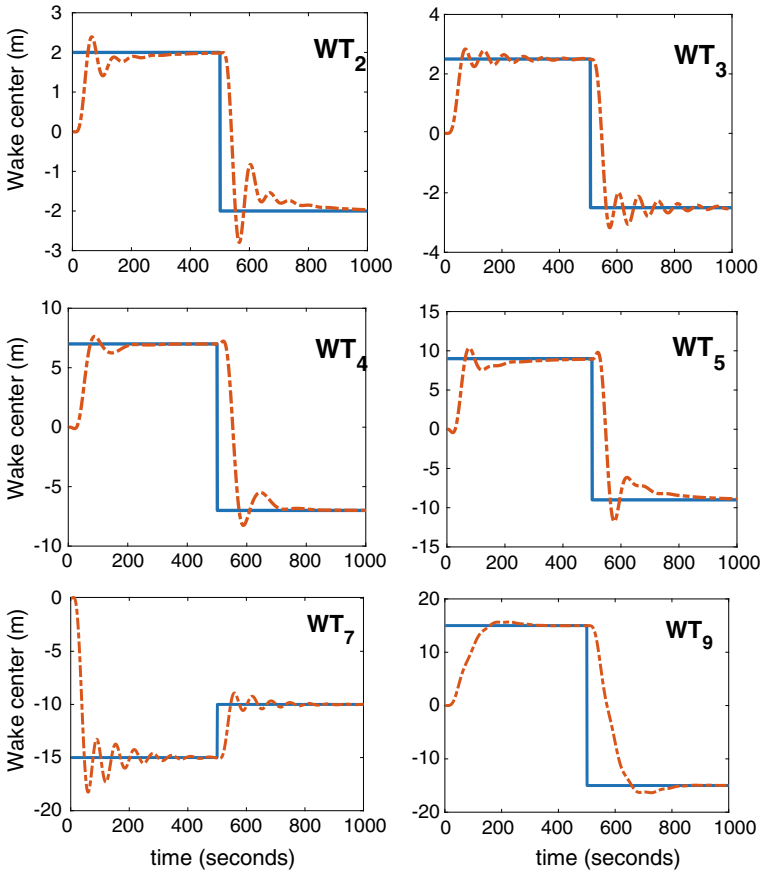

Fig. 5.18 Wake center estimated by transfer function model (orange dotted line) and reference wake center (blue solid line) for upstream turbines of WT_{12}

The powers for non-yawed (P_{ny}) and yawed (P_y) configuration are calculated considering a freestream wind speed $v_0 = 10$ m/s. Further, the wind speed at each downstream turbine is calculated based on Gaussian wake model. For each turbine, the power captured when upstream turbines are yawed is more than that in non-yawed configuration. Quantitatively, a 1.7% increase in the total wind farm power is observed when operated in yawed configuration. Among the similar studies carried out for power maximization based on yaw correction, in [1] the authors have conducted a wind tunnel test for which the effect of yawing the upstream turbine is analyzed on downstream turbine. The increase in the power coefficient of downstream turbine is validated by experimental study for a downstream distance of 3D. An advantage of the proposed methodology includes the computation time since the blocks involve transfer function models. However, it is limited by the dynamic effects in atmospheric boundary layer such as turbulent mixing of wakes. LIDAR-

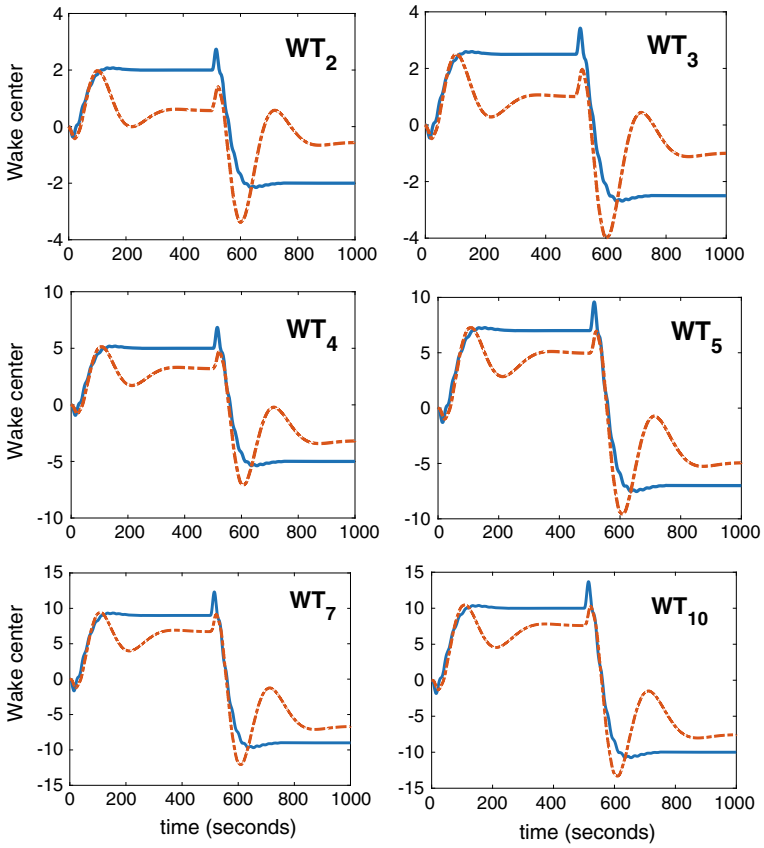

Fig. 5.19 Wake center estimated by transfer function model (blue solid line) and Kalman filter (orange dotted line) for upstream turbines of WT_{12}

based measurement of wind speed aids in controller action for appropriate yaw angle corrections. Further, industrial experiments from General Electric reveal that wake management-based control increases the plant output in the range 0.5–2% [8].

The current work proposes a novel transfer function-based closed-loop wake control strategy for wind farms which aims to track wake center of upstream turbine for power maximization at the downstream turbine. A data-driven approach is used to determine transfer functions between input yaw angle and output wake center for a multi-model scenario. Further, for multiple wind turbine scenario, the effective wind speed deficit is used to model effective wake center for a particular upstream turbine (WT_{12}) in our case. Utilizing advanced control algorithms, wake management incorporates data with random wind characteristics and micro-siting information. The proposed methodology is compared with KF technique. Results reveal that KF-based wake center estimation suffers from uncertainties in wind speed which are handled accurately by LIDAR-based measurement. Further, a 1.7% increase in total wind power is found when upstream turbines are operated in the yawed mode.

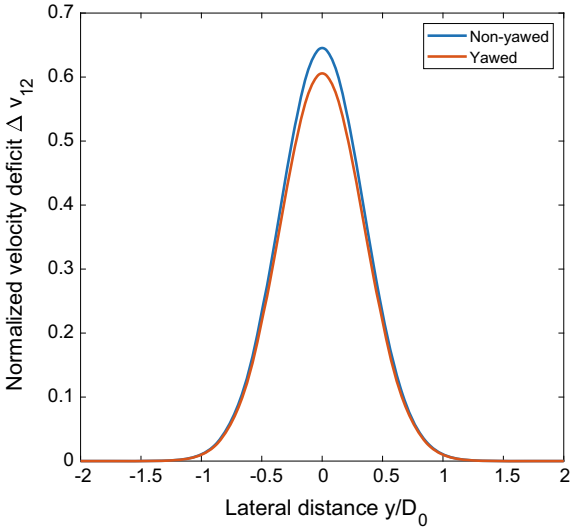

Fig. 5.20 Effective velocity deficit for WT_{12} for non-yawed and yawed condition

Table 5.3 Individual turbine power in non-yawed and yawed condition

Wind turbine	Upstream turbine	Power (P_{ny}) (MW)	Power (P_y) (MW)	% change
WT_1	NA	2.8274	2.8274	0.00
WT_2	NA	2.8274	2.8223	–0.1800
WT_3	NA	2.8274	2.8223	–0.1800
WT_4	1, 2	1.5074	1.5116	+0.2786
WT_5	2, 3	2.6816	2.6916	+0.3729
WT_6	1, 4	2.0666	2.0891	+1.0887
WT_7	2, 4, 5	2.0561	2.1541	+4.7663
WT_8	3, 5	2.0162	2.1130	+4.8011
WT_9	1, 4, 6, 7	2.0053	2.1016	+4.8022
WT_{10}	2, 5, 7, 9	2.0001	2.0884	+4.4414
WT_{11}	1, 2, 4, 6, 9	2.0761	2.0962	+0.9681
WT_{12}	2, 3, 4, 5, 7, 9, 10	1.9821	1.9959	+0.6962
WT_{13}	3, 5, 8	2.0752	2.0965	+0.9782
WT_{14}	2, 3, 4, 5, 7, 9, 10, 12	1.9701	1.9862	+0.8172
WT_{15}	2, 5, 7, 8, 10, 12, 13, 14	1.9970	2.0866	+4.4867
		$\sum P_{ny} = 32.916$	$\sum P_y = 33.483$	

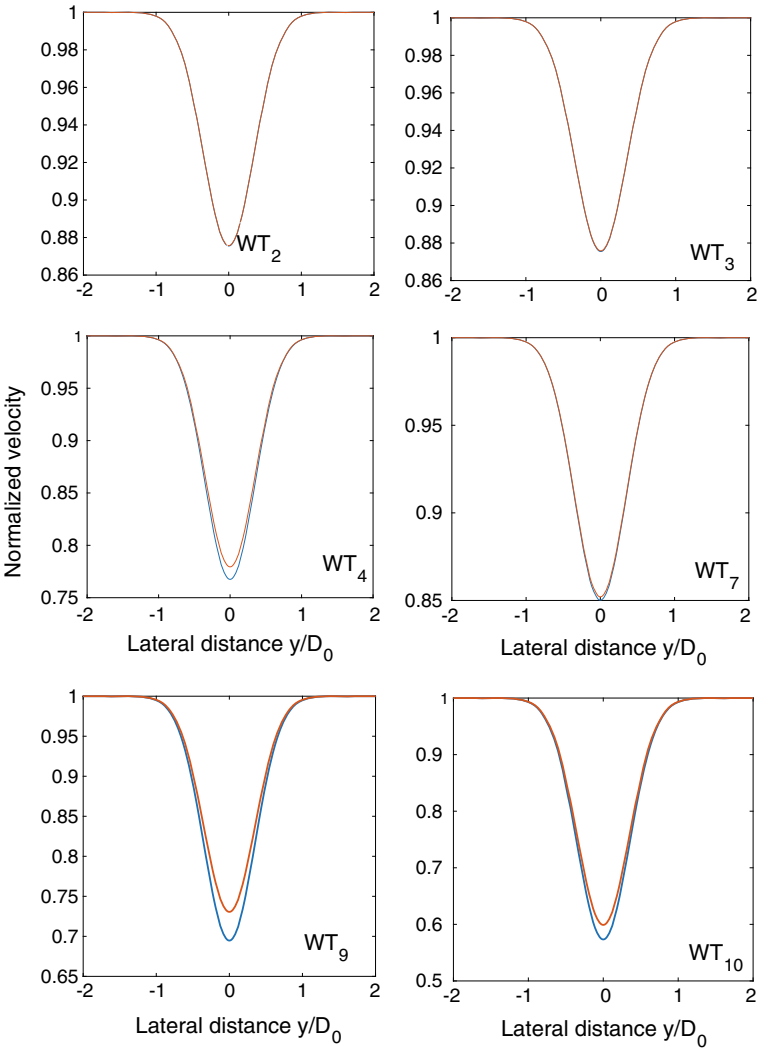

Fig. 5.21 Normalized velocity for WT_{12} for non-yawed (blue) and yawed (orange) condition

References

1. Adaramola M, Krogstad PÅ (2011) Experimental investigation of wake effects on wind turbine performance. Renew Energy 36(8):2078–2086
2. Antonini EG, Romero DA, Amon CH (2019) Improving CFD wind farm simulations incorporating wind direction uncertainty. Renew Energy 133:1011–1023
3. Barthelmie RJ, Pryor SC (2019) Automated wind turbine wake characterization in complex terrain. Atmos Meas Tech Discuss, 1–31

4. Bastankhah M, Porté-Agel F (2014) A new analytical model for wind-turbine wakes. Renew Energy 70:116–123
5. Beyer F, Luhmann B, Raach S, Stuttgarter PWC (2015) Shadow effects in an offshore wind farm - potential of vortex methods for wake modelling
6. Bianchi FD, Mantz RJ, Battista HD (2007) Wind turbine control systems. Springer, London
7. Boersma S, Doekemeijer B, Gebraad P, Fleming P, Annoni J, Scholbrock A, Frederik J, van Wingerden JW (2017) A tutorial on control-oriented modeling and control of wind farms. In: 2017 American control conference (ACC). IEEE
8. Burra R, Ambekar A, Narang H, Liu E, Mehendale C, Thirer L, Longtin K, Shah M, Miller N (2014) GE brilliant wind farms. In: 2014 IEEE symposium on power electronics and machines for wind and water applications. IEEE
9. Cacciola S, Bertelè M, Schreiber J, Bottasso C (2016) Wake center position tracking using downstream wind turbine hub loads. J Phys: Conf Ser 753:032036
10. Campagnolo F, Petrović V, Schreiber J, Nanos EM, Croce A, Bottasso CL (2016) Wind tunnel testing of a closed-loop wake deflection controller for wind farm power maximization. J Phys: Conf Ser 753:032006
11. Chen CT (2001) Direct adaptive control of chemical process systems. Ind Eng Chem Res 40(19):4121–4140
12. Chowdhury S, Zhang J, Messac A, Castillo L (2012) Unrestricted wind farm layout optimization (UWFLO): investigating key factors influencing the maximum power generation. Renew Energy 38(1):16–30
13. Dar Z, Kar K, Sahni O, Chow JH (2017) Windfarm power optimization using yaw angle control. IEEE Trans Sustain Energy 8(1):104–116
14. Deb D, Tao G, Burkholder J, Smith D (2005) An adaptive inverse control scheme for a synthetic jet actuator model. In: Proceedings of the 2005, American control conference. IEEE
15. Deb D, Tao G, Burkholder J, Smith D (2008) Adaptive synthetic jet actuator compensation for a nonlinear aircraft model at low angles of attack. IEEE Trans Control Syst Technol 16(5):983–995
16. Dou B, Guala M, Lei L, Zeng P (2019) Experimental investigation of the performance and wake effect of a small-scale wind turbine in a wind tunnel. Energy 166:819–833
17. Doubrawa P, Barthelmie R, Wang H, Pryor S, Churchfield M (2016a) Wind turbine wake characterization from temporally disjunct 3-d measurements. Remote Sens 8(11):939
18. Doubrawa P, Barthelmie RJ, Wang H, Churchfield MJ (2016b) A stochastic wind turbine wake model based on new metrics for wake characterization. Wind Energy 20(3):449–463
19. Dunne F, Pao L, Wright A, Jonkman B, Kelley N (2010) Combining standard feedback controllers with feedforward blade pitch control for load mitigation in wind turbines. In: 48th AIAA aerospace sciences meeting including the new horizons forum and aerospace exposition. American Institute of Aeronautics and Astronautics
20. Fleming P, Annoni J, Shah JJ, Wang L, Ananthan S, Zhang Z, Hutchings K, Wang P, Chen W, Chen L (2017) Field test of wake steering at an offshore wind farm. Wind Energy Sci 2(1):229–239
21. Fleming PA, Gebraad PM, Lee S, van Wingerden JW, Johnson K, Churchfield M, Michalakes J, Spalart P, Moriarty P (2014) Evaluating techniques for redirecting turbine wakes using SOWFA. Renew Energy 70:211–218
22. Gebraad P, Fleming P, van Wingerden J (2015) Wind turbine wake estimation and control using FLORIDyn, a control-oriented dynamic wind plant model. In: 2015 American control conference (ACC). IEEE
23. Gebraad PMO, Teeuwisse F, van Wingerden J, Fleming PA, Ruben SD, Marden JR, Pao LY (2014) A data-driven model for wind plant power optimization by yaw control. In: 2014 American control conference, IEEE
24. Howland MF, Bossuyt J, Martínez-Tossas LA, Meyers J, Meneveau C (2016) Wake structure in actuator disk models of wind turbines in yaw under uniform inflow conditions. J Renew Sustain Energy 8(4):043301
25. Ioannou PA, Sun J (1995) Robust adaptive control. Prentice-Hall Inc, Upper Saddle River

26. Iungo GV (2016) Experimental characterization of wind turbine wakes: wind tunnel tests and wind LiDAR measurements. J Wind Eng Ind Aerodyn 149:35–39
27. Jiménez Á, Crespo A, Migoya E (2009) Application of a LES technique to characterize the wake deflection of a wind turbine in yaw. Wind Energy 13(6):559–572
28. Jonkman J, Butterfield S, Musial W, Scott G (2009) Definition of a 5-MW reference wind turbine for offshore system development. Technical report
29. Katic I, Højstrup J, Jensen N (1987) A simple model for cluster efficiency. A. Raguzzi, pp 407–410
30. Landau ID, Lozano R, M'Saad M, Karimi A (2011) Adaptive control. Springer, London. https://doi.org/10.1007/978-0-85729-664-1
31. Larsen G, Larsen T, Chougule A (2017) Medium fidelity modelling of loads in wind farms under non-neutral abl stability conditions a full-scale validation study. J Phys: Conf Ser 854(1):012026
32. Machefaux E, Larsen GC, Troldborg N, Gaunaa M, Rettenmeier A (2014) Empirical modeling of single-wake advection and expansion using full-scale pulsed lidar-based measurements. Wind Energy 18(12):2085–2103
33. Maeda T, Yokota T, Shimizu Y, Adachi K (2004) Wind tunnel study of the interaction between two horizontal axis wind turbines. Wind Eng 28(2):197–212
34. Manwell JF, McGowan JG, Rogers AL (2009) Wind energy explained. Wiley Ltd, New York
35. Nath A, Deb D, Dey R, Das S (2018) Blood glucose regulation in type 1 diabetic patients: an adaptive parametric compensation control-based approach. IET Syst Biol 12(5):219–225
36. Nguyen NT (2018) Model-reference adaptive control. Springer International Publishing, Berlin. https://doi.org/10.1007/978-3-319-56393-0
37. Patel R, Deb D (2018) Parametrized control-oriented mathematical model and adaptive backstepping control of a single chamber single population microbial fuel cell. J Power Sourc 396:599–605
38. Qian GW, Ishihara T (2018) A new analytical wake model for yawed wind turbines. Energies 11(3):665
39. Raach S, Schlipf D, Borisade F, Cheng PW (2016) Wake redirecting using feedback control to improve the power output of wind farms. In: 2016 American control conference (ACC). IEEE
40. Raach S, Schlipf D, Cheng PW (2016) Lidar-based wake tracking for closed-loop wind farm control. J Phys: Conf Ser 753:052009
41. Rezaei V (2014) LIDAR-based robust wind-scheduled control of wind turbines. In: 2014 American control conference. IEEE
42. Schlipf D, Kühn M (2008) Prospects of a collective pitch control by means of predictive disturbance compensation assisted by wind speed measurements. In: Proceedings of the 9th German wind energy conference DEWEK, 26th to 27th November, Bremen, Germany
43. Schlipf D, Fischer T, Carcangiu CE, Rossetti M, Bossanyi E (2010) Load analysis of look-ahead collective pitch control using lidar. In: Proceedings of the 10th German wind energy conference DEWEK
44. Schlipf D, Schlipf DJ, Kühn M (2012) Nonlinear model predictive control of wind turbines using LIDAR. Wind Energy 16(7):1107–1129
45. Scientific C (2016) Finance grade performance, zephir 300. Technical report, 14532 131 Avenue NW Edmonton AB T5L 4X4 Canada. https://s.campbellsci.com/documents/ca/product-brochures/zephir300_br.pdf
46. Shahalami SH, Farsi D (2018) Analysis of load frequency control in a restructured multi-area power system with the kalman filter and the LQR controller. AEU - Int J Electron Commun 86:25–46
47. Simley E, Pao L, Frehlich R, Jonkman B, Kelley N (2011) Analysis of wind speed measurements using continuous wave LIDAR for wind turbine control. In: 49th AIAA aerospace sciences meeting including the new horizons forum and aerospace exposition. American Institute of Aeronautics and Astronautics
48. Sun F, Hu X, Zou Y, Li S (2011) Adaptive unscented kalman filtering for state of charge estimation of a lithium-ion battery for electric vehicles. Energy 36(5):3531–3540

49. Thomsen K, Sørensen P (1999) Fatigue loads for wind turbines operating in wakes. J Wind Eng Ind Aerodyn 80(1–2):121–136
50. Vali M, Petrovic V, Boersma S, van Wingerden JW, Pao LY, Kuhn M (2018) Model predictive active power control of waked wind farms. In: 2018 annual American control conference (ACC). IEEE
51. Wang H, Barthelmie RJ, Doubrawa P, Pryor SC (2016) Errors in radial velocity variance from doppler wind lidar. Atmos Meas Tech 9(8):4123–4139

Chapter 6
BESS Life Enhancement for Hybrid Wind Farms

A battery energy storage system (BESS) is a system that stores energy via the use of a battery technology for it to be used when needed later on. Intermittent wind power not only increases the cost of specifically constructed BESS needed in stochastic wind power generation but also leads to degraded battery life. This chapter deals with battery optimization by a wind wake management technique aimed at reducing the operational cost. A two-turbine wind farm is studied, and battery charging and discharging events are identified based on the forecast error of wind speed. The life cycle count is determined based on an empirical relationship between the counts of charging and discharging cycles and depth of discharge of battery.

Three different conditional analysis of wind farm layout exist and are as follows: (i) without wake, (ii) without wake management, and (iii) with wake management. Further, the operating cost and life cycle count for the BESS are assessed based on a global battery aging model that accounts for temperature changes. Results are validated for two datasets, and it is found that the battery operational cost is minimum with the implementation of wake management technique on upwind turbine.

6.1 Introduction

Power output from a wind energy source is subjected to high variation owing to random nature of wind. Dispatch of wind power not only suffers from fluctuations but also from the cost involved from the ancillary support. Battery energy storage systems (BESS) pose a cost-efficient solution to mitigate the fluctuations in wind output [2]. BESS-based energy dispatch is governed by operational constraints which often decide the discharging capabilities for a battery system. Penalty faced by the wind energy operators typically is considerably high if the forecasted power levels do not meet the assured ones. Such intermittency can jeopardize system stability and enhance dependency on storage systems [25]. Thus, integrating storage systems and renewable sources for an optimized grid operation are challenging [28].

H. S. Dhiman and D. Deb, *Decision and Control in Hybrid Wind Farms*,
Studies in Systems, Decision and Control 253,
https://doi.org/10.1007/978-981-15-0275-0_6

Various studies have discussed optimization of wind-battery hybrid system operation but the possibility under wind wakes remains unexplored. Wind forecasting is an important market procedure to ensure a reliable grid-connected operation. Catalao et al. have presented forecasting methods based on temporal scales with short-term and medium-term wind forecasting in electricity markets [6]. However, wind prediction encounters challenges in terms of nonlinearity of wind speed time series which is handled better by advanced machine learning algorithms like support vector regression and extreme learning machine.

Du et al. present a new hybrid wind forecasting model that encapsulates the ensemble empirical mode decomposition [40, 41] for extracting the main features of the wind speed time series and have used multi-objective moth-flame optimization to obtain optimal parameters for neural network [14]. The proposed method is then applied at a wind farm Sotavento in Spain. Four time series with 1500 data points are taken and are segregated into training (1200) and testing (300) set. Results reveal that the proposed model outperformed Generalized neural network and Wavelet neural network with respect to error attributes like RMSE and MAE. Accuracy in wind speed prediction determines the dependency on the storage systems to outlay the economic blueprint for the entire system. Hao et al. described a detailed two-stage model that incorporates the error in wind power forecasts initially to forecast a more stable and reliable wind power by using multi-objective grey wolf optimizer (MOGWO) based on extreme learning machine (ELM model) [21, 29, 38, 39], and for model validation, three datasets from Ontario, Canada, and Galicia, Spain, are used, and the proposed model is compared with benchmark models like persistence model, ARIMA, backpropagation neural network, and Elman neural networks.

The operation of BESS is governed by state of charge (SoC) at a given time. The SoC estimation and forecasting plays an important role in battery charging and discharging characteristics. Conventionally, SoC is defined as the charge present in the battery as a percentage of full charge capacity. The estimation of SoC of a battery system finds its primary application in hybrid electric vehicles and storage systems for renewable energy sources (solar and wind). Parameters like open-circuit voltage (OCV) and transfer impedance directly influence the SoC. Among many methods, Kalman filtering [32], extended Kalman filtering [7, 9, 34, 36, 45], and unscented Kalman filtering [42] are commonly used.

Kalman filter-based SoC estimation is carried out to estimate the battery capacity by considering an equivalent circuit of battery in terms of voltage source, resistors, and capacitors. The relationship between SoC and open-circuit battery voltage is often reported as nonlinear over different temperature ranges [43]. Kalman filter was initially presented in 1960 that essentially involves discrete mathematical expressions to model the state estimation along with process and measurement noise [20, 31]. Yu et al. discussed SoC estimation in lithium-ion batteries using Kalman filter [44]. The authors consider a dual-polarization model equivalent to second-order model for a battery. To validate the model, experimental analysis is carried out for a Li-ion phosphate battery with rated voltage of 2.5 V and capacity of 280 mAh. Results indicate an error of 0.5%. Mastali et al. discussed two models, extended Kalman filter and dual Kalman filter, for estimating SoC considering the effect of battery

geometry [32]. Extended Kalman filter and dual extended Kalman filter techniques are used for fixed parameter and varying parameters battery models. Two geometries with cylindrical and prismatic shapes are considered and results reveal an estimation error of 4% .

Chen et al. presented SoC estimation for a Li-ion battery using a feedforward neural network (FFNN) framework and extended Kalman filtering [7] to model a battery specifically at low temperatures with unknown initial SoC. FFNN is used to trace a neural network for mapping the inputs SoC, battery current, surface temperature, and polarization state to output battery terminal voltage. Further, SoC estimation is also used in hybrid electric vehicles in harmony with battery management system (BMS). Due to the dynamic nature of the battery, SoC determination is done online for predicting the remaining life so as to take preventive steps before potential failure. Claude et al. carried out an extended Kalman filter (EKF) based experimental validation for Li-ion battery [9] by considering a double RC electrical circuit whose parameters are calculated by determining the voltage drop upon application of charge/discharge signals. Polynomial equations relating to open-circuit voltage and SoC with fourth and sixth-order degree have been determined with an error approximately in the range of 4–18% between experimental values and those determined by EKF. Further, Chen et al. demonstrated an online SoC estimation for Li-ion battery using an improved unscented Kalman filter (IUKF) method [8]. The battery parameters are identified offline and a relationship between open-circuit voltage and SoC is obtained in MATLAB. In order to overcome the limitations posed by improper modeling of battery and process noise, an adaptive model and noise algorithm is proposed. Experimental results suggested the superiority of IUKF over adaptive UKF with an error as low as 1.5%.

Coulomb counting and machine learning-based methods like artificial neural networks and support vector machines are also used for estimating SoC of a battery [26]. Commercially available BESS include lead acid battery (LA), lithium-ion battery (Li-ion), sodium sulfur (NaS), and nickle cadmium (NiCd) battery. Among these, lead acid battery is used for providing reserve capacity in wind farms owing to its deep charging and discharging.

Wind farm operation not only suffers from forecasting errors but also from wake effect created due to upwind turbines. The aforementioned aerodynamic phenomenon leads to reduction in effective power captured at the downstream turbines. Early wake model developed by N. Jensen encapsulates the development of wake behind rotor diameter [24]. Jensen's wake model is utilized for wind farm power calculations [35], and other works have been validated and tested to accommodate the power losses in wind and the losses are found in acceptable range [5, 10, 33]. Velocity deficit due to wake effect can be minimized by either axial induction method that alters the pitch of the upwind turbine or by redirection of the wake behind the upwind turbine by changing the yaw angle. Control-oriented wake redirection has been explored by Fleming et al. with a high-fidelity simulation tool to investigate the wake redirection on the power capture capability of the downstream turbine [17]. Further, Gebraad et al. have demonstrated a novel dynamic wake model for estimating wake center, effective wind speed, and power production for downstream turbines in a wind farm [18].

Experimental analysis has also revealed yaw angle control of the upstream turbine to deflect the wake field behind rotor and enhance the power capturing capabilities of downstream turbine [22, 23]. Repositioning the downstream turbine can significantly reduce the rotor shadow under upstream turbine as described by Gebraad et al., as it improves velocity profile and increases net power capture [19].

With a hybrid wind farm operation, the focus is also laid on the accurate forecasts needed to schedule BESS dispatch. On the lines of wind forecasting, our previous work based on hybrid machine intelligent SVR variants [13], we now extend the hybrid wind farm operation by considering the wake phenomenon. A typical BESS-enabled wind farm is subjected to erratic power dispatch, and in order to optimize the overall system cost and lessen the hurdles in frequent maintenance, a wake management technique is implemented and validated for a two-turbine wind farm. The major contribution of this chapter includes BESS cost estimation for every kilowatt (kW) of wind power forecasted in the presence of wakes with inaccuracy in forecasting error. Further, the life cycle improvement of the BESS with appropriate wake management technique based on yaw angle is investigated for a two-turbine wind farm layout. This chapter is organized as follows: Sect. 6.2 discusses the problem formulation where the energy reservoir model for state of charge (SoC) forecast is discussed for battery along with the forecast strategy for wind speed and BESS cost model. Section 6.3 throws light on results followed by discussion in Sect. 6.4.

6.2 Problem Formulation

With reference to wind speed forecasting, deterministic and probabilistic forecasting methods are used. However, with advances in deterministic forecasting methods like support vector regression and ensemble models, here probabilistic approach is not considered with each wind regime representing a unique distribution profile. Dhiman et al. have discussed hybrid variants of machine intelligent SVR models for wind forecasting and wind ramp events [13]. The current scenario of BESS for wind power integration involves significant error in forecasting wind speed which is then assessed to either charge or discharge the BESS. In case the forecasted wind speed exceeds the actual wind speed, the deficit power is then compensated by discharging the BESS given the SoC constraints are not violated. However, in presence of wind wakes, the actual wind speed at the downstream turbine is much less than the freestream wind speed at the upwind turbine, and the deficit in power generated is then compensated by the BESS. Since the storage devices are expensive initial investments, erratic charging and discharging schedules can significantly hamper battery life and hence the operational cost. A yaw angle based wake management strategy redirects the wake stream behind the upwind turbine to reduce the velocity deficit caused, and thus increases the power captured by the downstream turbine.

6.2.1 Wind Forecasting Using Least Square Support Vector Regression

Least square support vector regression (LSSVR), a variant of the original formulation of Suykens et al. [37], which chooses equality constraints and minimizes the square of the penalty term in the loss function, is applied for accurate forecasts in many diverse areas as illustrated in Fig. 6.1.

Mathematically, LSSVR is expressed as

$$f(x) = w^{\mathrm{T}}\phi(x) + b, \tag{6.1}$$

with $w \in \mathrm{R}^{\mathrm{n}}$ as the weight vector, T representing vector transform, $x_i \in \mathrm{R}^{\mathrm{n}}$, $y \in \mathrm{R}$, and b as a bias term:

$$\min \ \frac{1}{2} \parallel w \parallel^2 + \frac{1}{2}\gamma_z \sum_{i=1}^{n} \varepsilon_i^2 \tag{6.2}$$

$$\textbf{s.t.} \ \ y_i = w^{\mathrm{T}}\phi(x_i) + b + \varepsilon_i, \ \ (i = 1, 2, \ldots, n), \tag{6.3}$$

where γ_z is the margin parameter and ε_i is the error term for each x_i, and using Lagrange multipliers, we have

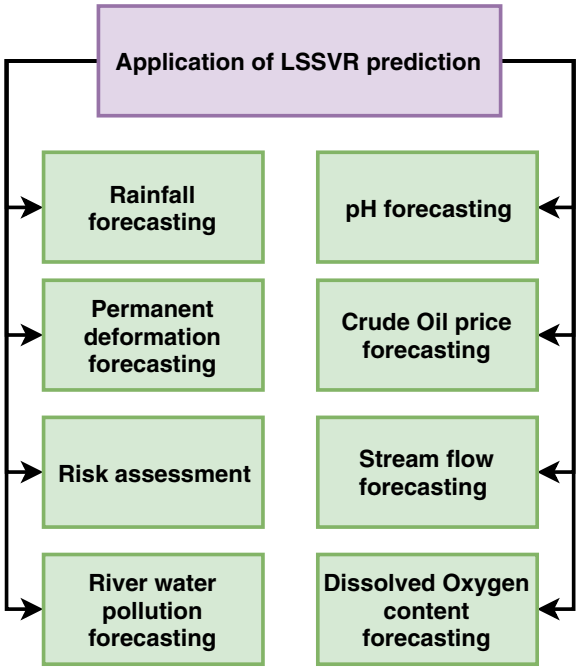

Fig. 6.1 Applications of LSSVR

$$L(w, b, \varepsilon, \alpha) = \frac{1}{2} \parallel w \parallel^2 + \frac{1}{2}\gamma_z \sum_{i=1}^{n} \varepsilon_i^2 - \sum_{i=1}^{n} \alpha_i (w^T \phi(x_i) + b + \varepsilon - y_i). \quad (6.4)$$

The Karush–Kuhn–Tucker (KKT) conditions for this formulation are obtained by partial differentiation with respect to $w, b, \varepsilon, \alpha$ given as

$$\begin{cases} \dfrac{\partial L}{\partial w} = 0 \Rightarrow w = \displaystyle\sum_{i=1}^{n} \alpha_i \phi(x_i) \\ \dfrac{\partial L}{\partial b} = 0 \Rightarrow \displaystyle\sum_{i=1}^{n} \alpha_i = 0 \\ \dfrac{\partial L}{\partial \varepsilon} = 0 \Rightarrow \gamma_z \varepsilon_i = \alpha_i \\ \dfrac{\partial L}{\partial \alpha} = 0 \Rightarrow w^T \phi(x_i) + b + \varepsilon - y_i = 0 \end{cases}$$

$$\begin{bmatrix} k(x, x^T) + \gamma_z^{-1} I & e \\ e^T & 0 \end{bmatrix} \begin{bmatrix} \alpha \\ b \end{bmatrix} = \begin{bmatrix} y \\ 0 \end{bmatrix}, \quad (6.5)$$

$$f_{LS-SVR}(x) = \sum_{i=1}^{n} \alpha_i k(x, x_i) + b, \quad (6.6)$$

where I is the identity matrix of appropriate dimension and $k(x, x_i)$ is the kernel function. The parameter α which is a Lagrangian multiplier is half the size of that in conventional ε-SVR regression problem. This smaller sized matrix increases computation time significantly. The parameter w essentially assigns a quantitative weight to each training sample while the bias term b is more of a correction term. The term ε is tolerance error that can be imposed on support vectors during training phase. Errors more than ε are penalized with a term C. The regressor given by (6.6) provides a solution to the optimization problem of a size smaller than the ε-SVR regressor and is therefore computationally faster. This technique is used to predict wind speed under three different cases, and the respective wind power is calculated. If the actual wind power exceeds the predicted one, the excess power is used to charge BESS, else discharging occurs.

Liu et al. studied the parameter optimization methods in tandem with LSSVR for forecasting dissolved oxygen content in transformer oil during incipient faults [30]. The data for dissolved gases is collected from several power companies, and imperialist competition algorithm (ICA) is used to find optimal hyperparameters for LSSVR. The method is compared with several other methods like back propagation neural network, generalized regression neural network, and radial basis function neural network. Results reveal that ICA-LSSVR-based forecasting yields better results in terms of MAPE and R^2.

In terms of river flow forecasting, Adnan et al. carried out a hybrid forecasting method based on LSSVR and Gravitational search algorithm (HLSGA) where two catchment areas on the upper Indus basin of Pakistan are selected [3]. The mean annual data for 32 years is chosen to study the hybrid method. In order to validate the method, n datasets are divided into $n-1$ sets for training. Further, various input combinations based on the autocorrelation values of the river flow data. Results reveal that HLSGA method outperforms model 5 regression tree (M5RT) and multiple linear regression (MLR) in terms of RMSE and MAE. Further, the effect of log transformation on the river flow time series is also analyzed, and the forecasting results of log-HLSGA are compared with HLSGA. The log transformation reduces skewness in the time-series data and yields better forecasts for all methods when compared to the original methods.

6.2.2 SoC Estimation Based on Energy Reservoir Model

The SoC estimation for battery is carried out using standard Kalman filter, extended Kalman filter [32], unscented Kalman filtering technique [4] based on battery model. Energy reservoir model (ERM) is based on the BESS charging and discharging powers. SoC is then estimated depending on the current available energy in the battery in terms of kWh and is expressed as

$$x_{SoC}(t) = x_{SoC}(t_0) - \frac{\Delta t/3600}{Q_{batt}} \sum_{i=1}^{T} (p_{dis}(i) + \eta_b p_{ch}(i) + p_s), \tag{6.7}$$

where $x_{SoC}(t)$, $x_{SoC}(t_0)$ are the estimated SoC at time interval t and initial SoC, respectively, p_{dis}, p_{ch}, η_b, and p_s are the discharging power, charging power, efficiency, and self-discharging scale factor, respectively. Charging and discharging powers are calculated based on the equations

$$p_{batt} = \begin{cases} p_{ch} = P_{wind} - \hat{P}_{wind} > 0 \\ p_{dis} = \hat{P}_{wind} - P_{wind} > 0, \end{cases} \tag{6.8}$$

where P_{wind} and $\hat{P}_{wind}$ are the actual and forecasted wind powers. The ERM is computationally rich and deals with linear equations which are easier to implement. In matrix form, ERM can be expressed as

$$H = \frac{-1/3600}{Q_{batt}} \begin{bmatrix} 1 \\ \eta_b \\ p_s \end{bmatrix}, \tag{6.9}$$

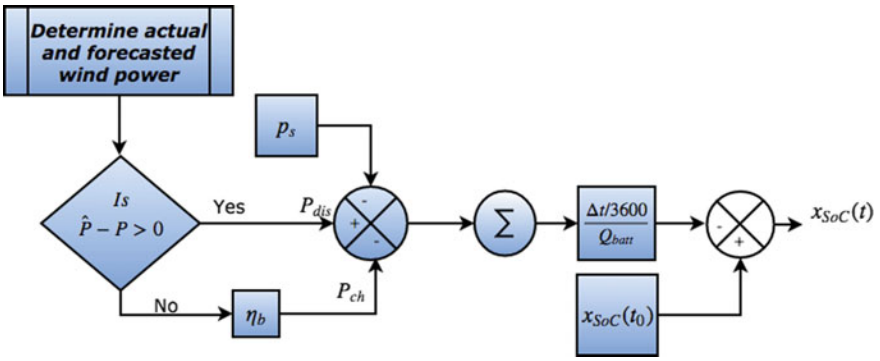

Fig. 6.2 Flowchart for SoC forecast based on charging/discharging powers

$$P_p = \begin{bmatrix} \Delta t p_{dis}(1) & \Delta t p_{ch}(1) & \Delta t \\ \Delta t (p_{dis}(1) + p_{dis}(2)) & \Delta t (p_{ch}(1) + p_{ch}(2)) & 2\Delta t \\ \vdots & \vdots & \vdots \\ \Delta t \sum_{i=1}^{T} p_{dis}(i) & \Delta t \sum_{i=1}^{T} p_{ch}(i) & n\Delta t \end{bmatrix},$$

where Δt is the time horizon (in seconds) for the next SoC estimate and first two columns of the P_p matrix represent the cumulative sum of discharging and charging power in kWh, respectively. In the present study, the ERM is used based on charging and discharging power calculated from the error in wind power forecasting. The SoC can be estimated as

$$x_{SoC} = P_p H + x_{SoC}(t_0), \tag{6.10}$$

where $x_{SoC}(t_0)$ is the randomly generated initial SoC calculated using random function generator MATLAB. The ERM model for SoC estimation is subjected to constraints ($x_{SoC}^{min} < x_{SoC} < x_{SoC}^{max}$) and upon violation of these constraints, the surplus power can be fed to neighboring wind farm(s).

The flowchart for ERM for SoC estimation is illustrated in Fig. 6.2.

Furthermore, in case the forecasted wind power $\hat{P}_{wind}$ exceeds P_{wind}, the BESS is allowed to discharge to compensate for deficit power. However, if the magnitude of discharge power violates the SoC limits, the wind farm operator decides to pay penalty or borrow deficit power from neighboring wind farms. In the present scenario with two wind turbines, the objective is to obtain accurate wind forecasts to minimize the duty on BESS. Based on the SoC calculated from (6.10), the depth of discharge ($x_{DoD} = 100 - x_{SoC}$) is determined for the BESS charging/discharging event.

6.2.3 Operational Cost Model for BESS

Charging and discharging of batteries according to the forecasting error, poses an operational cost to be incurred. For a lithium-ion battery, a linear relationship between number of life cycles (N_{cyc}) and logarithm of depth of discharge (x_{DoD}) is obtained in [15] and is given as

$$N_{cyc} = m \times \log(x_{DoD}) + c, \tag{6.11}$$

where m and c are slope and intercept for the linear equation (6.11), with $m = -1808$ and $c = 8644.5$.

The cost of BESS for each charging/discharging event can be calculated if the battery's health condition is known. Farzin et al. have discussed a model for BESS that determines the operational cost of BESS depending on number of life cycles left with battery in use [16] and is given as

$$C_{batt} = B_{batt} \sum_{i=1}^{N-1} \left[\frac{1}{N_{cyc}(i+1)} - \frac{1}{N_{cyc}(i)} \right], \tag{6.12}$$

where N_{cyc} is the life cycle count at the end of ith charging/discharging event, and B_{batt} is the capital cost of the BESS.

Battery aging is a complex process and is not only dependent on depth of discharge but also on the ambient temperature that accelerates the aging [27]. A mathematical model that describes the relationship between number of life cycles, depth of discharge, and ambient temperature is given as

$$N_{cyc} = \begin{cases} \left(12850e^{-(9.738*x_{DoD})} + 3210e^{-(1.429*x_{DoD})}\right), & T_{amb} \leq 20°C \\ \left(12850e^{-(9.738*x_{DoD})} + 3210e^{-(1.429*x_{DoD})}\right) \\ \left(37.68T_{amb}^{-1.101} - 0.3897\right), & T_{amb} > 20°C, \end{cases}$$

where x_{DoD} and T_{amb} are the depth of discharge and ambient temperature. Figure 6.3 illustrates the number of BESS cycles as a function of depth of discharge and ambient temperature. For ambient temperature of more than 20° C, the battery life is affected in terms of reduction in cycle count.

6.2.4 Wake Management for Wind Farms

The reduction in wind speed due to upwind turbines leads to lesser power extraction at the downstream turbines. A wake redirection approach where the yaw angle for upwind turbine is varied to deflect the wake stream away from downstream rotor improves the wind speed profile [12].

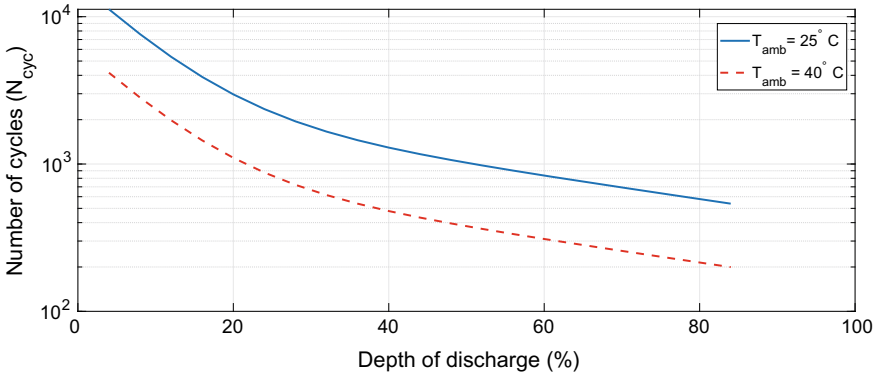

Fig. 6.3 Number of BESS cycles as a function of x_{DoD} and ambient temperature

The improved velocity profile then further improves the power captured at the downstream turbine. The wind speed under wake calculated based on Jensen's wake model is

$$v_j = v_0\left(1+\left(\sqrt{1-C_T}-1\right)\left(\frac{r_0}{r_x}\right)^2\right),\ r_x = r_0+\alpha_y x, \tag{6.13}$$

where v_j, v_0 are the wind speed under wake effect and freestream wind speed [24]. The factor α_y gives an idea about how quickly wake expands behind rotor. The wake stream is deflected by an angle ϕ as shown in Figure 5.5 for a given yaw angle misalignment γ and wind direction θ given as

$$\phi = (0.6a+1)\gamma+\theta, \tag{6.14}$$

where a is the axial induction factor and θ is the wind speed direction which is 0° in the present case [11].

Similarly, using wake management by varying the yaw angle (from 0° to γ°), the wind speed v_j^{γ} at the downstream turbine is given as

$$v_j^{\gamma} = \begin{cases} v_0\left[1-2a\left(\frac{1}{YY}\right)^2\times\cos^2(4.5\phi)\right],\ \phi\le\phi_{th} \\ v_0,\ \ \phi>\phi_{th}, \end{cases} \tag{6.15}$$

where $YY = 1+2\alpha_y Z\cos\phi$, $Z = \frac{x}{D_0}$ is the turbine spacing factor and ϕ_{th} is the threshold wake angle (here $\phi_{th} = 20°$).

6.3 Numerical Simulation for Proposed Methodology

In the present study, a wind farm with two-turbine (adj)s is considered where WT_1 is the upwind turbine and WT_2 is the downstream turbine as illustrated in Fig. 5.5. The wind speed (v_0) is collected for all the wind farm sites mentioned in Table 6.1. The data is collected every 10 min for all the datasets labeled as **X1** (Bishop & Clerks, Massachusetts), **X2** (Blandford, Massachusetts), **X3** (Paxton, Massachusetts), and **X4** (Middelgrunden, Denmark) at hub heights 15m, 60m, 78m, and 10 m, respectively.

The wind speed for WT_2 is calculated under wake effect using (6.13) and (6.15). The downstream distance between WT_1 and WT_2 is $5D_0$. Table 6.2 highlights the turbine and BESS parameters used.

In wake aerodynamics, since the thrust coefficient of wind turbine varies with speed, using look-up table we find C_T for wind speed data under consideration. For this purpose, GE2.5-120 wind turbine model is selected and the curve as shown in Fig. 6.4 between C_T and wind speed is imported [1].

Wind forecasting is carried out using Least square support vector regression for Cases I, II, and III. The wind speed data is segmented into training (800) and testing (200) sets. Figure 6.6 illustrates the wind speed scenario under freestream, waked and yawed ($\gamma = 5°$) turbine conditions depicted by symbols v_0, v_j, and v_j^{γ}, respectively. Further, the charging and discharging powers for BESS are calculated from (6.8) and SoC is determined based on (6.10). The BESS life cycle and operational cost ($/kWh) are determined for three cases (as shown in Fig. 6.5) with fixed rotor diameter and yaw angle ($\gamma = 5°$) in case of upwind turbine:

Table 6.1 Description of wind datasets

Dataset	Site coordinates	Data duration
Bishop and Clerks	41.574° N, 70.249° E	Jan 1, 2011–Jan 7, 2011
Blandford	42.223° N, 72.968° E	Jan 1, 2011–Jan 7, 2011
Paxton	42.303° N, 71.897° E	Jan 1, 2011–Jan 7, 2011
Middelgrunden	55.691° N, 12.670° E	Feb 1, 2019–Feb 7, 2019

Table 6.2 Wind turbine and BESS parameters

Parameters	Value
Rotor diameter (D_0)	120 m
x_{SoC}^{max}	90%
x_{SoC}^{min}	10%
$x_{SoC}(t_0)$	81.47%
Charging efficiency (η_b)	91.86%
Self-discharge factor (kW)	1.545
Battery capital cost (B_{batt})	250 $/kWh

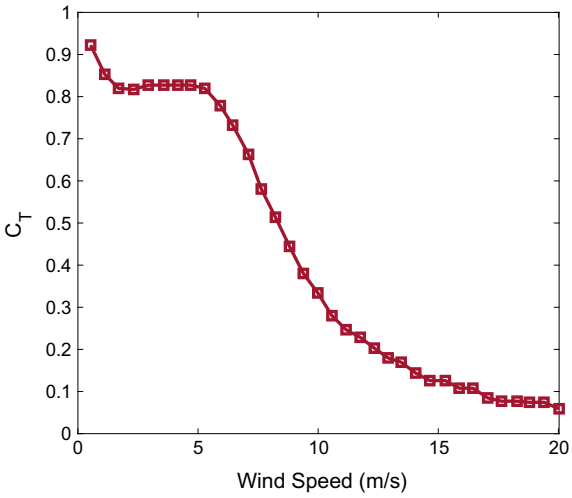

Fig. 6.4 Variation of thrust coefficient (C_T) with freestream wind speed

- Case I (without wake effect for a two-turbine wind farm layout): The BESS charging and discharging powers are calculated based on the forecast error.
- Case II (considering wake effect of WT_1 on WT_2 given the wind turbines operate in stable atmospheric boundary layer): The wind power for WT_2 is forecasted considering wake effect.
- Case III: Considering wake management strategy with variation in the yaw angle of WT_1.

Table 6.3 highlights the operational cost (B_{batt}) for different BESS battery ratings. A fixed yaw angle of 5° for WT_1 gives a saving of 11.22% in BESS operational cost for battery rating of 300 kWh for dataset X1. Further, we observe that the operational cost increases with BESS rating for all the cases.

A BESS rating of 1000 kWh however gives minimum operational cost but is subjected to size constraints. An optimal BESS rating is preferred for wind farm operation. The operational cost is determined for different yaw angles and is found minimum for $\gamma = 15°$, suggesting an optimal yaw angle setting for upwind turbine as shown in Fig. 6.7. Further, we observe from Fig. 6.8 that the life cycle count of BESS varies monotonically with depth of discharge for all the datasets.

The life cycle count starts from the same initial point since the initial SoC is same for all the cases. However, case I is an ideal scenario that does not practically exist for a wind farm due to the spacing constraints. The life cycle count is evaluated using (6.11) for all the three cases with $Q_{batt} = 500$ kWh, and it is found that a wake management technique of varying yaw angle by 5° increases life cycle count of BESS by 5.86%, 4.19%, 5.64% and 29.53% for datasets **X1**, **X2**, **X3** and **X4**, respectively.

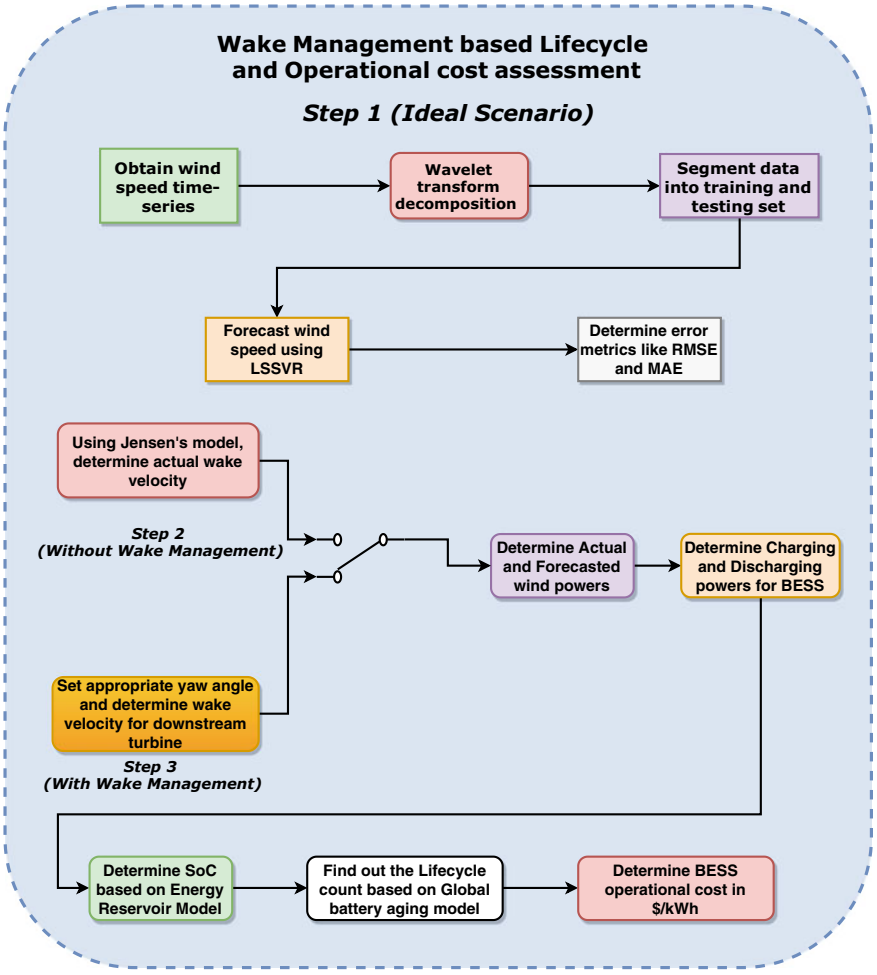

Fig. 6.5 Flowchart for proposed methodology

6.3.1 Operational Cost and Life Enhancement for Hilly Wind Site

Wind speed distribution and variability is high in hilly areas. The rapid changes in speed and direction can cause large discharging events. In order to test the validity of the proposed scheme, two wind datasets from hilly area are undertaken and BESS operational cost along with life cycle improvement is studied. The wind speed data for Challicum hills, Australia labeled as dataset **Z1** and Longyuan wind farm in Tibet labeled as dataset **Z2** is collected for the month of May 2019 with 10 min interval.

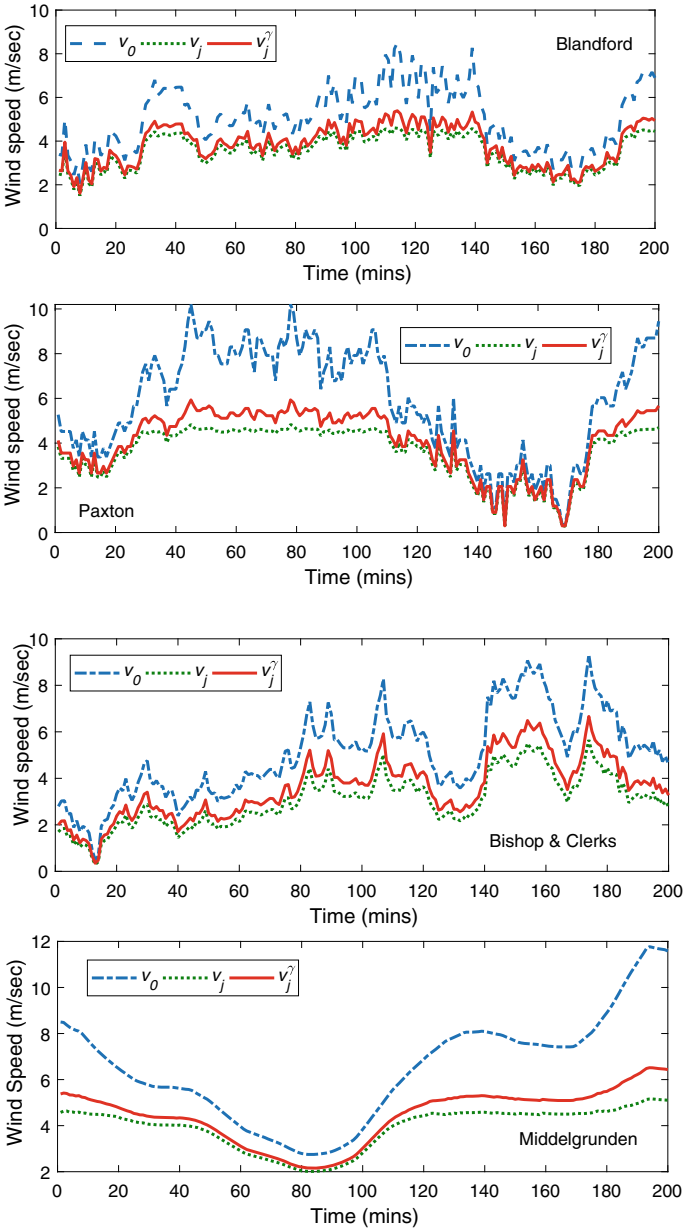

Fig. 6.6 Wind speed under different wake scenarios

Table 6.3 Operational cost (OC) for different datasets for $\gamma = 5°$

Dataset	Rating (kWh)	Case I	Case II	Case III	% saving in OC	% saving in life cycles
X1	300	0.0217	0.0603	0.0536	11.22	12.63
	400	0.0316	0.0666	0.0617	7.35	7.93
	500	0.0417	0.0704	0.0665	5.53	5.86
	750	0.0576	0.0754	0.0728	3.46	3.58
	1000	0.0646	0.0779	0.0760	2.53	2.59
X2	300	0.0558	0.0570	0.0525	7.91	8.59
	400	0.0598	0.0614	0.0581	5.31	5.61
	500	0.0603	0.0640	0.0614	4.02	4.19
	750	0.0612	0.0674	0.0657	2.52	2.59
	1000	0.0621	0.0691	0.0678	1.84	1.85
X3	300	0.0217	0.0527	0.0466	11.51	13.01
	400	0.0210	0.05893	0.0541	7.22	7.78
	500	0.0352	0.0615	0.0582	5.34	5.64
	750	0.0506	0.0658	0.0636	3.27	3.38
	1000	0.0568	0.0679	0.0663	2.37	2.42
X4	300	0.0102	0.0437	0.0219	10.56	12.63
	400	0.0121	0.0501	0.0421	6.73	8.52
	500	0.0135	0.0567	0.0438	6.12	7.11
	750	0.0187	0.0627	0.0548	4.18	6.92
	1000	0.0212	0.0656	0.0598	2.54	3.35

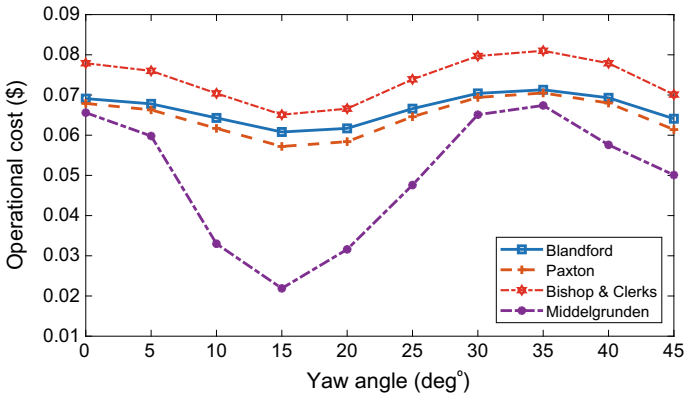

Fig. 6.7 Operational cost for different yaw angles

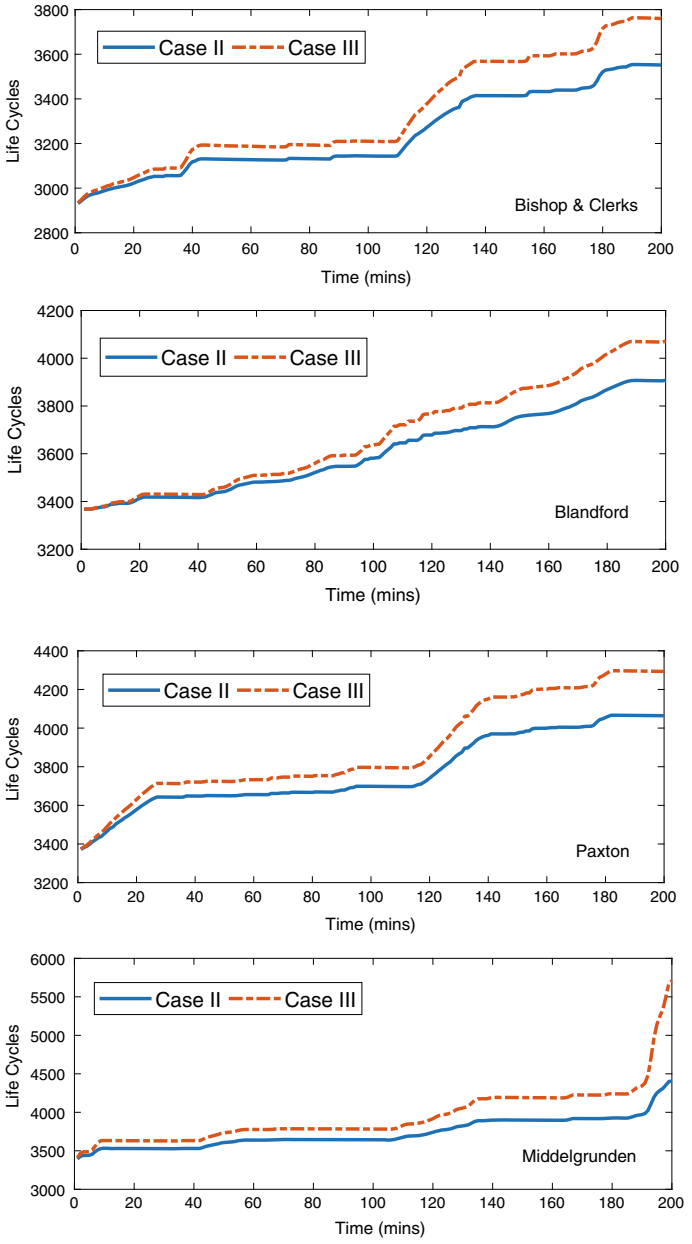

Fig. 6.8 BESS life cycle without (case II) and with (case III) wake management

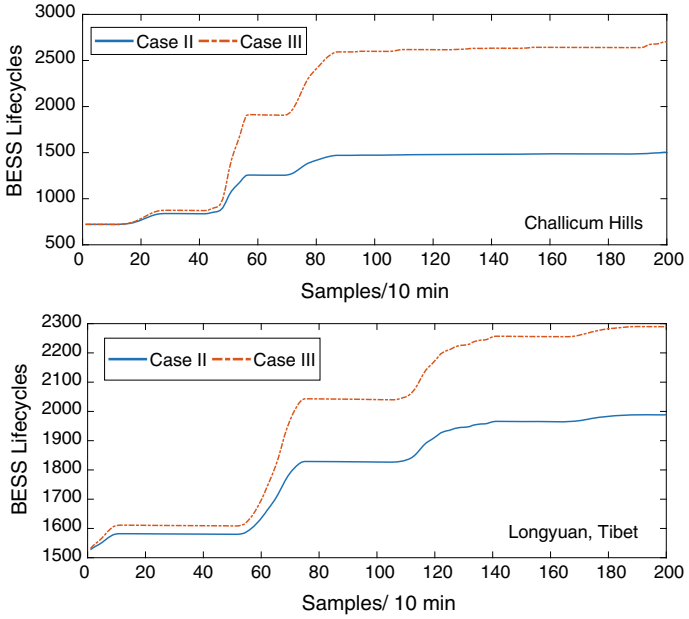

Fig. 6.9 Life cycle count without (Case II) and with wake management (Case III) for hilly wind sites

Table 6.4 Operational cost (OC) for hilly wind datasets for $\gamma = 5°$

Dataset	BESS rating (kWh)	Case II	Case III	% saving in OC	% saving in life cycles
Z1	500	0.1662	0.0925	44.37	79.74
	750	0.2077	0.1403	32.46	48.05
	1000	0.2335	0.1720	26.33	35.74
Z2	500	0.1217	0.1092	13.17	15.16
	750	0.1375	0.1253	8.87	9.73
	1000	0.1438	0.1341	6.72	7.20

Figure 6.9 illustrates the life cycle without (Case II) and with wake management (Case III) for hilly sites.

From Table 6.4, we can see that for hilly wind sites, the methodology adopted for estimating operational cost and determining life cycle count of BESS is validated. For a BESS rating of 500 kWh, the % saving in operational cost is 44.37% while % saving in life cycles is 79.74%.

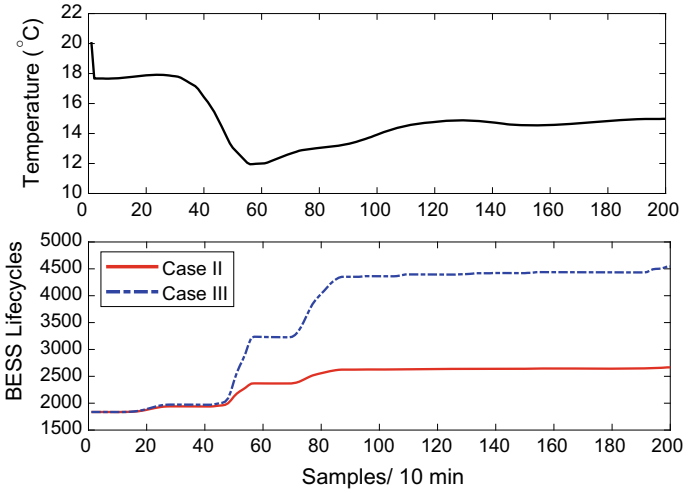

Fig. 6.10 BESS life cycle count based on global battery aging model for dataset **Z1**

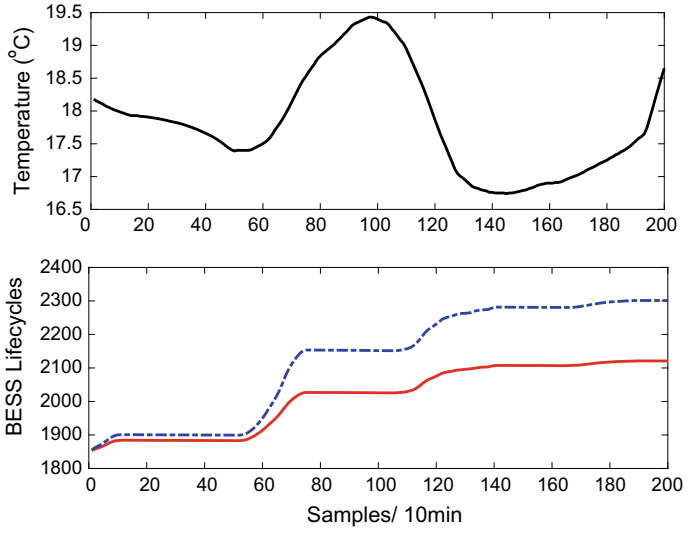

Fig. 6.11 BESS life cycle count based on global battery aging model for dataset **Z2**

6.3.2 Operational Cost Based on Global Battery Aging Model

Since the current data for BESS is available experimentally by knowing voltage level of wind farms apriori, we have incorporated the global battery aging model for life cycle and operational cost assessment. For validation of the proposed method, the life cycle assessment along with operating cost of BESS are determined based on

Table 6.5 Operational cost (OC) based on Global battery aging model for $\gamma = 5°$

Dataset	BESS rating (kWh)	Case II	Case III	% saving in OC	% saving in life cycles
Z1	500	0.1361	0.1262	7.274	15.69
	750	0.1626	0.1561	3.997	10.62
	1000	0.1961	0.1899	3.161	5.31
Z2	500	0.0999	0.0808	19.13	23.65
	750	0.1119	0.0994	11.16	12.57
	1000	0.1179	0.1086	7.84	8.51

global battery aging model for two different wind datasets labeled as **Z1** and **Z2**. Apart from wind speed data, the temperature data is collected for the two wind farm sites. The data available in °K is converted into °C. Figures 6.10 and 6.11 illustrate the life cycle for Cases II and III as explained in the previous section.

The % saving in operating cost for dataset **Z1** is 7.274% for a BESS rating of 500 kWh and 3.161% for a rating of 1000 kWh. Similarly, for dataset **Z2**, the % saving in operating cost for a BESS rating of 500 kWh is 19.13% while for 1000 kWh it is 7.84%.

6.4 Discussion

Based on the proposed methodology for BESS life enhancement and operating cost minimization, we discuss primarily two main cases as described in the previous section. Case II that involves operation of downstream turbine without yaw angle misalignment results in higher operational cost than Case III. It is also worthwhile to note that, the BESS operational cost increases with increase in its capacity owing to higher investment costs. Further, the % saving in life cycles decreases as we increase BESS rating as depicted in Tables 6.3, 6.4, and 6.5. It is also found that with ambient temperature taken into account the proposed methodology holds a good agreement for saving in operational cost and life cycles. The current methodology involves the availability of actual and forecasted wind powers that essentially determines the charging and discharging schedules of BESS. Hence, the SoC estimation largely depends on the accuracy of the forecasting method used. Several other methods like KF, EKF, and UKF require the physical and electrical parameters of the battery model to determine the SoC. In the proposed methodology, only actual and forecasted wind power schedule is needed.

The present study deals with BESS optimization in terms of operational cost and life cycle count. The wind power forecasting accuracy is treated as a measure for charging and discharging the BESS. Energy reservoir model is used to estimate the SoC during charging/discharging event and based on that the depth of discharge is

determined for calculating the life cycle count. A two-turbine wind farm with yaw angle for upwind turbine $\gamma = 15^{\circ}$ results in minimal BESS operational cost for a wake management strategy and leads to optimum usage of BESS in terms of life cycle count. Further, in order to analyze the effect of ambient temperature on the BESS performance, a global battery aging model is considered and life cycle assessment along with operating cost is determined. Results reveal a significant improvement in BESS performance when upstream turbine is operated in yaw mode.

References

1. General electric ge 2.5 - 120 - 2,50 mw - wind turbine. https://en.wind-turbine-models.com. Accessed 12 April 2019
2. Abdeltawab HH, Mohamed YARI (2015) Market-oriented energy management of a hybrid wind-battery energy storage system via model predictive control with constraint optimizer. IEEE Trans Ind Electron 62(11):6658–6670
3. Adnan RM, Yuan X, Kisi O, Anam R (2017) Improving accuracy of river flow forecasting using LSSVR with gravitational search algorithm. Adv Meteorol 2017:1–23
4. Andre D, Appel C, Soczka-Guth T, Sauer DU (2013) Advanced mathematical methods of SOC and SOH estimation for lithium-ion batteries. J Power Sourc 224:20–27
5. Barthelmie RJ, Hansen K, Frandsen ST, Rathmann O, Schepers JG, Schlez W, Phillips J, Rados K, Zervos A, Politis ES, Chaviaropoulos PK (2009) Modelling and measuring flow and wind turbine wakes in large wind farms offshore. Wind Energy 12(5):431–444
6. Catalao JPS, Pousinho HMI, Mendes VMF (2010) Hybrid wavelet-PSO-ANFIS approach for short-term wind power forecasting in Portugal. IEEE Trans Sustain Energy
7. Chen C, Xiong R, Yang R, Shen W, Sun F (2019a) State-of-charge estimation of lithium-ion battery using an improved neural network model and extended kalman filter. J Clean Prod 234:1153–1164
8. Chen Z, Yang L, Zhao X, Wang Y, He Z (2019b) Online state of charge estimation of li-ion battery based on an improved unscented kalman filter approach. Appl Math Model 70:532–544
9. Claude F, Becherif M, Ramadan H (2017) Experimental validation for li-ion battery modeling using extended kalman filters. Int J Hydrog Energy 42(40):25509–25517
10. Crespo A, Hernández J, Frandsen S (1999) Survey of modelling methods for wind turbine wakes and wind farms. Wind Energy 2(1):1–24
11. Dar Z, Kar K, Sahni O, Chow JH (2017) Windfarm power optimization using yaw angle control. IEEE Trans Sustain Energy 8(1):104–116
12. Dhiman H, Deb D, Muresan V, Balas V (2019a) Wake management in wind farms: an adaptive control approach. Energies 12(7):1247
13. Dhiman HS, Deb D, Guerrero JM (2019b) Hybrid machine intelligent SVR variants for wind forecasting and ramp events. Renew Sustain Energy Rev 108:369–379
14. Du P, Wang J, Yang W, Niu T (2019) A novel hybrid model for short-term wind power forecasting. Appl Soft Comput 80:93–106
15. EPRI (2010) Electric energy storage technology options. Technical report, Electric Power Research Institute, Palo Alto, California. https://www.epri.com/pages/product/1022261
16. Farzin H, Fotuhi-Firuzabad M, Moeini-Aghtaie M (2016) A practical scheme to involve degradation cost of lithium-ion batteries in vehicle-to-grid applications. IEEE Trans Sustain Energy 7(4):1730–1738
17. Fleming PA, Gebraad PM, Lee S, van Wingerden JW, Johnson K, Churchfield M, Michalakes J, Spalart P, Moriarty P (2014) Evaluating techniques for redirecting turbine wakes using SOWFA. Renew Energy 70:211–218

18. Gebraad P, Fleming P, van Wingerden J (2015) Wind turbine wake estimation and control using FLORIDyn, a control-oriented dynamic wind plant model. In: 2015 American control conference (ACC). IEEE
19. Gebraad PMO, Teeuwisse F, van Wingerden J, Fleming PA, Ruben SD, Marden JR, Pao LY (2014) A data-driven model for wind plant power optimization by yaw control. In: 2014 American control conference. IEEE
20. Grewal MS, Andrews AP (2014) Kalman filtering. Wiley Inc, New York
21. Hao Y, Tian C (2019) A novel two-stage forecasting model based on error factor and ensemble method for multi-step wind power forecasting. Appl Energy 238:368–383
22. Howland MF, Bossuyt J, Martínez-Tossas LA, Meyers J, Meneveau C (2016) Wake structure in actuator disk models of wind turbines in yaw under uniform inflow conditions. J Renew Sustain Energy 8(4):043301
23. Iungo GV (2016) Experimental characterization of wind turbine wakes: wind tunnel tests and wind LiDAR measurements. J Wind Eng Ind Aerodyn 149:35–39
24. Jensen N (1983) A note on wind generator interaction
25. Jin T, Tian Y, Zhang CW, Coit DW (2013) Multicriteria planning for distributed wind generation under strategic maintenance. IEEE Trans Power Deliv 28(1):357–367
26. Junping W, Quanshi C, Binggang C (2006) Support vector machine based battery model for electric vehicles. Energy Convers Manag 47(7–8):858–864
27. Layadi TM, Champenois G, Mostefai M, Abbes D (2015) Lifetime estimation tool of lead-acid batteries for hybrid power sources design. Simul Model Pract Theory 54:36–48
28. Liang C, Wang P, Han X, Qin W, Jia Y, Yuan T (2018) Battery energy storage selection based on a novel intermittent wind speed model for improving power system dynamic reliability. IEEE Trans Smart Grid 9(6):6084–6094
29. Liu H, Chen C, qi Tian H, fei Li Y, (2012) A hybrid model for wind speed prediction using empirical mode decomposition and artificial neural networks. Renew Energy 48:545–556
30. Liu J, Zheng H, Zhang Y, Li X, Fang J, Liu Y, Liao C, Li Y, Zhao J (2019) Dissolved gases forecasting based on wavelet least squares support vector regression and imperialist competition algorithm for assessing incipient faults of transformer polymer insulation. Polymers 11(1):85
31. Luo J, Peng J, He H (2019) Lithium-ion battery SOC estimation study based on cubature kalman filter. Energy Procedia 158:3421–3426
32. Mastali M, Vazquez-Arenas J, Fraser R, Fowler M, Afshar S, Stevens M (2013) Battery state of the charge estimation using kalman filtering. J Power Sourc 239:294–307
33. Porté-Agel F, Wu YT, Chen CH (2013) A numerical study of the effects of wind direction on turbine wakes and power losses in a large wind farm. Energies 6(10):5297–5313
34. Qiu Y, Li X, Chen W, min Duan Z, Yu L (2019) State of charge estimation of vanadium redox battery based on improved extended kalman filter. ISA Trans
35. Sethi JK, Deb D, Malakar M (2011) Modeling of a wind turbine farm in presence of wake interactions. In: 2011 International conference on energy, automation and signal. IEEE. https://doi.org/10.1109/iceas.2011.6147144
36. Sturm J, Ennifar H, Erhard S, Rheinfeld A, Kosch S, Jossen A (2018) State estimation of lithium-ion cells using a physicochemical model based extended kalman filter. Appl Energy 223:103–123
37. Suykens J, Vandewalle J (1999) Neural Process Lett 9(3):293–300
38. Wang J, Zhang W, Li Y, Wang J, Dang Z (2014) Forecasting wind speed using empirical mode decomposition and elman neural network. Appl Soft Comput 23:452–459
39. Wang J, Du P, Niu T, Yang W (2017) A novel hybrid system based on a new proposed algorithm-multi-objective whale optimization algorithm for wind speed forecasting. Appl Energy 208:344–360
40. Wang J, Yang W, Du P, Niu T (2018a) A novel hybrid forecasting system of wind speed based on a newly developed multi-objective sine cosine algorithm. Energy Convers Manag 163:134–150
41. Wang S, Zhang N, Wu L, Wang Y (2016) Wind speed forecasting based on the hybrid ensemble empirical mode decomposition and GA-BP neural network method. Renew Energy 94:629–636

42. Wang W, Wang X, Xiang C, Wei C, Zhao Y (2018b) Unscented kalman filter-based battery SOC estimation and peak power prediction method for power distribution of hybrid electric vehicles. IEEE Access 6:35957–35965
43. Xing Y, He W, Pecht M, Tsui KL (2014) State of charge estimation of lithium-ion batteries using the open-circuit voltage at various ambient temperatures. Appl Energy 113:106–115
44. Yu Z, Huai R, Xiao L (2015) State-of-charge estimation for lithium-ion batteries using a kalman filter based on local linearization. Energies 8(8):7854–7873
45. Zheng L, Zhu J, Wang G, Lu DDC, He T (2018) Differential voltage analysis based state of charge estimation methods for lithium-ion batteries using extended kalman filter and particle filter. Energy 158:1028–1037

Appendix

A.1 Barbalat's Corollary

Corollary A.1 *Suppose* $f(t) \in C^1(a, \infty)$ *and* $\lim_{t\to\infty} f(t) = \alpha$ *where* $\alpha < \infty$. *If* $\ddot{f}$ *is uniformly continuous, then* $\lim_{t\to\infty} \dot{f}(t) = 0$.

Proof We will prove this result by contradiction. Suppose $\lim_{t\to\infty} \dot{f}(t) \neq 0$. The $\forall \varepsilon > 0$ and a monotonic function $\{t_n\}$ such that $t_n \to \infty$ as $n \to \infty$ and $|\dot{f}(t_n)| \geq \varepsilon$ for all $n \in \mathbb{N}$. Since $\dot{f}(t)$ is a continuous function for such ε, $\forall \delta > 0$ such that $\forall n \in \mathbb{N}$

$$|t - t_n| < \delta \Rightarrow \left| f'(t) - f'(t_n) \right| \leq \frac{\epsilon}{2}. \tag{A.1}$$

Hence if $t \in \{t_n, t_n + \delta\}$ then

$$\begin{aligned} |\dot{f}(t)| &= |\dot{f}(t_n) - (\dot{f}(t_n) - \dot{f}(t))| \\ &\geq |\dot{f}(t_n)| - |\dot{f}(t_n) - \dot{f}(t)| \\ &\geq \varepsilon - \frac{\varepsilon}{2} \\ &\geq \frac{\varepsilon}{2}. \end{aligned} \tag{A.2}$$

Since $f(t) \in C^1$, we have,

H. S. Dhiman and D. Deb, *Decision and Control in Hybrid Wind Farms*,
Studies in Systems, Decision and Control 253,
https://doi.org/10.1007/978-981-15-0275-0

$$\begin{aligned}\left|\int_a^{t_n+\delta} \dot{f}(t)dt - \int_a^{t_n} \dot{f}(t)dt\right| &= \left|\int_{t_n}^{t_n+\delta} \dot{f}(t)dt\right| \\ &\geq \left|\dot{f}(t)dt\right| \\ &\geq \frac{\varepsilon}{2}dt \\ &= \frac{\varepsilon\delta}{2}. \end{aligned} \tag{A.3}$$

However,

$$\begin{aligned}\lim_{t\to\infty}\left|\int_a^{t_n+\delta} \dot{f}(t)dt - \int_a^{t_n} \dot{f}(t)dt\right| &= \lim_{t\to\infty} |f(t_n+\delta) - f(t_n)| \\ &= \lim_{t\to\infty} |f(t_n+\delta)| - |f(t_n)| \\ &= |\alpha| - |\alpha| = 0.\end{aligned}$$

This is a contradiction. Therefore $\lim_{t\to\infty} \dot{f}(t) = 0$. □

A.2 Wind Speed Datasets

- https://www.umass.edu/windenergy/resourcedata/format
- http://www.sotaventogalicia.com/en/real-time-data/historical
- http://www.soda-pro.com/web-services/meteo-data/merra

Multi-criteria decision-making source codes

A.3 Simple Additive Weighting

```
function [S,w,Xn]= saw(X)
tic
%normalize decision matrix according to beneficial
%and non-beneficial criteria
[m,n]=size(X);
for i=1:m
    for j=1:n
        Xn(i,j)=min(X(:,j))/X(i,j);
    end
end
Q=(Xn).*log(Xn);

%Construct criteria weight matrix w using Entropy method
for j=1:n
        E(j)=-1/log(m).*sum(Q(:,j));
```

```
        d(j)=abs(1-E(j));
end
for j=1:n
    w(j)=d(j)/sum(d);
end

%Construct weighted decision matrix v(i,j) and Calculate
%performance index S for all alternatives
    v=w.*Xn;
    disp('Performance index using SAW method')
    S=sum(v,2);
toc
end
```

A.4 Technique for Order of Preference by Similarity to Ideal Solution

```
%Deterministic TOPSIS

function [C,w,Xn,vplus,vminus,Splus,Sminus]=topsis(X)
tic
%Construct Decision matrix
%X=input('enter Decision matrix')
[m,n]=size(X);
%Construct normalized decision matrix
for i=1:m
    for j=1:n
        Xn(i,j)=X(i,j)./sqrt(sum(X(:,j).^2));
    end
end
Q=(Xn).*log(Xn);
%Construct criteria weight matrix w using Entropy method
    for j=1:n
        E(j)=-1/log(m).*sum(Q(:,j));
        d(j)=abs(1-E(j));
        %w(j)=d(j)/sum(d);
    end
for j=1:n
    w(j)=d(j)/sum(d);
end

%Construct weighted decision matrix v(i,j)
%wx=[0.1 0.4 0.3 0.2];
for i=1:m
   for j=1:n
        v(i,j)=w(j).*Xn(i,j);
    end
end

%Identify positive and negative ideal solutions
%for i=1:m
```

```
    for j=1:n
    vplus(j)=min(v(:,j));      %positive ideal solution
    vminus(j)=max(v(:,j));     %negative ideal solution
    end
%end
%Calculate Eucledian distance for Non-beneficial solution
 p=input('enter Lp norm type ');
for i=1:m
    for j=1:n
        xx(i,j)=(v(i,j)-vplus(j))^p;
        xxn(i,j)=(v(i,j)-vminus(j))^p;
    end
end

for i=1:m
        Splus(i)=(sum(xx(i,:)))^1/p;
        Sminus(i)=(sum(xxn(i,:)))^1/p;
end

disp('Performance index using TOPSIS method ');
%Rank the alternatives according to relative closeness
for i=1:m
    C(i)=Sminus(i)/(Splus(i)+Sminus(i));
    Rank=sort(C);
end

    %[Qp]=COPRAS(v)
    %[w,S]= saw(X)
toc
end
```

A.5 Complex Proportional Assessment

```
function [Qp,Xn,w]=COPRAS(X)
%Construct Decision matrix
[m,n]=size(X);
%Construct normalized decision matrix
for i=1:m
    for j=1:n
        Xn(i,j)=X(i,j)./sqrt(sum(X(:,j).^2));
       % Xn(i,j)=(1/(X(i,j)))./(sum(1./X(:,j)));
    end
end
Q=(Xn).*log(Xn);
%Construct criteria weight matrix w using
% Entropy method
    for j=1:n
        E(j)=-1/log(m).*sum(Q(:,j));
        d(j)=abs(1-E(j));
        %w(j)=d(j)/sum(d);
    end
```

```
for j=1:n
    w(j)=d(j)/sum(d);
end

%Construct weighted decision matrix v(i,j)

for i=1:m
   for j=1:n
        v(i,j)=w(j).*Xn(i,j);
    end
end
        [m,n]=size(v);

        for i=1:m
            Sm(i)=sum(v(i,:));
        end

        yy=sum(Sm);
        zz=(sum(1./Sm));
        %evaluate performance index
        %for each alternative
        for i=1:m

            Cp(i)=(yy./(Sm(i).*zz));
         end

        disp('Performance index using COPRAS method ')
         for i=1:m
            Qp(i)=Cp(i)/max(Cp);
        end

end
```

A.6 Fuzzy TOPSIS

```
%Fuzzy TOPSIS for hybrid operation of wind farm
%Enter fuzzy decision matrix L,M,U
%L=[3 5 5; 5 3 3; 5 3 1; 1 1 1];
%M=[5.667 8.33 7; 7 7 5; 8.33 5 2.33; 2.33 4.33 1];
%U=[9 9 9; 9 9 7; 9 7 5; 5 7 3];
L=input('enter L matrix ');
M=input('enter M matrix ');
U=input('enter U matrix ');

[m,n]=size(L);

%identify minimum lower TFN for each TFN
for i=1:n
    k(i)=min(L(:,i));
end
```

```
%compute normalized L,M,U matrices
for i=1:m
    for j=1:n
        NL(i,j)=k(j)./U(i,j);
    end
end

for i=1:m
    for j=1:n
        NM(i,j)=k(j)./M(i,j);
    end
end
for i=1:m
    for j=1:n
        NU(i,j)=k(j)./L(i,j);
    end
end

%declare weights for criteria for  L,M,U matrices
%WL=[5 7 3];
%WM=[7 9 5];
%WU=[9 9 7];
WL=[5,7,9];
WM=[7 9 9];
WU=[3 5 7];

%compute weighted normalized L,M,U matrices
for i=1:m
    for j=1:n
        WNL(i,j)=WL(j).*NL(i,j);
         WNM(i,j)=WM(j).*NM(i,j);
           WNU(i,j)=WU(j).*NU(i,j);
    end
end

%identify FPIS and FNIS solutions

for i=1:m
    for j=1:n
        FPL(j)=max(WNL(:,j));    %Positive ideal L soln
        FPM(j)=max(WNM(:,j));    %Positive ideal M soln
        FPU(j)=max(WNU(:,j));    %Positive ideal U soln


        FNL(j)=min(WNL(:,j));    %Negative ideal L soln
        FNM(j)=min(WNM(:,j));    %Negative ideal M soln
        FNU(j)=min(WNU(:,j));    %Negative ideal U soln

    end
end

%calculate distance of each element from FPIS & FNIS
for i=1:m
```

```
    for j=1:n
        %Positive distance L Matrix
        DL(i,j)=(WNL(i,j)-FPL(j))^2;

        %Positive distance M Matrix
        DM(i,j)=(WNM(i,j)-FPM(j))^2;

         %Positive distance U Matrix
        DU(i,j)=(WNU(i,j)-FPU(j))^2;

        %Negative distance L Matrix
        DNL(i,j)=(WNL(i,j)-FNL(j))^2;

        %Negative distance M Matrix
        DNM(i,j)=(WNM(i,j)-FNM(j))^2;

        %Negative distance U Matrix
        DNU(i,j)=(WNU(i,j)-FNU(j))^2;


    end
end
 %Aggregate positive & negative distance matrix
 APDM=sqrt(0.33.*(DL+DM+DU));
 ANDM=sqrt(0.33.*(DNL+DNM+DNU));

  %Compute distance degree for each alternative
  PD=sum(APDM,2); %summation across rows
  ND=sum(ANDM,2);

  %compute closeness coefficient
  for i=1:m
      CC(i)=ND(i)/(PD(i)+ND(i));
  end

  [kenny,ADDL] =FuzzyCOPRAS(WNL,WNM,WNU)
```

A.7 Fuzzy COPRAS

```
% kenny is the priority score for alternatives
function [Q,ADDL]= FuzzyCOPRAS(WNL,WNM,WNU)
[m,n]=size(WNL);
   ADDL=[sum(WNL,2) sum(WNM,2) sum(WNU,2)];

   %defuzzyfy into crisp numbers

     alpha=input('enter alpha cut value')

for k=1:length(alpha)
```

```
 for i=1:m
  Q(k,i)=2*ADDL(i,1)*(1-alpha(k))+0.5*(ADDL(i,3)
         -ADDL(i,2))*(1-alpha(k))^2;
 end
end

for i=1:4
Qmax(i)=max(Q(i,:));
end

alphacut=input('enter alpha cut value');
     switch alphacut
          case 0.2
               alphacut=1;
          case 0.4
               alphacut=2;
          case 0.6
               alphacut=3;
          otherwise
               alphacut=4;
     end
   kenny=(Q(alphacut,:)/Qmax(alphacut))*100;

NCS=input('enter normalized cost score ');
NCS2=input('enter normalized cost score ');

FPS=NCS.*kenny
FPS2=NCS2.*kenny
end
```

Epilogue

Having presented both the decision-making aspects and also the control aspects related to wake center estimation, involved in the wind farm profit maximization, what would tie both these aspects together for future work, is an integrated mechanism to compute wind turbine computational fluid dynamics (CFD) simulations. Such simulation, possibly in the form of a toolbox, should be capable of modeling wake effects for any given arrangement of upwind turbines, at any yawed condition and under a plethora of decision-making scenarios. Real-time adaptive control meant to enable profit maximization in such a way that decision-making is dynamic is needed.

For such an integrated decision and control toolbox of wind power management in wind farms, the toolbox needs to be provided with an extensive database of criteria and attributes for different types of wind farms and wind turbines therein. In order to ensure that the chosen criteria and attributes are exhaustive in terms of all possible variants of wind turbines and wind farms and the conditions therein, it is important to study a large number of wind farms and also collate extensive data through the process of an exhaustive survey of experts prior to the selection of the prospective choices in decision-making.

Apart from such a simulation framework, it is also needed to carry out exhaustive wind tunnel tests for different decision-making attributes, criteria, and also with different advanced controllers under yawed and pitched conditions of turbine blades. As explained in Chap. 4, fuzzy set theory is useful in decision-making when the goals, limitations, and outcomes of actions taken are imprecisely available, and since exhaustive wind tunnel tests and exhaustive survey of experts cannot intrinsically remove the inherent stochastic nature of wind, fuzzy logic-based decision making like fuzzy TOPSIS and fuzzy COPRAS are envisioned to be continued force to reckon with in the area of wind farm power generation.

This indicative multipronged approach of optimization will need to be further extended to an extensive research of BESS for deployment in onshore wind farms at different levels, so as to be able to continue to enhance life cycle count and reduce

H. S. Dhiman and D. Deb, *Decision and Control in Hybrid Wind Farms*,
Studies in Systems, Decision and Control 253,
https://doi.org/10.1007/978-981-15-0275-0

operational cost. There is extensive research going on in the estimation of SoC and models which are more advanced than the Energy reservoir model used in this book, would find appropriate use in further study in this field. Experimental work would need to be carried out for yaw angle control of different configurations of upwind turbines to ascertain minimal BESS operational cost for advanced wake management strategies.